Spin-1 atomic condensates in magnetic fields

A Dissertation
Presented to
The Academic Faculty

by

Wenxian Zhang

In Partial Fulfillment
of the Requirements for the Degree
Doctor of Philosophy in Physics

School of Physics
Georgia Institute of Technology
December 2005

Spin-1 atomic condensates in magnetic fields

Approved by:

Dr. Li You, Chair
School of Physics
Georgia Institute of Technology, Advisor

Dr. Michael S. Chapman
School of Physics
Georgia Institute of Technology

Dr. Chandra Raman
School of Physics
Georgia Institute of Technology

Dr. Mei-Yin Chou
School of Physics
Georgia Institute of Technology

Dr. Z. John Zhang
School of Chemistry and Biochemistry
Georgia Institute of Technology

Date Approved: April 21, 2005

For my father, Guangxi Zhang,

and

my son, Edwin Zhang

ACKNOWLEDGEMENTS

This is a great moment in my life and I would like to share this moment with all my friends, in Georgia Tech, in U.S.A, and in China. Without their help and support this work would not have been possible to complete.

First of all, I want to express my greatest gratitude to my thesis advisor, Professor Li You, for all the support and guidance. His experiences and keen insights into atomic, molecular, and optical physics were the most precious for the improvement of my research abilities.

Forever thanks to my friends Dr. Su Yi, Dr. Özgür Esat Müstecaplıoğlu, Dr. Duanlu Zhou, Bo Sun, and Dr. Yuheng Lan for terrific and vital discussions on some issues of my thesis work. Special thanks to Mingshien Chang and Professor Michael S. Chapman, their experimental support and great help are of key importance to the success of my thesis. Many thanks to Dr. Mei Zhang, Hai'an Wang and Hsiang-Hua Jen for the great "physical life" together.

On a personal note, I am indebted to my parents for their support and encouragement over all these years. Remorse preys upon my mind whenever I remembered my father, Guangxi Zhang, who passed away during my Ph. D. study at Georgia Tech. Many thanks to my wife, Huizhen Wang, who is always by my side throughout my graduate studies. She is the best and the most wonderful friend and has been always incredibly supportive to me in our life together.

This work was supported by the NSF under grant No. PHYS-0140073 and PHYS-0326315, and the ARO/NSA/ARDA/DARPA under grant No. DAAD19-01-1-0667.

TABLE OF CONTENTS

LIST OF TABLES

LIST OF FIGURES

SUMMARY

In this thesis we investigate the static, dynamic, and thermodynamic properties of atomic spin-1 Bose gases in external magnetic fields. At low magnetic fields the properties of single-component, or scalar condensates, are essentially unaffected but can become significantly altered for spinor Bose condensates as shown by our studies.

We first study the Bose-Einstein condensation of trapped spin-1 Bose gases by employing the Hartree-Fock approximation and the two-fluid model within a mean field approximation. Our detailed investigation reveals that the ferromagnetically interacting spin-1 condensates exhibit triple condensations while the antiferromagnetically interacting ones show double condensations.

The ground state structure of homogeneous and trapped spin-1 Bose condensates with ferromagnetic and antiferromagnetic interactions at zero temperature in magnetic fields are then investigated systematically. We further illuminate the important effect of quadratic Zeeman shift which causes a preferred occupation of the $|m_F = 0\rangle$ state through spin exchange collisions, $2|m_F = 0\rangle \leftrightarrow |m_F = 1\rangle + |m_F = -1\rangle$.

We also present detailed studies of the off-equilibrium coherent dynamics of spin-1 Bose condensates in magnetic fields within the single spatial mode approximation. Dynamical instabilities of the off-equilibrium oscillations are shown to be responsible for the formation of multiple domains as recently observed in several ^{87}Rb experiments.

Finally, we discuss briefly excited condensate states, or soliton-like states, in cigar-shaped spin-1 Bose condensates with an effective quasi-1D description, using the developed nonpolynomial Schrödinger equation.

CHAPTER I

INTRODUCTION

Bose-Einstein condensation (BEC) was first predicted theoretically by Bose [1] and Einstein [2] in 1920s, yet not realized in its original form for a weakly interacting gas until a decade ago when it was first achieved with dilute alkali atomic gases inside a magnetic trap [3, 4, 5]. As can be easily seen in the phase diagram, the Bose condensed state is an supercooled state. The thermodynamic ground state is actually a solid state, thus the Bose condensed state is meta-stable that may last up to more than a few minutes. The central theme of Bose-Einstein condensation in finite systems is the macroscopic occupation of a single particle state. The original idea that condensation occurs only in momentum space for an infinite system becomes simultaneous condensations in both momentum and coordinate space for a finite confined system. Experimental techniques such as laser cooling, magnetic trapping, and evaporative cooling, collectively enable cooling of an atomic alkali system down to nanokelvin (now even picokelvin [6]) temperatures, where the thermal de Broglie wave length of an atom, $\lambda_T = h/\sqrt{2\pi \mathsf{m} k_B T}$, is of the order of a few micrometer. The atoms thus behave quantum mechanically, distinguished from classical systems [3, 4, 5], and become quantum degenerate when the de Broglie wavelength of atoms is larger than the average distance between atoms (typical densities of atomic condensates range from 10^{13} to 10^{15} cm^{-3} and the average distance between atoms is less than 1 micrometer).

The realization of BEC in trapped dilute alkali atomic gases has stimulated significant interest because this system is an excellent test-bed for weakly interacting many body quantum theory. Many branches of research in trapped condensates remain active even 10 years after the initial discoveries [7]. For example, the formation of a

vortex in a rotating condensate manifests its superfluid property as first demonstrated experimentally by Matthews *et al.* with a phase imprinting technique [8, 9], followed by Madison *et al.* and Abo-Shaeer *et al.* with a laser beam "stirrer" [10, 11, 12], and Hodby *et al.* with a "rotating bucket" method [13]. A state of vortex lattice can now be routinely produced as reported by Abo-Shaeer *et al.*, Raman *et al.* [11, 12], Engels *et al.* [14], and Bretin *et al.* [15].

Many studies have been devoted to the properties of a condensate in a double well potential and in an optical lattice relevant to strongly interacting condensed matter systems. For a simple double well model system, one expects to find Josephson like dynamical effects, Rabi oscillations, and self-trappings in different interaction regimes [16, 17, 18]. Optical lattices created by standing wave laser beams consist of an array of wells where each well can contain a small sub-condensate. Coherent tunnelling, similar to the Josephson junction like oscillation, was first observed in an optical lattice system by Anderson and Kasevich [19] and was followed by other groups on various condensed matter effects, cumulating with the observation of the interference pattern of the superfluid to Mott-insulator phase transition formed by releasing the trapping potential [20, 21, 22, 23]. Bloch oscillations are also observed when condensates in optical lattices are accelerated [24, 25], and Hofstadter butterfly effect is predicted for an array of atoms placed in a super-strong effective magnetic field created by laser beams [26].

Lower dimensional (1D or 2D) quantum gases consist of another hot topical area and many novel properties appear in these systems [27, 28, 29, 30, 31]. A 1D Boson system can be solved exactly with the technique of Bethe ansatz and such a system has many known counter-intuitive properties. For example, the interaction between atoms is "weak" in the high-density limit but becomes "strong" in the low-density limit. A 1D system in the low density limit is usually referred as a Tonks-Girardeau gas in which the particles are impenetrable and exhibit Fermion-like features [27, 28, 31].

BEC-BCS (Bardeen-Cooper-Schrieffer) crossover, at which trapped dilute ultracold fermionic atoms form a bosonic molecular condensate and/or Cooper pairs near a Feshbach resonance, is yet another prominent and highly debated new phenomenon in recent years. Regal *et al.* first reported the appearance of condensation of fermionic ^{40}K atom pairs, similar to Cooper pairs in a superconductor, on the BCS side of the Feshbach resonance where weakly bound molecular condensate is not supported [32]. Similar results were also reported with higher percentages of condensate (80% vs 15% of Regal *et al.*) by Zwierlein *et al.* in ^{6}Li systems at MIT and the 80% condensate is argued to be actually composed of short-range atomic pairs, or essentially molecules on the BCS side [33]. While some of these debates can be traced to the differences of a Feshbach resonance being broad or narrow, much theoretical work have been done [34, 35, 36, 37, 38, 39]. Ohashi and Griffin recently proposed a new concept capable of reconciling molecules and Cooper pairs and giving rise to a continuous phase transition from the BCS to BEC [40].

Spinor condensates are the topic I shall concentrate on in this thesis. It arises when more than one hyperfine states of atoms are trapped simultaneously. Despite its early appearance in atomic condensate research, it was not an actively pursued topic, evidenced by only a few available experiments for pseudo-spin-half condensates [41, 42, 43, 44] and spin-1 condensates [45, 46, 47, 48, 49, 50, 51, 52]. The study on spinor condensate has received significant boosts recently with more experimental set-ups being built for spin-1 and spin-2 condensates [53, 54, 55, 56]. Experimentally spin-1 or spin-2 condensates are confined spatially with optical traps. The releasing of the spin degrees of freedom enables one to study both static and dynamic spin properties of a condensate absent in a magnetically trapped single component (scalar) condensate.

Making use of a Feshbach resonance, one can adjust the interaction strength between atoms in a scalar Bose condensate by changing the magnitude of an external

magnetic field, the interaction between atoms then changes from repulsive to attractive when the magnetic field crosses the Feshbach resonant region [57, 58, 59]. In this way one may control the static, dynamic, and thermodynamic properties of a single component condensate. Typically the magnetic field is in the range of several hundred Gausses and the relative Zeeman shift between open and closed channels is responsible for the tuning [60]. This picture becomes richer for a spinor condensate, even in much smaller magnetic fields, e.g. less than 1 Gauss, because Zeeman shifts are different for different spin components. It turns out, as we will show later, the leading term of the Zeeman effect, the linear one, has little effect on the properties of a spin-1 condensate but the quadratic term can significantly affect both the static and dynamic properties [45, 48, 53]. Many theoretical studies in the past have been devoted to the properties of a spinor condensate in a negligible magnetic field [50, 51, 52] and only a few touched on the topic of a nonzero magnetic field [61, 62, 63]. In this thesis, we focus on the properties of atomic spin-1 Bose gases in external magnetic fields.

The thesis is organized as follows. We briefly review the history of Bose-Einstein condensation and other current topical areas of atomic quantum gases in chapter . In chapter , we discuss the two body contact pseudo-potential interaction and outline a second quantized description of the Hamiltonian and the mean field Gross-Pitaevskii equation for both interacting scalar and spin-1 atomic Bose gases. This procedure for a spin-1 system can be extended straight forwardly to higher atom spin gases such as a spin-2 Bose gas. We present in chapter several analytical results in the ideal gas limit, the Thomas-Fermi limit for repulsively interacting scalar Bose gases, and the critical atom number for an attractively interacting scalar Bose condensate.

In chapter 2.2 we study the Bose-Einstein condensation of a harmonically trapped interacting spin-1 Bose gas. Due to the conservations of the total number of atoms and the total magnetization, both the ideal and antiferromagnetically interacting

spin-1 Bose gases exhibit double phase transitions, the ferromagnetically interacting Bose gases, on the other hand, exhibit triple condensations. We also find that in a certain range of temperatures a spin-1 Bose gas with ferromagnetic interaction can display phase separation between different condensed components.

We have carried out the study of the effect of magnetic fields because they are inevitable in experimental environment. For a scalar condensate, only strong magnetic fields, usually in the range of hundreds of Gausses, may affect its properties due to the change of the magnitude or sign of the s-wave scattering length through a Feshbach resonance. For a spinor condensate, the effect of a magnetic field is more direct, from its coupling to atomic magnetic dipole moments. In chapter 3.6 we systematically investigate the ground states of a homogeneous and a harmonically trapped interacting spin-1 Bose gas in a uniform external magnetic field. The quadratic Zeeman shift is shown to greatly affect the ground state structures. We find in general that the quadratic Zeeman effect causes a preferred occupation of the $|0\rangle$ component, thus the stronger the applied magnetic fields, the more atoms in the $|0\rangle$ state.

In chapter 4.6, we investigate the dynamical properties of an off-equilibrium spin-1 Bose condensate in an external magnetic field. Again, the linear Zeeman effect can be eliminated mathematically by changing to an interaction picture. The quadratic Zeeman effect thus completely determines the coherent oscillation of a spin-1 Bose condensate under the single spatial mode approximation. By analyzing the stability of the dynamics, we find that ferromagnetically interacting spin-1 condensates are dynamically instable and can evolve into a multi-domain structure as observed in a ^{87}Rb spin-1 condensate confined in a cigar-shaped trap.

In chapter 5.6, we discuss the collective excited eigenstate of a trapped spin-1 Bose condensate, a soliton state, and its dynamics with an effective quasi-1D non-polynomial Schrödinger equation description.

CHAPTER II

FORMULATION

2.1 Scalar atomic Bose gases

Before proceeding to the spin-1 atomic gases, let us summarize briefly the formulation of interacting spinless Bose gases. For an ultra-cold atomic gas in the same hyperfine state, the atomic interaction can be effectively described by a contact pseudo-potential,

$$V(\vec{r}-\vec{r}\,') = \frac{4\pi\hbar^2 a_{\rm sc}}{\mathsf{m}}\,\delta(\vec{r}-\vec{r}\,'),$$

characterized by the s-wave scattering length, $a_{\rm sc}$, as the dominant atomic interaction is isotropic and short ranged (for instance the famous van de Waals potential). $a_{\rm sc} > 0$ (< 0) denotes an overall repulsive (attractive) interaction. $a_{\rm sc}$ can be tuned using a Feshbach resonance as shown by many experimental groups [58, 59] with external uniform magnetic fields. $\hbar$ is the Plank's constant and m is the mass of the atom. This pseudo potential approximation (also called shape-independence approximation) simplifies the atomic interaction, $V(\vec{r}-\vec{r}\,')$, with an effective interaction $g\delta(\vec{r}-\vec{r}\,')$ independent of the details of the actual two-body potential.

With the contact pseudo-potential, the second quantized Hamiltonian of a single component scalar condensate is given by

$$H \;=\; \int d\vec{r}\left\{\Psi^\dagger\left[-\frac{\hbar^2}{2\mathsf{m}}\nabla^2 + V_{\rm ext}(\vec{r})\right]\Psi + \frac{g}{2}\Psi^\dagger\Psi^\dagger\Psi\Psi\right\},$$

where $\Psi(\vec{r})$ ($\Psi^\dagger(\vec{r})$) is the annihilation (creation) field operator which annihilates (creates) an atom at position $\vec{r}$, $V_{\rm ext}(\vec{r})$ is an external potential (usually a harmonic trap), and $g = 4\pi\hbar^2 a_{\rm sc}/\mathsf{m}$ is the interaction strength of the contact pseudo-potential.

The equation of motion for $\Psi(\vec{r})$ is obtained in Heisenberg picture as

$$i\hbar\frac{\partial}{\partial t}\Psi(\vec{r},t) = [\Psi, H] = \left[-\frac{\hbar^2}{2\mathsf{m}}\nabla^2 + V_{\rm ext}(\vec{r})\right]\Psi + g\Psi^\dagger\Psi^\dagger\Psi.$$

Within the mean-field theory, the field operator is approximated by its average value, $\Phi(\vec{r},t) \approx \langle\Psi(\vec{r},t)\rangle$, which is usually referred to as the wave function of the condensate or the order parameter. This approximation is valid if the number of condensed atoms, N, is large. The relative number fluctuation scales as $1/\sqrt{N}$ if one takes the condensate wave function as a coherent state. The dynamics of a condensate is then governed by the Gross-Pitaevskii (GP) equation [64, 65, 66, 67, 68, 69]

$$i\hbar\frac{\partial}{\partial t}\Phi(\vec{r},t) = \left[-\frac{\hbar^2}{2\mathsf{m}}\nabla^2 + V_{\rm ext}(\vec{r}) + g|\Phi(\vec{r},t)|^2\right]\Phi(\vec{r},t).$$

Another way to reach the GP equation is to start from the energy functional of the condensate,

$$E[\Phi,\Phi^*] = \int d\vec{r}\left\{\Phi^*\left[-\frac{\hbar^2}{2\mathsf{m}}\nabla^2 + V_{\rm ext}(\vec{r})\right]\Phi + \frac{g}{2}|\Phi|^4\right\},$$

and the GP equation is given by

$$i\hbar\frac{\partial}{\partial t}\Phi(\vec{r},t) = \frac{\delta E[\Phi,\Phi^*]}{\delta\Phi^*}.$$

By writing $\Phi(\vec{r},t) = \Phi(\vec{r})e^{-i\mu t/\hbar}$, we obtain the stationary state from solving the following equation

$$\left[-\frac{\hbar^2}{2\mathsf{m}}\nabla^2 + V_{\rm ext}(\vec{r}) + g|\Phi(\vec{r})|^2\right]\Phi(\vec{r}) = \mu\Phi(\vec{r}),$$

with $\Phi(\vec{r})$ being normalized to the total number of atoms N. The condensate ground state corresponds actually to the lowest μ stationary state of the above equation.

When the interaction term is small the properties of a condensate in a harmonic trap is close to the ideal gas limit whose wave function can be approximated as a Gaussian function. When the interaction is strong and repulsive, one reaches the so-called Thomas-Fermi limit where the wave function flattens due to the repulsive

interaction between atoms and one can neglect the kinetic energy term. The density profile of the condensate is then given by $n(\vec{r}) = |\Phi(\vec{r})|^2 = [\mu - V_{\rm ext}(\vec{r})]/g$ when $\mu > V_{\rm ext}(\vec{r})$ and $n = 0$ otherwise. When the interaction is attractive, a condensate in a uniform trap is unstable because the system tends to collapse [70, 71]. But for a confined system the zero-point energy (scales as N) may balance the weak attractive interaction (scales as N^2) if N is small [5, 72, 73]. Above a critical point, N_c, the interaction can not be balanced any more by the zero-point energy and the system becomes also unstable.

2.2 Spinor atomic Bose gases

For spinor atomic Bose gases at an ultra-low temperature, the collisions (interactions) between atoms become more complicated than in single-component gases. Ho, and independently Ohmi and Machida first discussed this issue [50, 51]. In this thesis we shall follow mainly Ho's arguments and procedures for convenience. Alkali atoms have two hyperfine states, typically, $F_{\rm high} = I + 1/2$ and $F_{\rm low} = I - 1/2$, where I is the quantum number of the nuclear spin, and $s = 1/2$ is the valence electron spin of the atom. For ^{87}Rb and ^{23}Na atoms, $I = 3/2$, thus $F_{\rm high} = 2$ and $F_{\rm low} = 1$. The energy splitting between them is usually in the range of $\sim$GHz, many orders of magnitude of typical trap frequencies which range from 1Hz to several kHz.

For an ideal spinor Bose gas, individual atom does not decay from the $F_{\rm high}$ states to the $F_{\rm low}$ states through spontaneous dipolar relaxation because of the conservation of the angular momentum which requires that the orbital angular momentum must be different by 1 before and after the transition. Two-photon processes may happen but usually they have a much lower rate which means longer time and are negligible for atoms in current experimental systems. For a spinor Bose gas with spin dependent interaction, the elastic collision would not change the hyperfine state due to the same reason as above. But the inelastic collision might change the atoms' hyperfine

state. At high temperatures above a few millikelvin, when the kinetic energy of an atom is comparable to its hyperfine energy splitting, atoms in any hyperfine state might be generated in principle after an inelastic collision. While it is forbidden at low temperatures to convert an atom into its $F_{\rm high}$ state through a collision of two atoms in their $F_{\rm low}$ state because of the conservation of the total energy. The reverse process is allowed. An atom acquired the kinetic energy corresponding to the hyperfine splitting would surely escape from the trap [74]. As a result, the ground state of the optically trapped spin-1 Bose gases consists only of atoms with $F_{\rm low}$ state.

For an ultra-cold spin-1 Bose gas, such as ^{87}Rb and ^{23}Na atoms, the ground state is composed of atoms in all Zeeman state $|F=1, m_F=+1,0,-1\rangle$ (hereafter denoted as $|+\rangle, |0\rangle, |-\rangle$) inside a far off resonant optical trap. There are two scattering channels for collisions of two $|F=1\rangle$ atoms, one of which has the total spin of the two atoms $|F_{\rm tot}=F_1-F_2=0\rangle$ and the other $|F_{\rm tot}=F_1+F_2=2\rangle$. The s-wave scattering lengthes of these two channels are denoted by a_0 and a_2, respectively. The interaction between two spin-1 atoms can thus be described by

$$V(\vec{r}_1-\vec{r}_2) \;=\; (g_0P_0+g_2P_2)\delta(\vec{r}_1-\vec{r}_2),$$

where $g_{0,2}=4\pi\hbar^2 a_{0,2}/\mathsf{m}$ and $P_{0,2}$ is the projection operator of the state of the atom pair (1 and 2) onto the total hyperfine spin state,

$$P_{F_{\rm tot}} \;=\; \sum_m |F_{\rm tot},m\rangle\langle F_{\rm tot},m|.$$

Similarly we can also project the operator $\vec{F}_1\cdot\vec{F}_2$ onto the total spin space

$$\vec{F}_1\cdot\vec{F}_2 \;=\; \sum_{F_{tot}=0,2}\frac{1}{2}\left[F_{\rm tot}(F_{\rm tot}+1)-F_1(F_1+1)-F_2(F_2+1)\right]P_{F_{\rm tot}}.$$

Substituting $F_1=F_2=1$ and $F_{\rm tot}=0$ or 2, we obtain

$$\vec{F}_1\cdot\vec{F}_2 \;=\; P_2-2P_0.$$

On the other hand we have the identity $P_0+P_2=1$. So we can express P_0 and P_2 as

$$P_0 \;=\; \frac{1}{3}\left(1-\vec{F}_1\cdot\vec{F}_2\right),$$

$$P_2 \;=\; \frac{1}{3}\left(2+\vec{F}_1\cdot\vec{F}_2\right).$$

Finally this leads to the rotationally invariant form

$$V(\vec{r}_1-\vec{r}_2) \;=\; \left(c_0+c_2\vec{F}_1\cdot\vec{F}_2\right)\delta(\vec{r}_1-\vec{r}_2),$$

where $c_0=(g_0+2g_2)/3$ and $c_2=(g_2-g_0)/3$. The interaction energy is less when the spins of the two colliding atoms align parallel to each other for $c_2<0$ and antiparallel for $c_2>0$. Thus the interaction is ferromagnetic if $c_2<0$ and antiferromagnetic if $c_2>0$.

The Hamiltonian of a spin-1 bosonic gas thus can be written down in the second quantized form as

$$\begin{aligned} H \;=\; & \int d\vec{r}\left[\Psi_i^\dagger\left(-\frac{\hbar^2}{2\mathsf{m}}\nabla^2+V_{\rm ext}(\vec{r})\right)\Psi_i+\frac{c_0}{2}\Psi_i^\dagger\Psi_j^\dagger\Psi_j\Psi_i\right. \\ & \left.+\frac{c_2}{2}\Psi_i^\dagger\Psi_k^\dagger\left(F_\alpha\right)_{ij}\left(F_\alpha\right)_{kl}\Psi_l\Psi_j\right], \end{aligned} \tag{1}$$

where $\Psi_i(\vec{r})$ $[\Psi_i^\dagger(\vec{r})]$ is the quantum field operator annihilating (creating) an atom in state $|i\rangle$ at $\vec{r}$, and $i,j,k,l=+,0,-$ and $\alpha=x,y,z$. Repeated indices are assumed to be summed. $F_{\alpha=x,y,z}$ are spin-1 matrices given by

$$F_x=\frac{1}{\sqrt{2}}\begin{pmatrix}0&1&0\\1&0&1\\0&1&0\end{pmatrix},\quad F_y=\tfrac{i}{\sqrt{2}}\begin{pmatrix}0&-1&0\\1&0&-1\\0&1&0\end{pmatrix},\quad F_z=\begin{pmatrix}1&0&0\\0&0&0\\0&0&-1\end{pmatrix}, \tag{2}$$

with the quantization axis taken along the z-axis direction.

The equation of motion for the field operators can be expressed in the Heisenberg's picture as

$$\begin{aligned} i\hbar\frac{\partial}{\partial t}\Psi_+(\vec{r},t) \;=\; & \left(-\frac{\hbar^2}{2\mathsf{m}}\nabla^2+V_{\rm ext}(\vec{r})+c_0\sum_j\left(\Psi_j^\dagger\Psi_j\right)\right)\Psi_+ \\ & +c_2\left(\Psi_+^\dagger\Psi_++\Psi_0^\dagger\Psi_0-\Psi_-^\dagger\Psi_-\right)\Psi_++c_2\Psi_-^\dagger\Psi_0\Psi_0, \\ i\hbar\frac{\partial}{\partial t}\Psi_0(\vec{r},t) \;=\; & \left(-\frac{\hbar^2}{2\mathsf{m}}\nabla^2+V_{\rm ext}(\vec{r})+c_0\sum_j\left(\Psi_j^\dagger\Psi_j\right)\right)\Psi_0 \end{aligned}$$

$$
\begin{aligned}
& +c_2\left(\Psi_+^\dagger\Psi_+ + \Psi_-^\dagger\Psi_-\right)\Psi_0 + 2c_2\Psi_0^\dagger\Psi_+\Psi_-, \\
i\hbar\frac{\partial}{\partial t}\Psi_-(\vec{r},t) &= \left(-\frac{\hbar^2}{2\mathsf{m}}\nabla^2 + V_{\rm ext}(\vec{r}) + c_0\sum_j\left(\Psi_j^\dagger\Psi_j\right)\right)\Psi_- \\
& +c_2\left(\Psi_-^\dagger\Psi_- + \Psi_0^\dagger\Psi_0 - \Psi_+^\dagger\Psi_+\right)\Psi_- + c_2\Psi_+^\dagger\Psi_0\Psi_0.
\end{aligned}
$$

Similar to the procedure for the GP equation of a scalar condensate, one obtains the coupled GP equations for a spin-1 condensate within mean field theory as follows,

$$
\begin{aligned}
i\hbar\frac{\partial}{\partial t}\Phi_+ &= \left[-\frac{\hbar^2}{2\mathsf{m}}\nabla^2 + V_{\rm ext} + c_0 n + c_2(n_+ + n_0 - n_-)\right]\Phi_+ + c_2\Phi_0^2\Phi_-^*, \\
i\hbar\frac{\partial}{\partial t}\Phi_0 &= \left[-\frac{\hbar^2}{2\mathsf{m}}\nabla^2 + V_{\rm ext} + c_0 n + c_2(n_+ + n_-)\right]\Phi_0 + 2c_2\Phi_+\Phi_-\Phi_0^*, \\
i\hbar\frac{\partial}{\partial t}\Phi_- &= \left[-\frac{\hbar^2}{2\mathsf{m}}\nabla^2 + V_{\rm ext} + c_0 n + c_2(n_- + n_0 - n_+)\right]\Phi_- + c_2\Phi_0^2\Phi_+^*,
\end{aligned}
$$

where $n_i = |\Phi_i|^2$ is the density of the ith component and $n = \sum_i n_i$ is the total density of the atomic gas.

CHAPTER III

BOSE-EINSTEIN CONDENSATION OF TRAPPED INTERACTING SPIN-1 ATOMS

3.1 Introduction

It has been known for a long time that the spin degrees of freedom of an atom become accessible if a far-off-resonant optical trap is used to provide equal confinement for all Zeeman states, instead of the more widely used magnetic traps for spin polarized atoms [50, 51, 52, 75]. Several earlier experiments have produced fascinating observations of spinor condensates, a superfluid with internal degrees of freedom, e.g., with ^{23}Na atoms in $F = 1$ [45, 46] and $F = 2$ [76] and ^{87}Rb atoms in $F = 1$ [49, 56, 77] and $F = 2$ [53, 54, 55], spin domains and interdomain tunnelling [47, 48], as well as the generation of coreless vortex states [78, 79, 80, 81]. These properties exist only because of the spinor nature of the condensate order parameter, and thus are generally not expected to occur in a magnetically trapped condensate.

Despite these and other related successes with spinor condensates, our knowledge remains limited regarding the condensation thermodynamics of spin-1 atoms. In a sense, the spin-1 condensate constitutes a type of quantum fluid unfamiliar to many of us. On the experimental side, it remains a significant challenge to produce a spinor condensate, as evidenced by the disproportionally small numbers of spinor BEC experiments in operation. In this chapter, we will revisit the topic of the condensation thermodynamics for a system of trapped spin-1 atoms. Of particular interest to us is the question of the so-called double condensations for a spin-1 system constrained by two global conservations [82]. Using the Bogoliubov-Popov approximation, Isoshima

et al. first investigated the thermodynamics of the BEC phase transition for a spin-1 gas [82]. Huang *et al.* studied analytically the effect of a magnetic field on the transition temperature [83]. While an attempt to find the zero-magnetic-field phase diagram was made through numerical simulations in Ref. [82], there still exist several question marks to the overall picture of BEC for a spin-1 Bose gas, especially for ferromagnetically interacting atoms such as ^{87}Rb. Limited by the computation procedure within the Bogoliubov-Popov approximation, only a few data points were made available in the earlier studies by Isoshima *et al.* [82].

In this chapter we will investigate systematically the phase diagram of a spin-1 Bose gas for both ferromagnetic and antiferromagnetic interactions. Instead of the Bogoliubov approach, we will adopt the Hartree-Fock-Popov approximation and employ a semiclassical approximation to the noncondensed atoms within the mean field theory. We will also enforce the thermodynamics for a finite trapped system with a fixed total atom number N and a total magnetization M. Recent studies have significantly verified the accuracy of this approximation when applied to similar systems [84]. As will be discussed in detail later our results indicate that double condensations will occur for a spin-1 gas with antiferromagnetic interactions, while triple condensations are more likely for ferromagnetic interactions [85].

We start with a review of several additional features of a BEC for an ideal gas of spin-1 atoms in a spherical harmonic trap in Sec. 2.2.2. This is followed by the formulation of an interacting spin-1 gas in Sec. 2.2.3, then a brief sketch of the Hartree-Fock-Popov theory and two fluid model used for our investigation. We outline the detailed numerical algorithm employed to solve the coupled two-fluid model for the quantum gas at different temperatures in Sec. 2.2.4 and present the results of our study in Sec. 2.2.5. We conclude with some discussions and remarks in Sec. 2.2.6.

3.2 BEC of an ideal gas of spin-1 atoms

In this section, we briefly review the phenomenon of BEC for a trapped noninteracting gas of spin-1 atoms following the pioneering study of Isoshima *et al.* [82]. At thermal equilibrium, we adopt the standard Bose-Einstein distribution, and treat the spinor degree of freedom as degenerate internal states in the absence of an external magnetic field. The average number of atoms at each single atom state of an energy ε_j for the component $|i\rangle$, is then conveniently given by

$$N_{i,j} = \frac{\mathsf{z}_i e^{-\beta\varepsilon_j}}{1 - \mathsf{z}_i e^{-\beta\varepsilon_j}}, \tag{3}$$

with $\beta = 1/(k_B T)$ at temperature T. k_B is the Boltzmann constant. The fugacity z_i can be expressed in terms of the chemical potential for the ith component μ_i as $\mathsf{z}_i = \exp(\beta\mu_i)$. In the thermodynamic limit, one can follow the usual approach by making a semiclassical approximation for a continuous description of the single particle density of states, and treating the ground state population separately as it can become macroscopic due to Bose-Einstein condensation. The total number of atoms for a given internal state in all motional excited states of the trap is thus found to be

$$N_i^T = \sum_{j=1}^{\infty} N_{i,j} = \left(\frac{k_B T}{\hbar\omega}\right)^3 g_3(\mathsf{z}_i), \tag{4}$$

where we have assumed atoms are confined in a spherical harmonic trap with a frequency ω independent of the atomic internal state $|i\rangle$. $g_\nu(x) = \sum_{n=1}^{\infty}(x^n/n^\nu)$ is the standard Bose function [86, 87, 88]. We note that the conservations of the total number of atoms $N = N_+ + N_0 + N_-$ and total magnetization $M = N_+ - N_-$ lead to the chemical potentials for different spin components expressible as $\mu_\pm = \mu \pm \eta$ and $\mu_0 = \mu$. These identities remain valid in the presence of atom-atom interactions. μ and η are effectively independent Lagrange multipliers used to guarantee the conservation of N and M, respectively. Taking the single atom trapped ground state to be zero energy, the Bose distribution (3) shows that μ_i is negative at high temperatures and

reaches zero when the spin component $|i\rangle$ condenses. η is positive (negative) for a positive M (negative), which acts as a fictitious applied magnetic field physically.

As was first pointed out in Ref. [82], there exists an interesting double condensation phenomenon for a spin-1 gas because of the presence of M conservation. When the temperature is lowered, the $|+\rangle$ component first condenses for a system with a positive M because its phase space density is largest, reflecting the fact that N_+ is the largest component population. Thus we first arrive at $\mu_+ = 0$. This consideration leads to the critical temperature T_1 governed by the following equations:

$$N = \left(\frac{k_B T_1}{\hbar\omega}\right)^3 \left[g_3(1) + g_3(e^{\beta\mu}) + g_3(e^{2\beta\mu})\right], \tag{5}$$

$$M = \left(\frac{k_B T_1}{\hbar\omega}\right)^3 \left[g_3(1) - g_3(e^{2\beta\mu})\right]. \tag{6}$$

On further lowering of the temperature, however, the remaining two components $|0\rangle$ and $|-\rangle$ condense simultaneously, rather than sequentially with the less populated component of the two condensing last. This is precisely due to the conservation identities as discussed before. The relationships $\mu_\pm = \mu \pm \eta$ and $\mu_0 = \mu$ lead to a mathematical certainty: when μ_+ is zero, if either μ_0 or μ_- becomes zero, both must be zero. At this second critical temperature T_2, both $\mu_0 = 0$ and $\mu_- = 0$, which imply that the $|0\rangle$ and $|-\rangle$ components condense simultaneously. This second condensation where all three components condense, occurs at the temperature T_2 of

$$T_2 = \frac{\hbar\omega}{k_B}\left[\frac{N-M}{3g_3(1)}\right]^{1/3}. \tag{7}$$

In Fig. 1, we illustrate the M dependence of the double condensations for an ideal Bose gas of spin-1 atoms. $T_c = [N/g_3(1)]^{1/3}(\hbar\omega/k_B) \approx 0.94N^{1/3}\hbar\omega/k_B$ is the condensation temperature for $M = N$, i.e., for a single component gas with all atoms polarized in state $|+\rangle$.

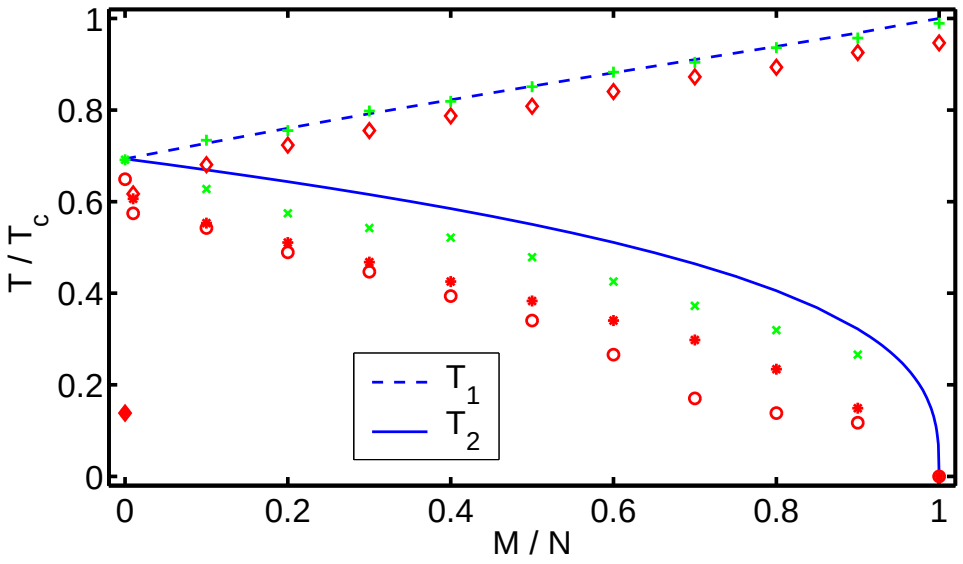

Figure 1: BEC for a gas of spin-1 atoms with $M > 0$ ($M < 0$). For noninteracting atoms, the $|+\rangle$ ($|-\rangle$) component condenses first at T_1 (dashed line) while the $|0\rangle$ and $|-\rangle$ ($|+\rangle$) components condense simultaneously at T_2 (solid line). For ^{23}Na atoms with antiferromagnetic interactions, double condensations persist according to our theoretical study. The $|+\rangle$ component (denoted by $+$) condenses first, which is then followed by the condensation of the $|-\rangle$ component (denoted by $\times$). The $|0\rangle$ component is unpopulated in the low temperature limit. For ^{87}Rb atoms with ferromagnetic interactions, our study reveals the potential for triple condensations. First, the $|+\rangle$ component condenses (denoted by $\diamond$), which is then followed by the second condensation for the $|-\rangle$ component (denoted by $*$), and finally the third condensation for the $|0\rangle$ component occurs (denoted by $\circ$).

3.3 BEC of an interacting gas of spin-1 atoms

3.3.1 Formulation

Our model system of the interacting spin-1 atoms is described by a Hamiltonian in second quantized form [50, 51, 52] in Eq. (1). It is easy to check that both the total number of atoms and the total magnetization

$$\begin{aligned} N &= \int d\vec{r}(|\Psi_+|^2 + |\Psi_0|^2 + |\Psi_-|^2), \\ M &= \int d\vec{r}(|\Psi_+|^2 - |\Psi_-|^2) = \int d\vec{r}\Psi_i^\dagger (F_z)_{ij}\Psi_j, \end{aligned}$$

commute with the Hamiltonian [Eq. (1)], and are thus constants of motion. To study the minimal energy ground state, we therefore introduce two Lagrange multipliers μ and η, to fix the total atom number and magnetization of the system in our numerical minimization. It turns out that μ is in fact the chemical potential of the system and η is an effective magnetic field. The Gibbs free energy is then given by

$$\begin{aligned} G &= H - \mu N - \eta M \\ &= \int d\vec{r}\Big\{\Psi_i^\dagger(\mathcal{L}_{ij} - \eta(F_z)_{ij})\Psi_j + \frac{c_0}{2}\Psi_i^\dagger\Psi_j^\dagger\Psi_j\Psi_i \\ &\quad + \frac{c_2}{2}\Psi_i^\dagger\,(F_\alpha)_{ij}\,\Psi_j\Psi_k^\dagger\,(F_\alpha)_{kl}\,\Psi_l\Big\}, \end{aligned} \tag{8}$$

where

$$\mathcal{L}_{ij} = \left[-\frac{\hbar^2}{2\mathsf{m}}\nabla^2 - \mu + V_{\rm ext}(\vec{r})\right]\delta_{ij}. \tag{9}$$

The atomic interactions are conveniently parametrized in explicit form through the two s-wave scattering lengths a_0 and a_2 between two spin-1 atoms [50, 51, 52]

$$c_0 = \frac{4\pi\hbar^2}{\mathsf{m}}\left(\frac{a_0 + 2a_2}{3}\right), \qquad c_2 = \frac{4\pi\hbar^2}{\mathsf{m}}\left(\frac{a_2 - a_0}{3}\right). \tag{10}$$

In this chapter, we attempt to find the mean field ground state of our spin-1 Bose gas system, which corresponds to the state with the lowest Gibbs free energy.

3.3.2 Hartree-Fock-Popov theory and the two-fluid model

The field operator $\Psi(\vec{r},t)$ evolves in the Heisenberg picture according to

$$i\hbar\frac{\partial}{\partial t}\Psi(\vec{r},t) \;=\; [\Psi,G]\,.$$

For the system of a spin-1 Bose gas as considered here, the above equation becomes

$$\begin{aligned}
i\hbar\frac{\partial}{\partial t}\Psi_+(\vec{r},t) &= \mathcal{L}_{++}\Psi_+ - \eta\Psi_+ + c_0\sum_j\left(\Psi_j^\dagger\Psi_j\right)\Psi_+ + c_2\left(\Psi_+^\dagger\Psi_+ + \Psi_0^\dagger\Psi_0 - \Psi_-^\dagger\Psi_-\right)\Psi_+ \\
&\quad + c_2\Psi_-^\dagger\Psi_0\Psi_0, \\
i\hbar\frac{\partial}{\partial t}\Psi_0(\vec{r},t) &= \mathcal{L}_{00}\Psi_0 + c_0\sum_j\left(\Psi_j^\dagger\Psi_j\right)\Psi_0 + c_2\left[\left(\Psi_+^\dagger\Psi_+ + \Psi_-^\dagger\Psi_-\right)\Psi_0 + 2\Psi_0^\dagger\Psi_+\Psi_-\right], \\
i\hbar\frac{\partial}{\partial t}\Psi_-(\vec{r},t) &= \mathcal{L}_{--}\Psi_- + \eta\Psi_- + c_0\sum_j\left(\Psi_j^\dagger\Psi_j\right)\Psi_- + c_2\left(\Psi_-^\dagger\Psi_- + \Psi_0^\dagger\Psi_0 - \Psi_+^\dagger\Psi_+\right)\Psi_- \\
&\quad + c_2\Psi_+^\dagger\Psi_0\Psi_0. \qquad (11)
\end{aligned}$$

Following the standard mean field theory procedure, i.e. taking $\Psi = \Phi + \delta\Psi$ with $\Phi = \langle\Psi\rangle$ denoting the condensate, after some tedious manipulations and calculations, we obtain a set of coupled Gross-Pitaevskii equations for the condensed components including their interactions with the noncondensed atoms as

$$\begin{aligned}
i\hbar\frac{\partial}{\partial t}\Phi_+ &= \left[-\frac{\hbar^2}{2\mathsf{m}}\nabla^2 + V_{\rm ext} - \mu - \eta + c_0(n+n_+^T) + c_2(n_+ + n_0 - n_- + n_+^T)\right]\Phi_+ \\
&\quad + c_2\Phi_0^2\Phi_-^*, \\
i\hbar\frac{\partial}{\partial t}\Phi_0 &= \left[-\frac{\hbar^2}{2\mathsf{m}}\nabla^2 + V_{\rm ext} - \mu + c_0(n+n_0^T) + c_2(n_+ + n_-)\right]\Phi_0 + 2c_2\Phi_+\Phi_-\Phi_0^*, \\
i\hbar\frac{\partial}{\partial t}\Phi_- &= \left[-\frac{\hbar^2}{2\mathsf{m}}\nabla^2 + V_{\rm ext} - \mu + \eta + c_0(n+n_-^T) + c_2(n_- + n_0 - n_+ + n_-^T)\right]\Phi_- \\
&\quad + c_2\Phi_0^2\Phi_+^*, \qquad (12)
\end{aligned}$$

and equations for the noncondensed parts $\delta\Psi_i$,

$$\begin{aligned}
i\hbar\frac{\partial}{\partial t}\delta\Psi_+(\vec{r},t) &= \left[-\frac{\hbar^2}{2\mathsf{m}}\nabla^2 + V_{\rm ext} - \mu - \eta + c_0(n+n_+) + c_2(2n_+ + n_0 - n_-)\right]\delta\Psi_+, \\
i\hbar\frac{\partial}{\partial t}\delta\Psi_0(\vec{r},t) &= \left[-\frac{\hbar^2}{2\mathsf{m}}\nabla^2 + V_{\rm ext} - \mu + c_0(n+n_0) + c_2(n_+ + n_-)\right]\delta\Psi_0, \qquad (13) \\
i\hbar\frac{\partial}{\partial t}\delta\Psi_-(\vec{r},t) &= \left[-\frac{\hbar^2}{2\mathsf{m}}\nabla^2 + V_{\rm ext} - \mu + \eta + c_0(n+n_-) + c_2(2n_- + n_0 - n_+)\right]\delta\Psi_-,
\end{aligned}$$

where $n = \sum_i n_i = \sum_i (|\Phi_i|^2 + n_i^T)$ is the total density of the atomic gas, with $n_i^T = \langle \delta\Psi_i^\dagger \delta\Psi_i \rangle$ the normal (noncondensed) gas density of the ith component. Instead of the Hartree-Fock-Bogoliubov (HFB) approximation as employed by Isoshima *et al.* [82], we use the Hartree-Fock-Popov (HFP) approximation to obtain the above equations. Within the HFP approximation, we neglect terms proportional to the anomalous noncondensate density $\langle \delta\Psi_i \delta\Psi_j \rangle$ as well as their complex conjugates. We also neglect cross component noncondensate terms proportional to $\langle \delta\Psi_i^\dagger \delta\Psi_j \rangle$ for $i \neq j$, similar to the random phase approximation. A more detailed formal discussion of the HFP theory can be found in Refs. [89, 90, 91, 92], and for the calculation of the phase diagram of Bose-Einstein condensation, it is an excellent approximation as confirmed recently in a set of detailed comparisons with experiments [84]. In addition, as will become clear later, the HFP approximation is also efficient from the numerical point of view, especially near regions of temperatures close to (but below) the critical temperature. The HFB approximation, on the other hand, is more difficult to handle numerically [82]. Although more rigorous at very low temperatures, the HFB approximation is expected to agree with the more transparent HFP approximation at higher temperatures. In deriving the equations for $\delta\Psi_i$, terms proportional to $\delta\Psi_i^\dagger$, $\delta\Psi_j$, and $\delta\Psi_j^\dagger$ for $j \neq i$ are also neglected. This is equivalent to the neglect of the "hole" component in the HFB approximation, and is thus expected to have a minor effect except that the temperature is very close to zero.

In the HFP approximation we adopt here, the normal fluid for noncondensed atoms is determined through the semi-classical approximation. We thus take $-i\hbar\nabla \to \vec{p}$, and approximate its distribution by the standard Bose-Einstein distribution in the phase space of $\{\vec{p}, \vec{r}\}$,

$$n_i^T(\vec{r}) = \int \frac{d\vec{p}}{(2\pi\hbar)^3} \frac{1}{e^{\varepsilon_i(\vec{p},\vec{r})/k_B T} - 1}, \tag{14}$$

with the HFP single particle energy spectrum,

$$\begin{aligned}
\varepsilon_+(\vec{p},\vec{r}) &= \frac{p^2}{2\mathsf{m}} + V_{\rm ext} - \mu - \eta + c_0(n+n_+) \\
&\quad + c_2\left(2n_+ + n_0 - n_-\right), \\
\varepsilon_0(\vec{p},\vec{r}) &= \frac{p^2}{2\mathsf{m}} + V_{\rm ext} - \mu + c_0(n+n_0) + c_2\left(n_+ + n_-\right), \\
\varepsilon_-(\vec{p},\vec{r}) &= \frac{p^2}{2\mathsf{m}} + V_{\rm ext} - \mu + \eta + c_0(n+n_-) \\
&\quad + c_2\left(2n_- + n_0 - n_+\right),
\end{aligned} \tag{15}$$

which are obtained by substituting $\delta\Psi_i(\vec{r},t) = \exp[-i\varepsilon_i(\vec{p},\vec{r})t/\hbar]u_i(\vec{r})$ into Eqs. (13) with $u_i(\vec{r})$ the eigenfunction for the excitation of the ith component. In the numerical implementation we use $[\mu - (3/2)]$ instead of μ in order to avoid negative levels at the points of both small $V_{\rm ext}$ and small p for an ideal gas. This modification also avoids the divergence of n_i^T near the edge of the condensate. This is precisely the correction of the zero-point energy between the semi-classical description and the quantum description.

Thus, we have formulated a coupled set of equations for both the condensate and the normal components; they are Eq. (12) for the condensed part and Eqs. (14) and (15) for the noncondensed atoms. These are the basis for our numerical investigations to be presented below.

3.4 Numerical method

In the numerical studies, we have developed the following algorithm self-consistently solving the coupled equations (12), (14), and (15), as an extension to the single component gas studied earlier [89]. Our algorithm is divided into the following steps:

- We find the condensate wave function $\Phi_i(\vec{r})$ and the chemical potential μ for a set of fixed normal gas density $n_i^T(\vec{r})$, by propagating Eqs. (12) in the imaginary time domain, as described in Refs. [93, 94].

- We compute the updated energy spectrum and normal gas density $n_i^T(\vec{r})$ from Eqs. (14) and (15) using the new condensate wave function and the chemical potential.

- We normalize the total number of atoms to N and adjust η accordingly [93].

- We repeat the above steps until convergence is reached. The convergence criterion is set to be that the condensate fraction $N^C(T)/N$ and the magnetization fraction M/N of successive iterations differ by less than 10^{-11} for most temperatures and less than 10^{-5} near the temperature region of phase transition.

At temperatures higher than the first BEC transition point, the above procedure converges rather quickly as the condensed component Φ_i is no more exists. In this case, we only need to solve Eqs. (14) and (15) self-consistently by adjusting μ and η.

3.5 Results and discussions

In this chapter, we focus on the illustration of our results for atoms inside a spherically symmetric harmonic trap

$$V_{\rm ext}(\vec{r}) = \frac{1}{2}\mathsf{m}\omega^2 r^2. \tag{16}$$

We take $N = 10^6$ and $\omega = (2\pi)100$ Hz, and use the spin-1 atom parameters for ^{23}Na and ^{87}Rb atoms as given in Table 1. As is shown, it is antiferromagnetic ($c_2 > 0$) for ^{23}Na atoms and ferromagnetic ($c_2 < 0$) for ^{87}Rb atoms.

Table 1: Atomic parameters for ^{23}Na and ^{87}Rb atoms [95, 96]. a_0 and a_2 are in units of Bohr radius and c_0 and c_2 in units of $(2\pi)10^{-12}$ Hz cm^3.

	a_0	a_2	c_0	c_2
^{23}Na	50.0	55.0	15.587	0.4871
^{87}Rb	101.8	100.4	7.793	-0.0361

3.5.1 Atoms with antiferromagnetic interactions (^{23}Na)

The interaction between ^{23}Na atoms is antiferromagnetic, i.e. $c_2 > 0$. The corresponding phase diagram we obtain is shown in Fig. 2. It clearly reveals the double phase transitions: one for the $|+\rangle$ component and the other for the $|-\rangle$ component. The $|0\rangle$ component of the condensate never shows up because the antiferromagnetic interaction favors an antiparallel alignment of the atomic spin, which is equivalent to a coherent superposition of the $|+\rangle$ and $|-\rangle$ states as explained in the discussion of order parameter symmetry at zero temperature in Ref. [50]. Our mean field result is also consistent with that of Isoshima *et al.* [82]. Similar to the case of an ideal gas, the transition temperature of the $|+\rangle$ component increases monotonically with M/N while that of the $|-\rangle$ component monotonically decreases. When the temperature decreases, the first condensed component is $|+\rangle$ because $M > 0$; the second condensed component is $|-\rangle$, which condenses at temperatures when $N_+^C + N_+^T - N_-^T > M$. Figure 3 shows typical density distributions of different components for a ^{23}Na gas. We see that $|\Phi_+|^2$ and $|\Phi_-|^2$ are always miscible [45, 97] and distributed mostly near the central region of the trap. We also note that $|\Phi_0|^2$ is always zero within this mean field study. All three components of the normal gas coexist. Both n_+^T and n_-^T peak at the edge of the condensate because of the shape of the net interaction potentials between the condensate and the normal gas. n_0^T is much flatter since $|\Phi_0|^2$ is zero.

We now comment on a particular feature related to the asymptotic behavior of the spin-1 gas of ^{23}Na atoms as $T \to 0$ for $M = 0$. The full quantum theory predicts a ground as a superfragmented Fock state with atoms equally distributed among the three spin components $|N_+ = N/3, N_0 = N/3, N_- = N/3\rangle$ [50, 52, 61, 62]. Such a state would give rise to a number fluctuation of order of N^2, and is impossible within the present mean field treatment. The mean field ground state is known to be $|N_+ = N/2, N_0 = 0, N_- = N/2\rangle$ [61, 98], consistent with our results. In an actual experiment, it is most likely that the mean field ground state is observed because

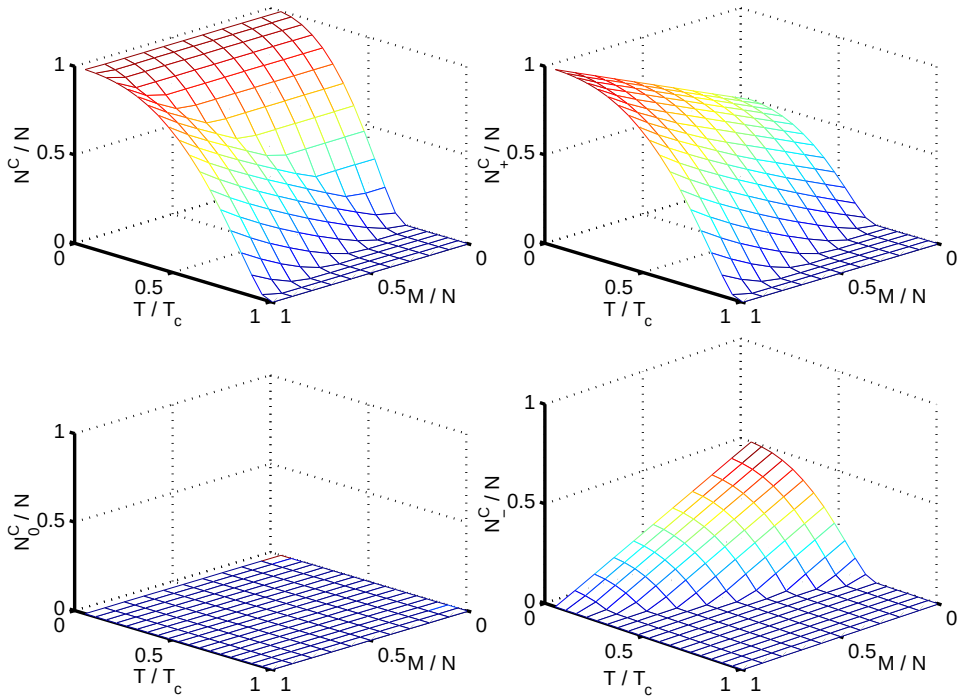

Figure 2: (Color) Double condensations for a spin-1 gas of ^{23}Na atoms. The upper left panel shows the total condensed fraction vs temperature and total magnetization. Similarly, the upper right one shows the fraction of condensed $|+\rangle$ component, the lower left the condensed $|0\rangle$ component, and the lower right the condensed $|-\rangle$ component.

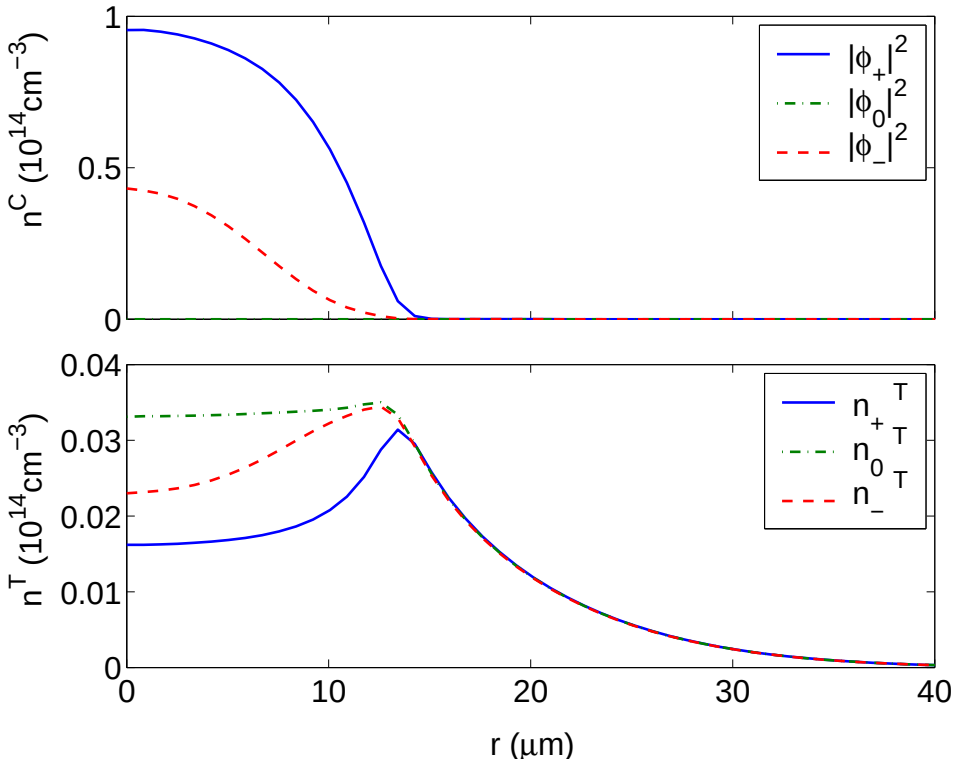

Figure 3: Typical density distributions for different spin components of a ^{23}Na gas ($T/T_c = 0.43, M/N = 0.4$). The upper panel is for the condensate and the lower one for the noncondensed atoms.

the full quantum state is not stable against various external sources of fluctuation or noises, e.g. that of the unshielded magnetic field [62], a small deviation of the total magnetization M from zero [61], or a temperature being not exactly zero. The mean field ground state, on the other hand, is more robust against these noise. In our numerical calculations, it is really impractical to set the temperature microscopically close to but above zero to probe the real ground state (for $M = 0$). We therefore enforced the ground state structure such that it asymptotically approaches that of the mean field ground state with a decrease of the temperature as shown in Fig. 2. With this convention, a related issue arises: the equivalence between states $|N_+ = N/2, N_0 = 0, N_- = N/2\rangle$ and $|N_+ = 0, N_0 = N, N_- = 0\rangle$ at zero temperature as first pointed out by Ho [50]. We note, however, that this equivalence is based on the assumption of an environment perfectly free of magnetic fields. The presence of even a tiny magnetic field, which is inevitable in the real world, would destroy this equivalence and cause the real ground state to be $|N_+ = N/2, N_0 = 0, N_- = N/2\rangle$, a convention we chose as indicated in Fig. 2.

3.5.2 Atoms with ferromagnetic interactions (^{87}Rb)

The phase diagrams for ^{87}Rb atoms with ferromagnetic interactions ($c_2 < 0$) are shown in Figs. 4 and 5. Only a sparse set of points was made available in the early work of Isoshima *et al.* [82] because the numerical solution becomes far more difficult to converge in this case. Based on our results, we see that when the temperature of the system decreases, triple condensations occur in general. When $M > 0$, the first condensed component is the $|+\rangle$ state (for $T < T_1$), the second one is the $|-\rangle$ state (for $T < T_2$), and the last one is the $|0\rangle$ state (for $T < T_3$). Our results show that the $|+\rangle$ component first condenses at T_1 and its population increases with decreasing temperature until T_2, at which the $|+\rangle$ condensed component is a little more than the total magnetization M. When temperature is lower than T_2, the $|-\rangle$ component

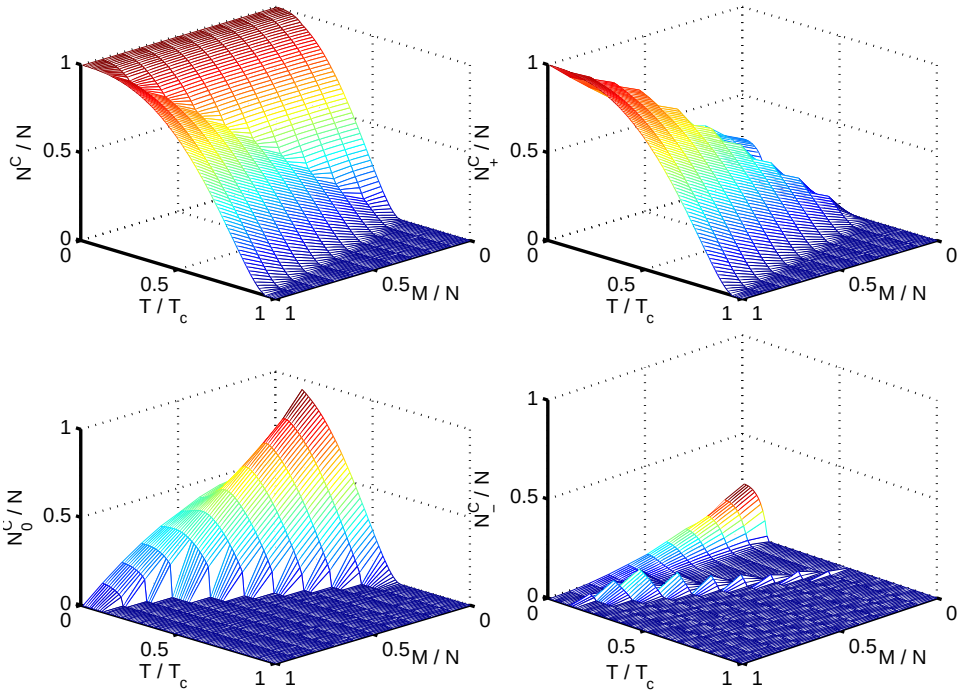

Figure 4: (Color) The same as in Fig. 2 but for a gas of ^{87}Rb atoms.

begins to condense as well. The two condensed components in states $|+\rangle$ and $|-\rangle$ both increase with decreasing temperature until the third critical temperature T_3, at which the $|0\rangle$ component starts to condense. Once the $|0\rangle$ component condenses, the $|-\rangle$ component starts to decrease and becomes very close to zero, while the $|+\rangle$ component is almost constant with respect to further decreasing of the temperature. This trend continues until the temperature is lower than T_4, when the condensed $|0\rangle$ component starts to decrease with decreasing temperature while the populations of the $|+\rangle$ and $|-\rangle$ condensed components increase. For the special case of $M = 0$, on the other hand, we observe only double condensations; the $|0\rangle$ component condenses first, followed by the simultaneous condensation of both the $|+\rangle$ and $|-\rangle$ components. This is again due to the special symmetry requirement that the $|+\rangle$ component be the same as the $|-\rangle$ component in order to keep $M = 0$. We note that in this case the fraction of condensed $|0\rangle$ component can reach as high as 94% at finite temperatures, much higher than the $\sim 50\%$ at zero temperature.

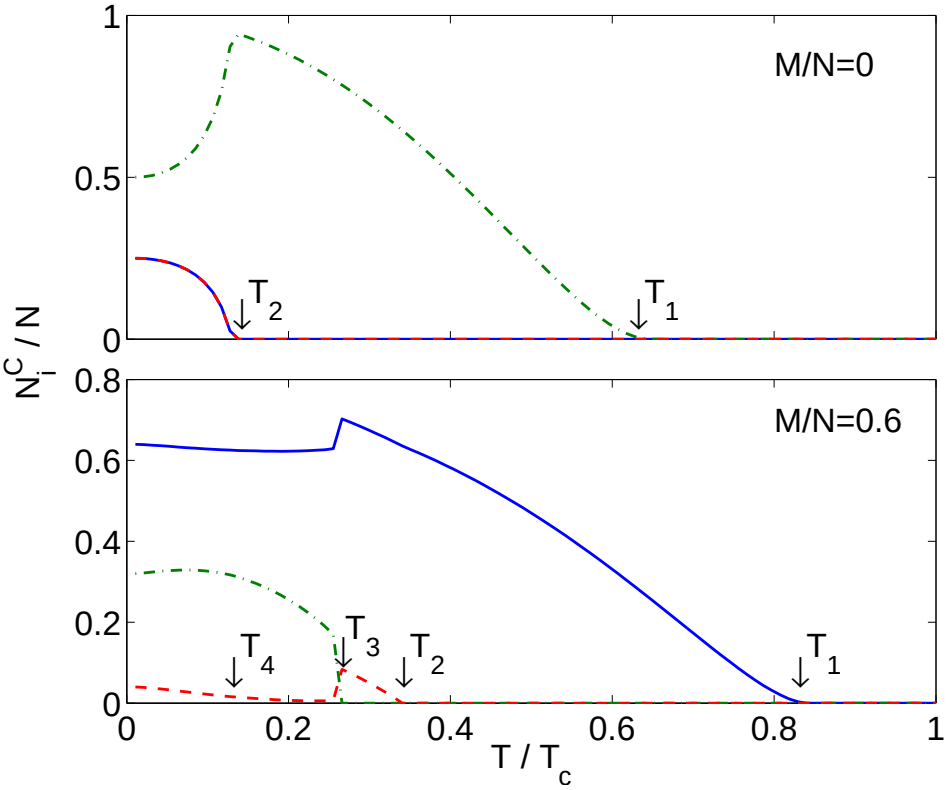

Figure 5: Double condensations for ^{87}Rb atoms when $M = 0$ (the upper panel) and triple condensations for $M/N = 0.6$ (the lower panel). The solid line denotes the fractional population of the condensed $|+\rangle$ component, the dot-dashed line denotes the $|0\rangle$ component, and the dashed line denotes the $|-\rangle$ component.

Figure 6 displays typical density distributions for a gas of ^{87}Rb atoms at different temperatures for $M/N = 0.6$. The right column corresponds to $T \in (T_3, T_2]$, where only the $|+\rangle$ and $|-\rangle$ components are condensed and the $|-\rangle$ component is quite small and is spatially located at the edge of the $|+\rangle$ component. Quite generally, we note that with the condensation of a component, its corresponding normal gas component would have a lower density. For instance, the normal gas density of the $|+\rangle$ component is low in the trap center where the $|+\rangle$ condensed component resides. The middle column of Fig. 6 is the typical density distribution when $T \in (T_4, T_3]$. The condensed $|+\rangle$ component stays at the center and is surrounded by the $|0\rangle$ component. The condensed $|-\rangle$ component is too small to be visible directly, but can be perceived from the shallow well in its normal gas component, which indicates that the condensed $|-\rangle$ component is not zero and is located around the edge of the condensed $|+\rangle$ component. The left column of Fig. 6 shows the density distributions when $T \in (0, T_4]$, where all three condensed components coexist near the center of the trap and are surrounded by their normal gas components.

These results for ^{87}Rb atoms can be understood in terms of the interplay of three factors: the ferromagnetic atom-atom interaction ($c_2 < 0$), the M conservation, and the miscibility between and among different components. The ferromagnetic interaction favors the most populated state, the M conservation sets an upper limit on the fraction of the condensed $|+\rangle$ component, and the immiscibility between the condensed $|+\rangle$ and $|-\rangle$ component sets an upper limit on the total fraction of the condensed $|+\rangle$ and $|-\rangle$ components. For instance, in the region $T \in (T_2, T_1]$, only the $|+\rangle$ component condenses. The ferromagnetic interaction plays a dominant role and thus more atoms condense into the $|+\rangle$ state with decreasing temperature. In the region of $T \in (T_3, T_2]$, the M conservation and the immiscibility begin to take their effect. The M conservation causes the increases to the condensed $|+\rangle$ and $|-\rangle$ components to be almost identical, while the immiscibility makes the condensed $|-\rangle$

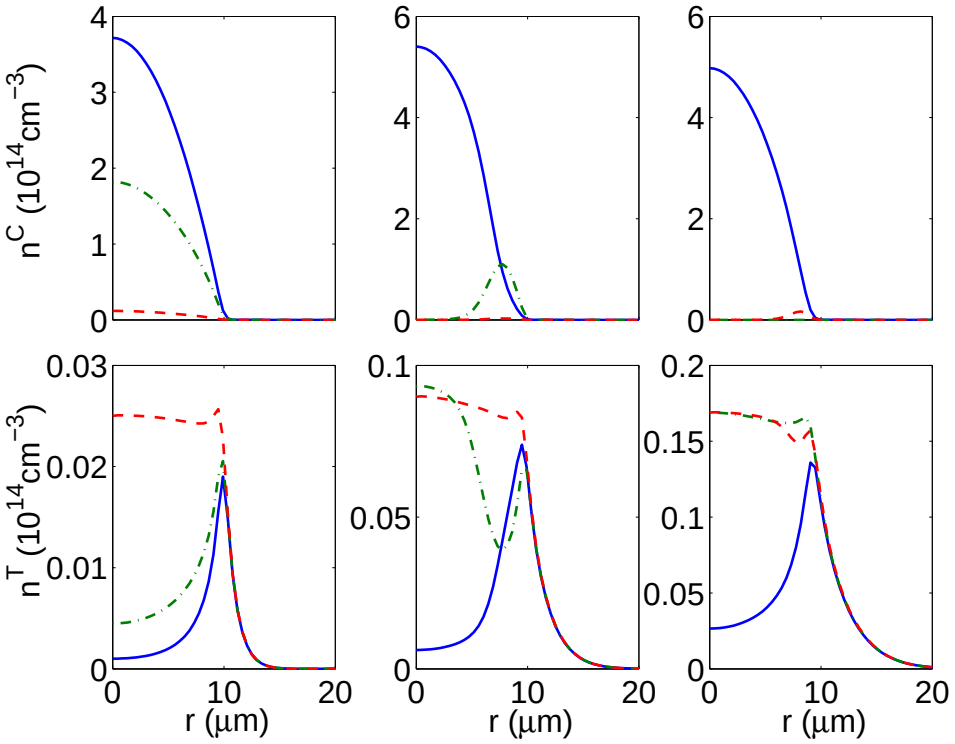

Figure 6: Typical density distributions for a gas of ^{87}Rb atoms at $M/N = 0.6$. The left column is $T/T_c = 0.11$, the middle one is 0.21, and the right one 0.32. The notations are the same as in Fig. 3.

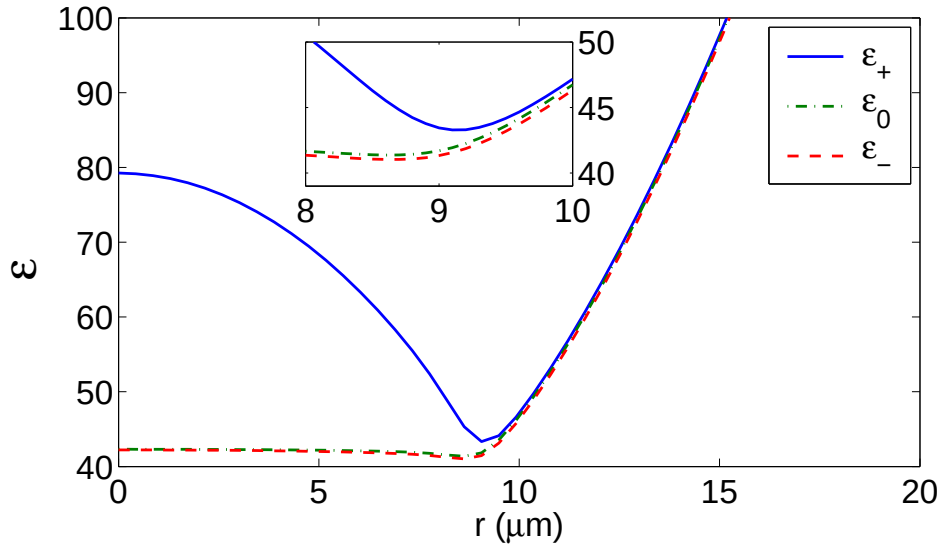

Figure 7: The lowest excitation level for a gas of ^{87}Rb atoms at $M/N = 0.6$, $T/T_c = 0.34$ (right before the condensation of the $|-\rangle$ component). The inset shows the details of a zoomed-in plot near the minimum.

component stay outside the condensed $|+\rangle$ component. The system becomes unstable with the increase of the $|+\rangle$ and $|-\rangle$ components because with more condensed $|+\rangle$ component, the condensed $|-\rangle$ component must be pushed out further. Near the third critical temperature T_3, the condensed $|-\rangle$ component suddenly decreases to almost zero and the condensed $|+\rangle$ component decreases to about M. Approximately, the total decreased amount from the $|+\rangle$ and the $|-\rangle$ components becomes the condensed $|0\rangle$ component. The system enters the region $T \in (T_4, T_3]$ in which the condensed $|0\rangle$ component increases steadily with lowering temperature because the condensed $|+\rangle$ and $|0\rangle$ components are miscible. The condensed $|+\rangle$ component is almost independent of the temperature because of the M conservation. With decreasing temperatures, more and more condensed $|0\rangle$ component finally suppresses the immiscibility between $|+\rangle$ and $|-\rangle$ component at T_4. All three condensed components become miscible, and both the $|+\rangle$ and $|-\rangle$ components increase to keep M conserved while the $|0\rangle$ component decreases.

Figure 7 shows the lowest excitation energy $\varepsilon = \varepsilon(p = 0)$ for the three components

of a ^{87}Rb gas at $M/N = 0.6$, $T/T_c = 0.34$ (right before the condensation of the $|-\rangle$ component). We see that the energy for the $|-\rangle$ component is lower than the corresponding ones for the other two states and takes a minimum near the spatial location of $r = 9$ μm, which is at the edge of the condensed $|+\rangle$ component. This result confirms that the $|-\rangle$ component condenses before the $|0\rangle$ component and surrounds the condensed $|+\rangle$ component.

3.6 Conclusions

We have studied the thermodynamics of Bose-Einstein condensation for a gas of spin-1 atoms with ferromagnetic and antiferromagnetic interactions using the mean field Hartree-Fock-Popov theory and the semiclassical approximation for the noncondensed components. Our results show that for antiferromagnetic interactions, double phase transitions persist as in a noninteracting gas: when $M > 0$, first the $|+\rangle$ component condenses, which is followed by the condensation of the $|-\rangle$ component on further decreasing of the temperature. The $|0\rangle$ component never condenses. For ferromagnetic interactions, on the other hand, our calculations reveal that the phase diagram becomes more complicated and a triple condensation scenario arises with decreasing temperatures: first the $|+\rangle$ component condenses, which is followed by the second condensation of the $|-\rangle$ component, and the third one for the $|0\rangle$ component. When the $|+\rangle$ and $|-\rangle$ components are the only condensed ones, they are immiscible. When all three components condense and the temperature is lower than T_4, they become miscible because of the presence of a large condensed $|0\rangle$ component. We have compared the numerically computed transition temperatures with that of an ideal gas as in Fig. 1. An overall lowering of the various transition temperatures due to atom-atom interactions is seen, consistent with the case of a single component interacting Bose gas, where the interaction-induced shift to the transition temperature has been

actively studied [99]. Quite generally a repulsive interaction tends to lower the transition temperature for a single component Bose gas [89]. In the case of a spin-1 Bose gas considered here, $c_0 > 0$ and $c_0 \gg |c_2|$ constitutes an overall repulsive interaction.

Finally, we note there also exists the possibility of a ferromagnetic phase transition for ^{87}Rb atoms, in addition to the Bose-Einstein condensation as studied here. In fact, as was investigated recently by Gu and Klemm [100], the ferromagnetic transition is generally predicted to occur before, i.e. at temperatures higher than, the Bose Einstein condensation. The present study, however, remains unchanged because we treated the system within the global constraint of the conservation of total magnetization, distinct from that required for a separate ferromagnetic phase transition [100]. As is evidenced from recent experiments, the total magnetization M is well conserved, even better than the conservation of the total number N [53, 77].

CHAPTER IV

MEAN FIELD GROUND STATE OF A SPIN-1 CONDENSATE IN A MAGNETIC FIELD

4.1 Introduction

Atomic Bose-Einstein condensates have provided a successful testing ground for theoretical studies of quantum many-body systems [7]. In most earlier Bose-Einstein condensation experiments, atoms were spatially confined with magnetic traps, which essentially freeze the atomic internal degrees of freedom [3, 4, 5]. Most studies were thus focused on scalar models, i.e. single-component quantum degenerate gases [101]. For such single-component systems, magnetic fields have no role to play except for being used to adjust the s-wave scattering length through Feshbach resonance. The emergence of spin-1 condensates [45, 46, 49, 53, 54, 55, 56] (of atoms with hyperfine quantum number $F = 1$) and spin-2 condensates ($F = 2$) [53, 54, 55] have created opportunities for understanding degenerate gases with internal degrees of freedom [50, 51, 52, 93, 102, 103].

In this chapter, we investigate the mean field ground state structures of a spin-1 atomic condensate in the presence of external magnetic fields (B) [94]. We focus on several aspects of the ground state properties strongly constrained by the requirement that elastic atom-atom collisions conserve both the total number of atoms (N) and the magnetization (M). Several earlier studies have focused on the global ground state structures when the conservation of M was ignored, or in the limiting case of a vanishingly small magnetic field ($B = 0$) [45, 50, 51, 52, 93, 102, 103]. As we show in this study, in the presence of a nonzero magnetic field, the conservation of M leads to ground state population distributions significantly different from those of the global

ground state.

The spin-1 Bose condensate in a magnetic field is described by the Hamiltonian (repeated indices are summed) [50, 51]

$$\begin{aligned} H &= \int d\vec{r}\,\Psi_i^\dagger(\mathcal{L}_{ij}+H_{ZM})\Psi_j + \frac{c_0}{2}\int d\vec{r}\Psi_i^\dagger\Psi_j^\dagger\Psi_j\Psi_i \\ &\quad +\frac{c_2}{2}\int d\vec{r}\Psi_k^\dagger\Psi_i^\dagger\left(F_\alpha\right)_{ij}\left(F_\alpha\right)_{kl}\Psi_j\Psi_l, \end{aligned} \tag{17}$$

where $\Psi_j(\vec{r})$ is the field operator that annihilates an atom in the j-th ($j=+,0,-$) internal state ($|F=1,m_F=+,0,-\rangle$) at location $\vec{r}$, $\mathcal{L}_{ij}=\left[-(\hbar^2\nabla^2/2\mathsf{m})+V_{\rm ext}(\vec{r})\right]\delta_{ij}$, and $V_{\rm ext}(\vec{r})$ an internal state independent trap potential. Terms with coefficients c_0 and c_2 of Eq. (17) describe elastic collisions of the spin-1 atom, where c_0 and c_2 are defined by Eq. (10) in terms of the scattering length a_0 (a_2) for two spin-1 atoms in the combined symmetric channels of total spin 0 (2). $F_{\alpha=x,y,z}$ are spin-1 matrices given by Eq. (2).

The external magnetic field B is taken to be along the quantization axis ($\hat{z}$). It induces a Zeeman shift on each atom expressible as

$$H_{ZM}(B)=\begin{pmatrix} E_+ & 0 & 0 \\ 0 & E_0 & 0 \\ 0 & 0 & E_- \end{pmatrix}.$$

According to the Breit-Rabi formula [104], the individual level shift can be expressed as

$$\begin{aligned} E_+ &= -\frac{E_{\rm HFS}}{8}-g_I\mu_I B-\frac{1}{2}E_{\rm HFS}\sqrt{1+y+y^2}, \\ E_0 &= -\frac{E_{\rm HFS}}{8}-\frac{1}{2}E_{\rm HFS}\sqrt{1+y^2}, \\ E_- &= -\frac{E_{\rm HFS}}{8}+g_I\mu_I B-\frac{1}{2}E_{\rm HFS}\sqrt{1-y+y^2}, \end{aligned} \tag{18}$$

where $E_{\rm HFS}$ is the hyperfine splitting [104], and g_I is the Lande g-factor for the atomic nuclei with nuclear spin $\vec{I}$. μ_I is the nuclear magneton and $y=(g_I\mu_I B+g_J\mu_B B)/E_{\rm HFS}$ with g_J the Lande g-factor for the valence electron with total angular momentum $\vec{J}$. μ_B is the Bohr magneton.

4.2 Mean field approximation

As in Chapter 2.2, at near zero temperatures and when the total number of condensed atoms is large, the ground state is essentially determined by the mean field term $\Phi_i = \langle \Psi_i \rangle$. Neglecting all quantum fluctuations we arrive at the mean field energy functional from Eq. (17) [52, 97]

$$H[\{\Phi_i\}] = H_S + E_0 N + \frac{c_2}{2}\langle \vec{F} \rangle^2 - \eta_0 \langle F_z \rangle + \delta \langle F_z^2 \rangle, \tag{19}$$

where the symmetric part

$$H_S = \int d\vec{r} \left[\Phi_i^* \mathcal{L}_{ij} \Phi_j + \frac{c_0}{2} \Phi_i^* \Phi_j^* \Phi_j \Phi_i \right], \tag{20}$$

is invariant under the exchange of spin component indices, thus is independent of the external B field. The Zeeman shift as given by the Breit-Rabi formula (18) can be conveniently parametrized by [97]

$$\begin{aligned} \eta_0 &= \frac{E_- - E_+}{2}, \\ \delta &= \frac{E_+ + E_- - 2E_0}{2}, \end{aligned} \tag{21}$$

which measure approximately the linear and quadratic Zeeman effects. The B-field dependence of η_0 and δ for a ^{87}Rb atom are displayed in Fig. 8. For current available experiments on ^{87}Rb and ^{23}Na atom gases, the magnetic field ranges from 1 mG to around 1 G. In this region, the linear Zeeman effect, η_0, is always 3-6 orders of magnitude larger than the quadratic Zeeman effect, δ. But we shall show later that the quadratic Zeeman effect plays a more important role despite of being smaller. The linear Zeeman effect is actually nulled by the conservation of the total magnetization M.

The elastic atomic collisions as described by the c_0 and c_2 parts of the Hamiltonian (17) conserve both N and M, which in the mean field approximation are given by

$$N = \sum_{j=\pm,0} \int d\vec{r} \, \langle \Psi_j^\dagger(\vec{r}) \Psi_j(\vec{r}) \rangle \approx \sum_{j=\pm,0} \int d\vec{r} \, |\Phi_j(\vec{r})|^2,$$

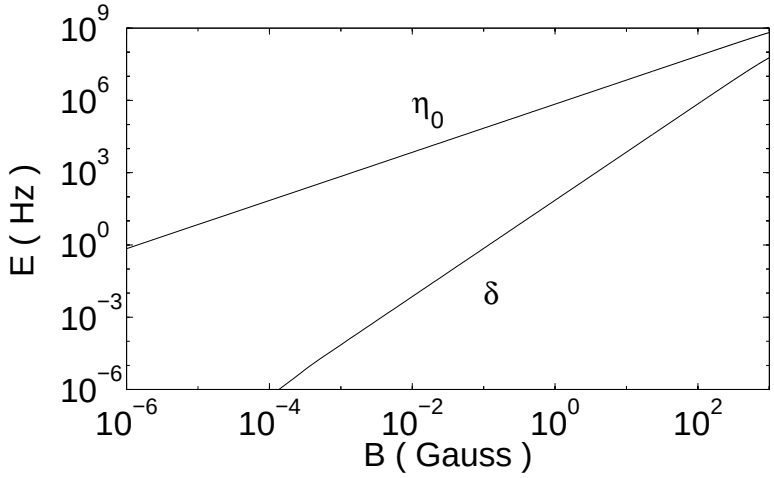

Figure 8: Approximate linear and quadratic Zeeman effects as characterized by parameters η_0 and δ versus magnetic field B for a ^{87}Rb atom.

$$\begin{aligned} M &= \int d\vec{r}[\langle\Psi_+^\dagger(\vec{r})\Psi_+(\vec{r})\rangle - \langle\Psi_-^\dagger(\vec{r})\Psi_-(\vec{r})\rangle] \\ &\approx \int d\vec{r}[|\Phi_+(\vec{r})|^2 - |\Phi_-(\vec{r})|^2]. \end{aligned} \tag{22}$$

In a typical experiment, the last stage before condensation consists of atomic evaporations, during which neither N nor M is conserved. For a scalar condensate, typically the ground state is obtained from a minimization of Eq. (19) subjected to the constraint of only N conservation. This gives rise to the Gross-Pitaevskii equation (GPE) and the associated condensate chemical potential, which mathematically is simply the Lagrange multiplier of the constrained minimization. A spin-1 condensate requires the introduction of two Lagrange multipliers during the minimization subjected to both the N and M conservation constraints, as was first performed in [45, 97].

When atomic interactions are ferromagnetic ($c_2 < 0$ as for ^{87}Rb atoms) and when the external B-field is negligible, Yi *et. al.* have shown previously that the ground state structure is simply a state where all individual atomic spins are aligned in the same direction [93]. In this case, the conservation of M can be simply satisfied by tilting the quantization axis away from the direction of the condensate spin. This

can always be done if a system described by (17) is rotationally symmetric, and thus contains the SO(3) symmetry [50]. The presence of a nonzero B field, on the other hand, breaks the rotational symmetry, [e.g. the linear Zeeman shift, reduces the SO(3) to SO(2) symmetry], thus the conservation of M has to be included in the minimization process directly.

The global ground state phase diagram including both linear and quadratic Zeeman effect was first investigated by Stenger *et al.* [45]. In their early study, although the M conservation was included in their formulation, it was not separately discussed, consequently their results do not easily apply to systems with fixed values of M. The ground state structures as given in Ref. [45] correspond to the actual ground state which is realized through a M non-conserving evaporation process (e.g. in the presence of a nonzero B-field) that has a reservoir for condensate magnetization. Our study, on the other hand, would explicitly discuss the phase diagram for fixed values of M, which could physically correspond to experimental ground states (with/without a B-field) due to a M conserving evaporation process. Although more limited, as our results can be traced to linear trajectories of $M = \text{const.}$ in the phase diagram of Ref. [45, 97], we expect them to be useful, especially in predicting ground state structures when a ready-made spinor condensate is subject to external manipulations that conserve both N and M.

When atomic interactions are anti-ferromagnetic ($c_2 > 0$), the global ground state was first determined to be a total spin singlet [52]. More elaborate studies, including quantum fluctuations, were performed by Ho and Yip [61] and Koashi and Ueda [62]. Unfortunately, these results [61, 62] do not correspond to actual ground states as realized in current experiments, because of the presence of background magnetic fields. For instance, the states as found in Ref. [61] are only possible if the magnetic field B is less than 70μG at the condensate density as realized in the MIT experiments [97]. The linear Zeeman shift (see Fig. 8) due to the presence of even a small magnetic

field can overwhelm atomic mean field interaction and typical atomic thermal energy, thus if it were not for the conservation of M, the ground state would simply correspond to all atoms condense into the lowest Zeeman sublevel of $|m_F = 1\rangle$.

We now minimize H of Eq. (19) by denoting $\Phi_j(\vec{r}) = \sqrt{N_j}\phi_j(\vec{r})e^{-i\theta_j}$, with a real mode function $\phi_j(\vec{r})$ ($\int \phi_j^2(\vec{r})d\vec{r} = 1$) and phase θ_j. It is easy to check that the phase convention of ferromagnetic/anti-ferromagnetic interactions as obtained previously [51] in the absence of a B-field still remains true, i.e.

$$\theta_+ + \theta_- - 2\theta_0 = 0, \qquad c_2 < 0 \ \text{(ferromagnetic)}, \tag{23}$$

$$\theta_+ + \theta_- - 2\theta_0 = \pi, \qquad c_2 > 0 \ \text{(anti-ferromagnetic)}. \tag{24}$$

4.3 Condensate ground state in a homogeneous system

In a homogeneous system such as a box type trap (of volume $\mathcal{V}$), adopting the above phase convention, the resulting ground state energy functional becomes ($+/-$ for $c_2 < 0$ and $c_2 > 0$ respectively)

$$\begin{aligned} H[\{N_i\}] &= H_S + E_0 N + \frac{c_2}{2\mathcal{V}}\left[(N_+ - N_-)^2 + 2N_0(\sqrt{N_+} \pm \sqrt{N_-})^2\right] \\ &\quad -\eta_0(N_+ - N_-) + \delta(N_+ + N_-). \end{aligned} \tag{25}$$

With everything expressed in terms of fractional populations and fractional magnetization $\rho_i = N_i/N$ and $m = M/N$, and note that $\rho_+ + \rho_- = 1 - \rho_0$, $\rho_+ - \rho_- = m$, Eq. (25) becomes

$$\begin{aligned} \frac{H[\{\rho_i\}]}{N} &= \frac{H_S}{N} + E_0 + \frac{c}{2}\left[(\rho_+ - \rho_-)^2 + 2\rho_0(\sqrt{\rho_+} \pm \sqrt{\rho_-})^2\right] \\ &\quad -\eta_0(\rho_+ - \rho_-) + \delta(\rho_+ + \rho_-), \end{aligned} \tag{26}$$

with an interaction coefficient $c = c_2 N/\mathcal{V}$, tunable through a change of condensate density.

We now minimize Eq. (26) under the two constraints $\rho_+ + \rho_0 + \rho_- = 1$ and $\rho_+ - \rho_- = m$. We restrict our discussion to the region $-1 < m < 1$ as the special

cases of $m = \pm 1$ are trivial. Because H_S, E_0, c, η_0, and m are all constants for given values of B, N, and $\mathcal{V}$, the only part left to be minimized is

$$\mathcal{F} \;=\; c\rho_0(\sqrt{\rho_+} \pm \sqrt{\rho_-})^2 + \delta(\rho_+ + \rho_-). \tag{27}$$

In the special case of $c = 0$, Eq. (27) reduces to

$$\mathcal{F} \;=\; \delta(\rho_+ + \rho_-). \tag{28}$$

The ground state is then very simple. When $\delta > 0$, which seems to be always the case for quadratic Zeeman shift, the minimum is reached by having as large an ρ_0 (thus as small an $\rho_+ + \rho_-$) as possible, namely

$$\rho_0 = 1 - |m|, \qquad \rho_+ = \begin{cases} |m|, & m \geq 0 \\ 0, & m < 0 \end{cases}, \qquad \rho_- = \begin{cases} 0, & m \geq 0 \\ |m|, & m < 0 \end{cases}. \tag{29}$$

When $\delta = 0$, we have (in general) three condensate components with $\rho_\pm = (1 - \rho_0 \pm m)/2$ and $0 \leq \rho_0 \leq 1 - |m|$.

For ferromagnetic interactions with $c < 0$, we define $x = \rho_+ + \rho_-$. The ground state is then determined by the minimum of

$$\mathcal{F} \;=\; g_+(x) + \delta x, \tag{30}$$

with $g_+(x) \equiv c(1-x)(x + \sqrt{x^2 - m^2})$. When $\delta = 0$, we find

$$\rho_\pm = \frac{1}{4}(1 \pm m)^2, \qquad \rho_0 = \frac{1}{2}(1 - m^2), \tag{31}$$

which is the same as obtained in [93, 102]. However with a nonzero $\delta > 0$, we find in general

$$\rho_\pm = \frac{1}{2}(x_0 \pm m), \qquad \rho_0 = 1 - x_0 \geq \frac{1}{2}(1 - m^2), \tag{32}$$

with x_0 being the root of equation $g'_+(x) + \delta = 0$, it turns out that there always exists one and only one solution to the equation. The equilibrium value for ρ_0 is larger than

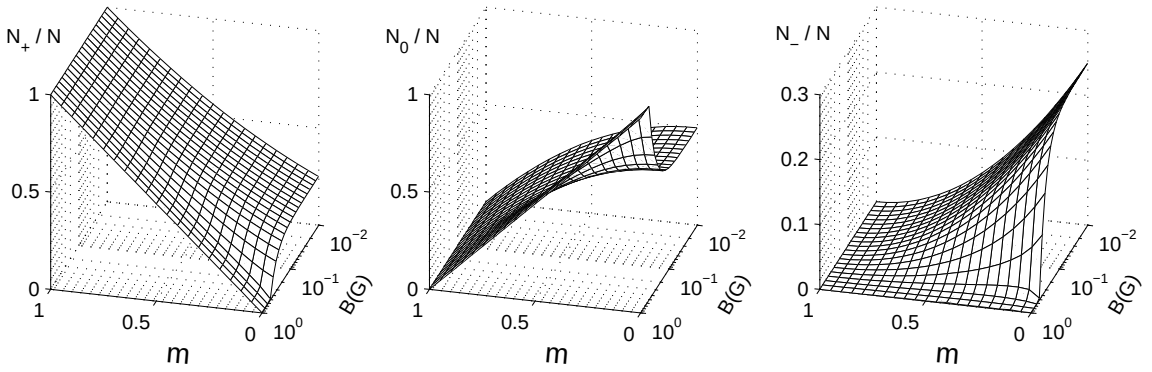

Figure 9: The dependence of fractional population for different spin component on m and B for a spin-1 ^{87}Rb homogeneous condensate with $N/\mathcal{V} = 5 \times 10^{14}\text{cm}^{-3}$.

the result of Eq. (31) because the quadratic Zeeman effect causes a lowering of the total energy if two $|m_F = 0\rangle$ atoms are created when an $|m_F = +1\rangle$ atom collides with an $|m_F = -1\rangle$ atom. Figure 9 displays the results of Eq. (32) for a typical ^{87}Rb condensate, for which the atomic parameters are $E_{\text{HFS}} = (2\pi)6.8347\text{GHz}$ [104], $a_0 = 101.8a_B$, and $a_2 = 100.4a_B$ (a_B is the Bohr radius) [95]. At weak magnetic fields, typically a condensate contains all three spin components. With the increasing of B-field, the quadratic Zeeman effect becomes important which energetically favors the $|0\rangle$ component, so typically only two components survive: the $|0\rangle$ component and the larger (initial population) of the $|+\rangle$ or $|-\rangle$ component, so the ground state becomes (for $m > 0$) $\rho_+ \simeq m$ and $\rho_0 \simeq 1 - m$.

Finally we consider the case of anti-ferromagnetic interactions for $c > 0$, we have then

$$\mathcal{F} \;=\; g_-(x) + \delta x, \tag{33}$$

with $g_-(x) = c(1-x)(x - \sqrt{x^2 - m^2})$. For $\delta = 0$, we again recover the standard result

$$\rho_0 = 0, \qquad \rho_\pm = \frac{1}{2}(1 \pm m), \tag{34}$$

if $m \neq 0$. When $m = 0$, the ground state is under-determined as many solutions are allowed as along as they satisfy $\rho_+ = \rho_- = (1 - \rho_0)/2$ with $\rho_0 \in [0, 1]$.

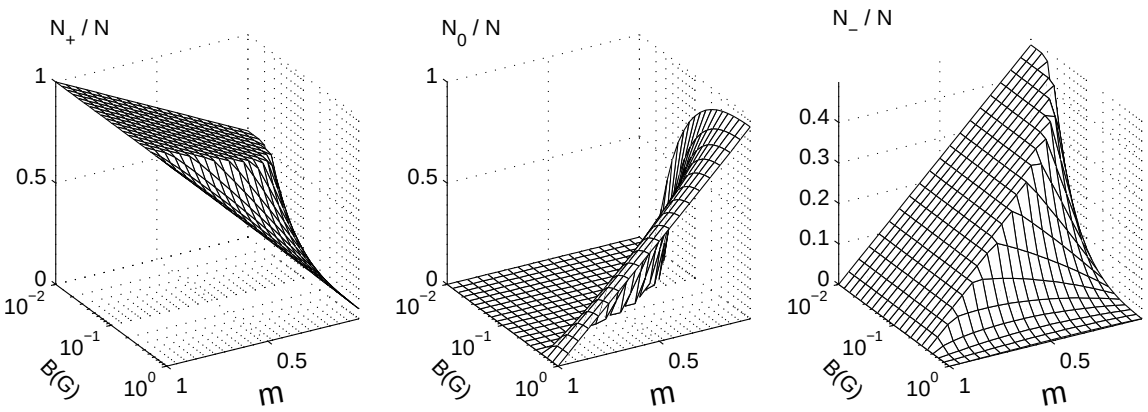

Figure 10: The same as in Fig. 9, but now for a spin-1 ^{23}Na condensate.

In an external B-field when $\delta > 0$, we first consider the special case of $m = 0$. It can be easily seen from Eq. (33) that $\rho_0 = 1$ is the ground state. For $m \neq 0$, we obtain the following result: when $\delta > c[1 - \sqrt{1 - m^2}]$, the ground state will have three condensate components with

$$\rho_\pm = (x_0 \pm m)/2, \qquad \rho_0 = 1 - x_0, \tag{35}$$

where x_0 is the root of equation $g'_-(x) + \delta = 0$; When $\delta \leq c[1 - \sqrt{1 - m^2}]$, only $|+\rangle$ and $|-\rangle$ components exist, i.e., $\rho_\pm = (1 \pm m)/2$.

Figure 10 is the typical results for a spin-1 ^{23}Na condensate. The atomic parameters are $E_{\rm HFS} = (2\pi)1.7716$ GHz [104], $a_0 = 50\ a_B$ and $a_2 = 55\ a_B$ [96]. At $B = 0$ there are only two condensate components, $|+\rangle$ and $|-\rangle$. For $B > 0$ but not very strong, there are two possibilities: three nonzero condensate components if $m < m_c$ and two nonzero condensate components if $m \geq m_c$, with $\delta(B) = c(1 - \sqrt{1 - m_c^2})$. When B-field gets stronger, i.e. $\delta(B) \geq c$, there are always three condensate components. Although the $|-\rangle$ component becomes smaller and smaller with increasing B, it never be zero exactly. Actually when B field is so strong that it overwhelms the spin dependent interaction, c term, the solution always approaches $\rho_0 \simeq 1 - |m|$ no matter what kind of interaction it is, ferromagnetic or antiferromagnetic interaction.

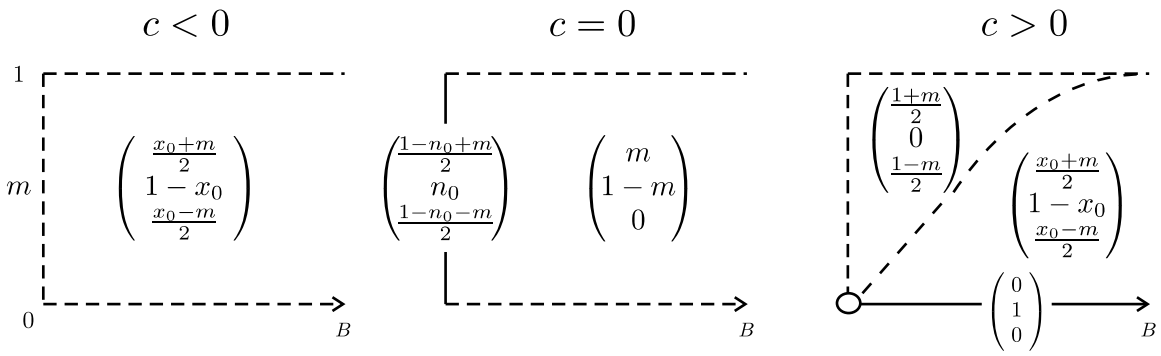

Figure 11: The ground state phase diagram for a homogeneous spin-1 condensate. Dashed curves and lines denote gradual transitions across the boundaries, solid lines denote discontinuous jumps. x_0 is the solution to equation $g'_{\pm}(x) + \delta = 0$ and the curves for $c > 0$ is determined by $\delta(B) = c[1 - \sqrt{1-m^2}]$. The open circle at $B = 0, m = 0$ for $c > 0$ denotes the family of degenerate ground state $[(1-\rho_0)/2, \rho_0, (1-\rho_0)/2]$.

Figure 11 summarizes the ground state structures of a homogeneous spin-1 condensate in a B-field for different c and m.

4.4 Condensate ground state inside a harmonic trap

In the previous section, we investigated in detail mean field ground state structures for a spin-1 condensate in a homogeneous confinement. For the case of a harmonic trap as in most experiments, there is no reason to believe *a priori* that the above conclusions still hold. In fact, the structures and phase diagrams as discussed before is only meaningful if the spatial mode function $\phi_j(\vec{r})$ for different spin components is identical. Otherwise, it would be impossible to classify the rich variety of possible solutions. When the spatial mode functions are the same, the spatial confinement simply introduces an average over the inhomogeneous density profile of the mode function.

The aim of this section, is therefore to determine the validity of the single mode approximation (SMA) in the presence of an external B-field and a harmonic trap. For simplicity, we assume the trap to be spherically symmetric. We employ numerical

methods to directly find the ground state solutions from the coupled Gross-Pitaevskii equation

$$\begin{aligned} i\hbar\frac{\partial}{\partial t}\Phi_+ &= [\mathcal{H}+E_+-\eta+c_2(n_++n_0-n_-)]\Phi_++c_2\Phi_0^2\Phi_-^*, \\ i\hbar\frac{\partial}{\partial t}\Phi_0 &= [\mathcal{H}+E_0+c_2(n_++n_-)]\Phi_0+2c_2\Phi_0^*\Phi_+\Phi_-, \\ i\hbar\frac{\partial}{\partial t}\Phi_- &= [\mathcal{H}+E_-+\eta+c_2(n_-+n_0-n_+)]\Phi_-+c_2\Phi_0^2\Phi_+^*, \end{aligned} \tag{36}$$

subject to the conservations of both N and M [Eqs. (22)]. $\mathcal{H}=-\hbar^2\nabla^2/2\mathsf{m}+V_{\rm ext}(\vec{r})+c_0n$, $V_{\rm ext}(\vec{r})=\mathsf{m}\omega^2r^2/2$, and $n=n_++n_0+n_-$ with $n_i=|\Phi_i|^2$. η is the Lagrange multiplier introduced to numerically enable the conservation of M.

It was shown previously that in the absence of an external B-field, and for ferromagnetic interactions, the SMA is rigorously valid despite the presence of a harmonic trap [93]. We can also show that in the presence of a nonzero B-field, the linear Zeeman shift does not affect the validity of the SMA because it can be simply balanced by the external Lagrange multiplier η. The quadratic Zeeman effect, on the other hand, can not be simply balanced, as it favors the production of two $|0\rangle$ atoms by annihilating one $|+\rangle$ and one $|-\rangle$ atom during a spin-exchange collision. Such unbalanced elastic collisions thus break the SO(3) symmetry of the freedom for an arbitrary quantization axis. Therefore, we do not in general expect the SMA to remain valid inside a nonzero B-field.

Numerically, we find the ground state solutions of Eq. (36) by propagating the equations in imaginary time. We typically start with an initial wave function as that of a complex Gaussian with a constant velocity: $\exp[-(x^2/2q_x^2+y^2/2q_y^2+z^2/2q_z^2)-i\vec{k}\cdot\vec{r}]$. q_x, q_y, q_z, and $\vec{k}$ are adjustable parameters which are checked to ensure that their choices do not affect the final converged ground state [93].

For $c_2=0$ or $c=0$, it is easy to check that SMA is always valid since the energy functional is symmetric with respect to spin component index. The fractional populations for each component is therefore the same as for a homogeneous system,

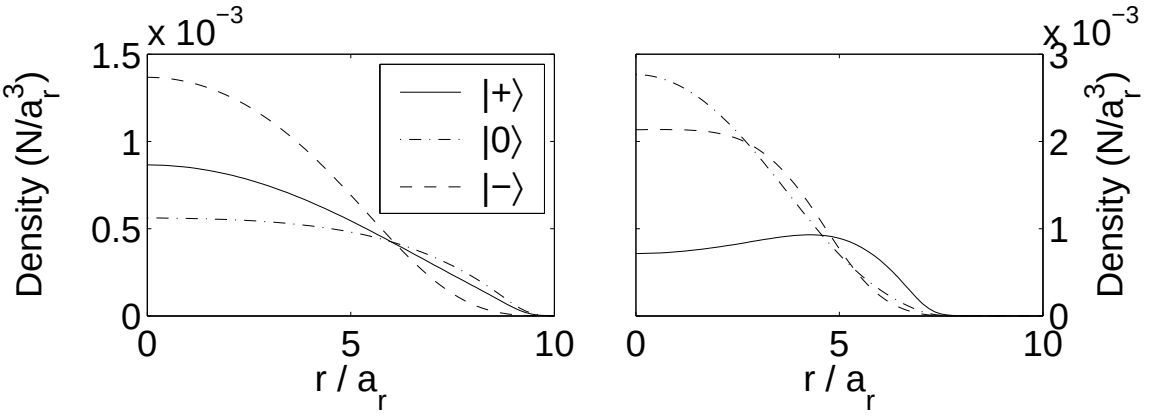

Figure 12: Typical densities of spatial mode functions for each components of a ^{87}Rb (a) and a ^{23}Na (b) condensate. The solid line denotes the $|+\rangle$ component, the dashed line the $|-\rangle$ component, and the dash-dotted line the $|0\rangle$ component. The parameters are, $N = 10^6, \omega = (2\pi)100$ Hz, $B = 1.0$ Gauss, and $m = 0.5$. $a_r = \sqrt{\hbar/\mathsf{m}\omega}$ is the length scale.

i.e. given by $[(1-\rho_0+m)/2, \rho_0, (1-\rho_0-m)/2]$ if $B = 0$, and $(m, 1-m, 0)$ if $B > 0$.

For ^{87}Rb and ^{23}Na condensates, which are believed to be ferromagnetic $c_2 < 0$ ($c < 0$) and anti-ferromagnetic $c_2 > 0$ ($c > 0$) respectively, Fig. 12 gives typical density distributions of spacial mode function, $n_j(\vec{r}) = |\phi_j(\vec{r})|^2$. Both panels in Fig. 12 clearly indicate that SMA is no longer valid. To get an overall idea of the validity of SMA we plot in Fig. 13 the overlap integrals of our mode functions with respect to the SMA mode function $\phi_{\rm SMA}(\vec{r})$ as determined from a scalar GP equation with a nonlinear coefficient $\propto c_0$ (due to the symmetric H_S only) [93]. For a ^{87}Rb condensate, we see the overlap is close to unity when B is small, therefore, SMA remains approximately applicable. But it becomes increasingly bad with the increase of B. We thus conclude that the SMA remains reasonable in a weak magnetic field while it is clearly invalid in a strong B-field. In fact, our numerical results confirm that the stronger the B-field, the worse the SMA gets. For typical system parameters, the dividing line occurs at a B-field of a fraction of a Gauss when the system magnetization M is not too small or too large. For a condensate with anti-ferromagnetic interactions, it was found earlier

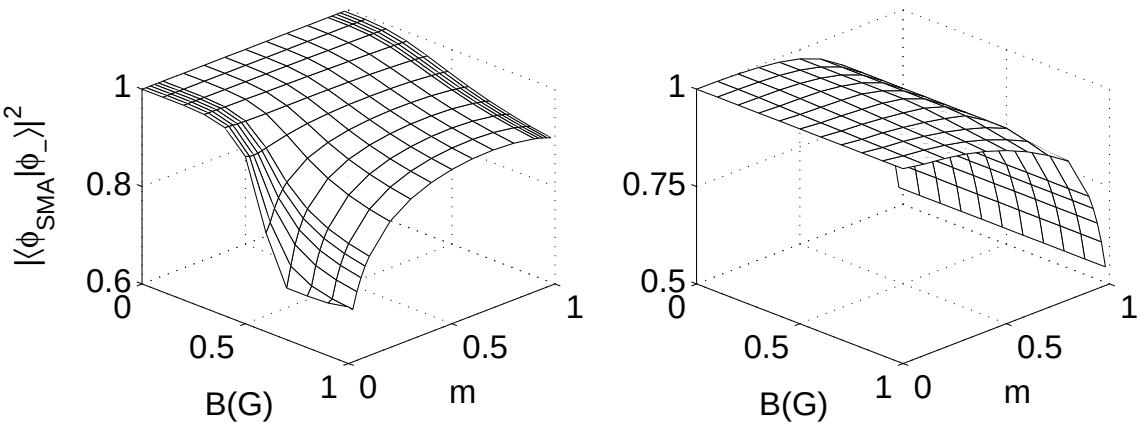

Figure 13: The overlap between the SMA mode function and the mode function for $|-\rangle$ component. Left panel is for a ^{87}Rb condensate. Right panel is for a ^{23}Na condensate. The atomic parameters are the same as in Fig. 12.

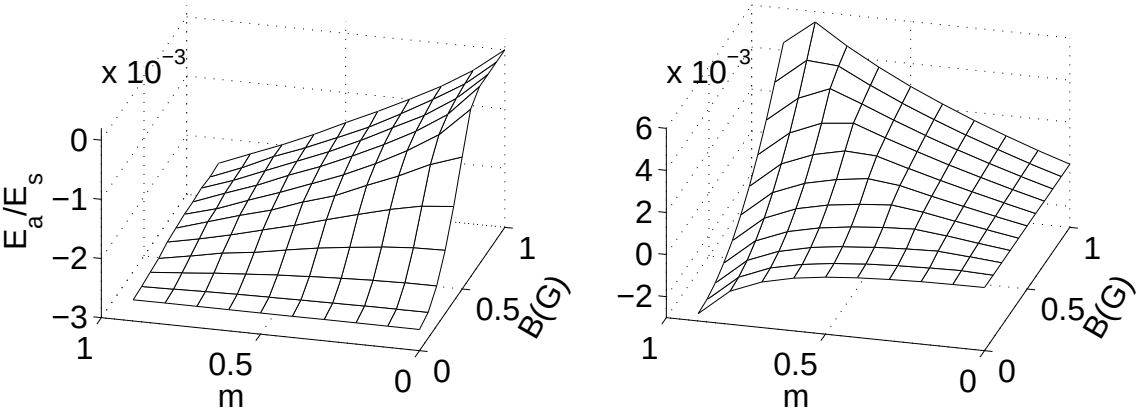

Figure 14: The same as in Fig. 13, but now comparing the spin asymmetric energy $E_a = c_2\langle\vec{F}\rangle^2/2 - (\eta_0+\eta)\langle F_z\rangle + \delta\langle F_z^2\rangle$ with the spin symmetric one H_s.

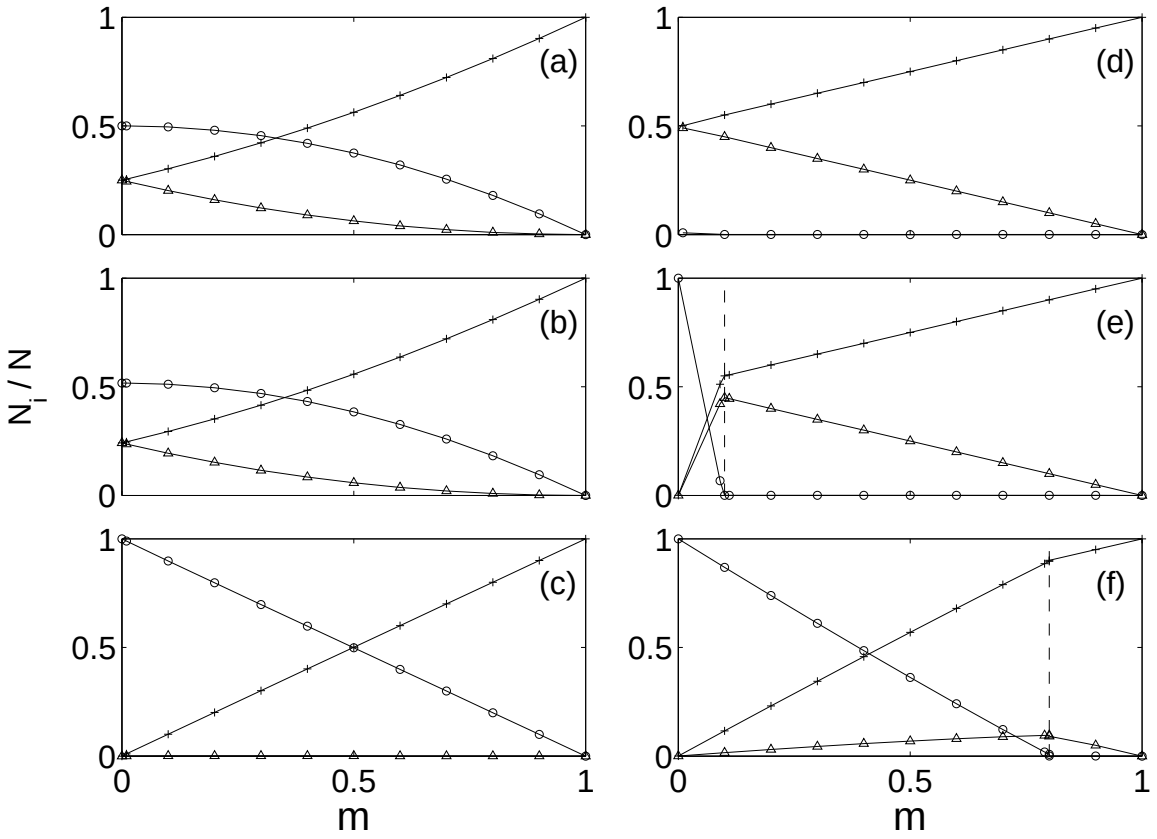

Figure 15: Fractional population for each spin component of a ^{87}Rb (left column) and a ^{23}Na (right column) condensate. The values of B-field from top row to bottom are $B = 0, 0.1, 1.0$ Gauss. The atomic parameters are the same as in Fig. 12. The solid lines with plus signs denote the $|+\rangle$ component, the lines with triangles are for the $|-\rangle$ component and the lines with open circles for the $|0\rangle$ component. The vertical dashed lines in (e) and (f) indicate the critical value m_c, the boundary between the two distinct regions discussed in the text. In (d), $m_c = 0$.

that SMA is violated in the limit of both large N and M even without an external B-field, while the case of $M = 0$ presents an exception where SMA remains strictly valid for $B = 0$ [93]. Figure 13 shows the overlap integral for a ^{23}Na condensate, indeed we see SMA is invalid except for the case of $M = 0$ where all atoms are in the $|0\rangle$ component. Remarkably, despite the seemingly large deviations from the SMA (as in Fig. 13), the spin asymmetric energy term remains very small in comparison to the spin symmetric term as evidenced in Fig. 14.

Figure 15 shows the dependence of fractional populations on the fractional magnetization for a ^{87}Rb (left column) and a ^{23}Na condensate (right column) at different B-fields. For ^{87}Rb atoms, these curves resemble the same dependence as for a homogeneous system where SMA is strictly valid. Nevertheless, we find the densities of mode functions can become quite different, i.e. SMA is not valid in general. For ^{23}Na atoms, the fractional component populations at different B-fields again follow the results as obtained previously for the homogeneous case. When $B = 0$ [as in Fig. 15(d)], the ground state distribution clearly obeys the same earlier (homogeneous) result $[(1+m)/2, 0, (1-m)/2]$, including the special case when $m = 0$ where it becomes $[(1-\rho_0)/2, \rho_0, (1-\rho_0)/2]$ with $\rho_0 \in [0, 1]$. For $B \neq 0$ [as in Fig. 15(e) and (f)], our numerical solutions reveal again two distinct regions; one for $m < m_c$ where all three components coexist, and another one for $m > m_c$ where only two components ($|+\rangle$ and $|-\rangle$) coexist. We find that m_c increases with the B-field, and is of course limited to $m_c < 1$. We conclude that despite the fact a harmonic trap induces spatially inhomogeneous distribution to condensate density, thus breaks the SMA in general, the overall ground state properties as measured by the fractional component distributions follow closely the results as obtained previously for the homogeneous case. Physically, we believe the above results can be understood as fractional populations relate to integrals of wave functions over all spaces, during which differences between wave functions can be averaged out. When only the $|+\rangle$ and $|-\rangle$ components coexist, in fact, the two constraints on N and M always give the fractional population $\rho_\pm = (1 \pm m)/2$ if $\rho_0 = 0$.

In summary, we find that inside a harmonic trap, the results remain largely the same as a homogeneous system, although the SMA becomes generally invalid. We find interestingly (see Fig. 16), the B field (or the δ) dependence of the critical value m_c that separates the two and three component condensate regions, remains almost identical as that given by the analytical formulae $\delta = c[1 - \sqrt{1 - m_c^2}\,]$ for a

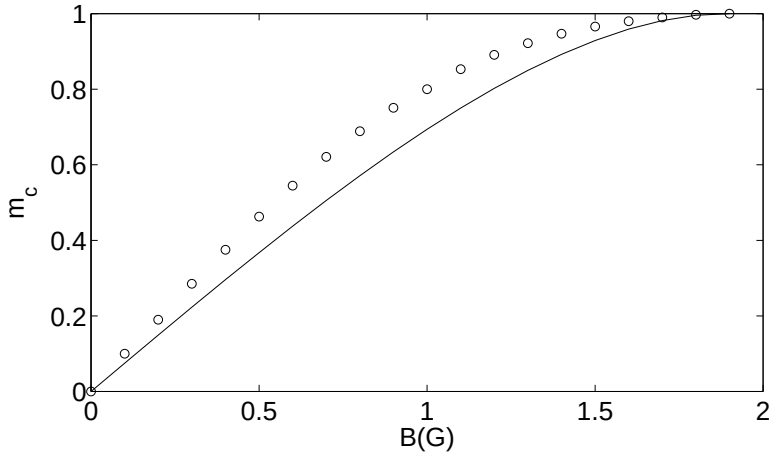

Figure 16: The B field dependence of the critical fractional magnetization m_c as computed numerically for a ^{23}Na condensate in a harmonic trap. The smooth curve corresponds to the result of $\delta = c[1-\sqrt{1-m_c^2}\,]$ (as from the homogeneous case) with an appropriately adjusted coefficient c (or density). The atomic parameters are the same as in Fig. 12.

homogeneous system. In a sense, this also points to the validity of the use of a mean field description, as the number of atoms is really large (10^6).

4.5 Effect of an inhomogeneous magnetic field

We have discussed the effect of a uniform magnetic field B in previous sections. We now consider an external B-field $\vec{B}(\vec{r}) = B_x(\vec{r})\hat{x} + B_y(\vec{r})\hat{y} + B_z(\vec{r})\hat{z}$, which satisfies $\nabla \cdot \vec{B}(\vec{r}) = 0$. Generally speaking, the Zeeman energy term, H_{ZM}^{ZQ}, is not diagonal in the Z-quantized (ZQ, according to T. Isoshima *et al.*'s notation [105]) representation $|\Psi_+(\vec{r}), \Psi_0(\vec{r}), \Psi_-(\vec{r})\rangle_{ZQ}$ since the local magnetic field $\vec{B}(\vec{r})$ is not always along the z-axis. But in a $\vec{B}$-quantized representation which chooses local z-axis always along the $\vec{B}(\vec{r})$, the Zeeman energy term, H_{ZM}^{BQ}, is still diagonal and given by the Breit-Rabbi formula (Eq. (18)). The relation between H_{ZM}^{ZQ} and H_{ZM}^{BQ} is found to be

$$H_{ZM}^{ZQ} = U^\dagger H_{ZM}^{BQ} U,$$

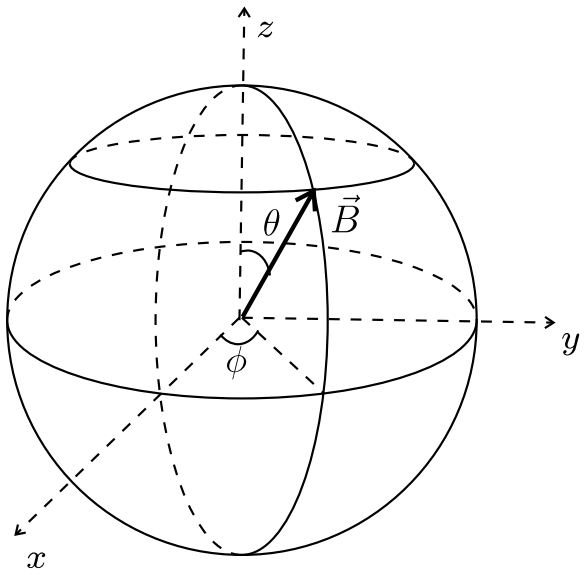

Figure 17: The magnetic field applied on the system at position $\vec{r}$.

where U is the unitary transformation which connects ZQ and BQ representations. The matrix U can be written as a product of two rotational matrices in spin space,

$$\begin{aligned} U &= e^{iF_y\theta}e^{iF_z\phi} \\ &= \begin{pmatrix} \frac{1}{2}(1+\cos\theta)e^{i\phi} & \frac{1}{\sqrt{2}}\sin\theta & \frac{1}{2}(1-\cos\theta)e^{-i\phi} \\ -\frac{1}{\sqrt{2}}\sin\theta e^{i\phi} & \cos\theta & \frac{1}{\sqrt{2}}\sin\theta e^{-i\phi} \\ \frac{1}{2}(1-\cos\theta)e^{i\phi} & -\frac{1}{\sqrt{2}}\sin\theta & \frac{1}{2}(1+\cos\theta)e^{-i\phi} \end{pmatrix}, \end{aligned} \tag{37}$$

where angles θ and ϕ are shown in Fig. 17.

After some tedious but straightforward calculations we find H_{ZM}^{ZQ} as follows, as in Isoshima *et al.* [105],

$$\begin{aligned} H_{ZM}^{ZQ} &= U^\dagger \begin{pmatrix} E_+(B) & 0 & 0 \\ 0 & E_0(B) & 0 \\ 0 & 0 & E_-(B) \end{pmatrix} U \\ &= \begin{pmatrix} H^{++} & H^{+0} & H^{+-} \\ H^{0+} & H^{00} & H^{0-} \\ H^{-+} & H^{-0} & H^{--} \end{pmatrix}, \end{aligned} \tag{38}$$

where $B = \left|\vec{B}(\vec{r})\right|$ and

$$\begin{aligned}
H^{++} &= \frac{1}{4}\left[E_+(1+\cos\theta)^2 + 2E_0\sin^2\theta + E_-(1-\cos\theta)^2\right], \\
H^{+0} &= -\frac{1}{\sqrt{2}}(\eta_0\sin\theta - \delta\sin\theta\cos\theta)e^{-i\phi}, \\
H^{+-} &= \frac{\delta}{2}\sin^2\theta e^{-i2\phi}, \\
H^{0+} &= (H^{+0})^* = -\frac{1}{\sqrt{2}}(\eta_0\sin\theta - \delta\sin\theta\cos\theta)e^{i\phi}, \\
H^{00} &= E_0\cos^2\theta + (E_+ + E_-)\frac{\sin^2\theta}{2} = E_0 + \delta\sin^2\theta, \\
H^{0-} &= -\frac{1}{\sqrt{2}}(\eta_0\sin\theta + \delta\sin\theta\cos\theta)e^{-i\phi}, \\
H^{-+} &= (H^{+-})^* = \frac{\delta}{2}\sin^2\theta e^{i2\phi}, \\
H^{-0} &= (H^{0-})^* = -\frac{1}{\sqrt{2}}(\eta_0\sin\theta + \delta\sin\theta\cos\theta)e^{i\phi}, \\
H^{--} &= \frac{1}{4}\left[E_-(1+\cos\theta)^2 + 2E_0\sin^2\theta + E_+(1-\cos\theta)^2\right]. \qquad (39)
\end{aligned}$$

We have used the definitions of η_0 and δ which denote the linear and quadratic Zeeman shift, respectively.

Now the GP Eq. (36) is modified as

$$\begin{aligned}
i\hbar\frac{\partial}{\partial t}\Phi_+ &= [\mathcal{H} + H^{++} - \eta + c_2(n_+ + n_0 - n_-)]\Phi_+ + c_2\Phi_0^2\Phi_-^* + H^{+0}\Phi_0 + H^{+-}\Phi_-, \\
i\hbar\frac{\partial}{\partial t}\Phi_0 &= [\mathcal{H} + H^{00} + c_2(n_+ + n_-)]\Phi_0 + 2c_2\Phi_0^*\Phi_+\Phi_- + H^{0+}\Phi_+ + H^{0-}\Phi_-, \qquad (40) \\
i\hbar\frac{\partial}{\partial t}\Phi_- &= [\mathcal{H} + H^{--} + \eta + c_2(n_- + n_0 - n_+)]\Phi_- + c_2\Phi_0^2\Phi_+^* + H^{-+}\Phi_+ + H^{-0}\Phi_0,
\end{aligned}$$

Propagating the above GP equation in imaginary time, we can find in principle the new ground state for a spin-1 condensate in an arbitrary magnetic field. As an example, we illustrate the results for a $\vec{B}(\vec{r})$,

$$\vec{B}(x,y,z) = \hat{z}B_0 + \hat{x}B'x - \hat{y}\frac{B'}{2}y - \hat{z}\frac{B'}{2}z.$$

Figure 18 shows the results we calculated for the ground state of ^{87}Rb spin-1 condensates in various magnetic fields for $B' = 0$ and $B' = 0.02$ G/cm. The trap parameters

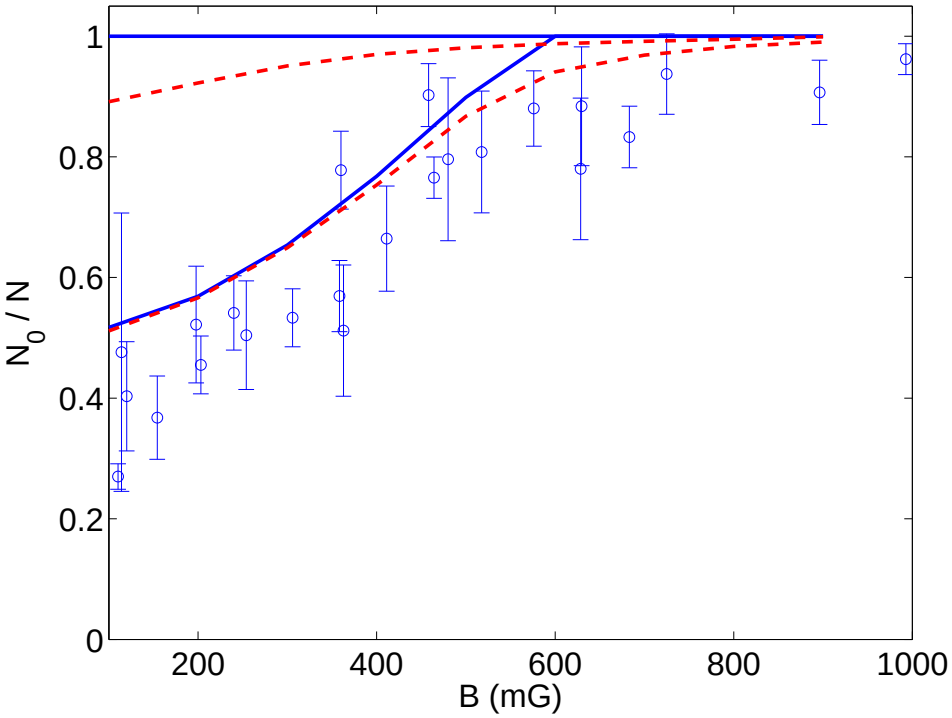

Figure 18: Comparison of theoretical calculation with experiment results. Circles with error bars denote experiment result, solid lines denote $B' = 0$ and dashed lines denote $B' = 0.02$ G/cm. The top pair of solid and dashed lines with diamond is for "antiferromagnetically interacting" ^{87}Rb condensate and the bottom pair is for ferromagnetically interacting one.

are close to that of experiments [53], $V_{\rm ext}(\vec{r}) = (1/2)\mathsf{m}(\omega_x^2 x^2 + \omega_y^2 y^2 + \omega_z^2 z^2)$ with $\omega_x = \omega_y = (2\pi)120$ Hz and $\omega_z = (2\pi)2550$ Hz. We also illustrate results for an "antiferromagnetic" ^{87}Rb spin-1 Bose condensate with $c_2' = -|c_2|$ in Fig. 18. Clearly the ^{87}Rb condensate result confirms a ferromagnetically interaction.

4.6 Conclusions

We have revisited the question of the mean field ground state structures of a spin-1 condensate in the presence of a uniform magnetic field. For a homogeneous system, when $c = 0$, there exist in general only two nonzero components $|+\rangle$ and $|0\rangle$, except that $B = 0$ where the ground state solution becomes indefinite; for ferromagnetic interactions when $c < 0$, the ground state in general has three nonzero components;

when $c > 0$ as for anti-ferromagnetic interactions, except for $m = 0$, there are two regions: one for $\delta > c[1 - \sqrt{1 - m_c^2}]$ where three nonzero components coexist and one for $\delta \leq c[1 - \sqrt{1 - m_c^2}]$ where only two components coexist. Inside a harmonic trap, these results remain largely true, although the SMA becomes generally invalid. We find interestingly (see Fig. 16), the B field (or the δ) dependence of the critical value m_c that separates the two and three component condensate regions, remains almost identical as that given by the analytical formulae $\delta = c[1 - \sqrt{1 - m_c^2}]$ for a homogeneous system. In a sense, this also points to the validity of the use of a mean field description, as the number of atoms is really large (10^6). We also investigated briefly the ground state in a nonhomogeneous magnetic field and compared directly with recent experimental results.

CHAPTER V

COHERENT SPIN MIXING DYNAMICS AND DOMAIN FORMATION IN A SPIN-1 ATOMIC BOSE CONDENSATE

5.1 Introduction

Different from a scalar or a pseudo-spin-1/2 two-component Bose condensate, a spin-1 Bose condensate has an inherent spin mixing mechanism, i.e., atoms can exchange among components through collisions $2|0\rangle \leftrightarrow |+\rangle + |-\rangle$. While most studies concentrate on condensates of atoms in a single hyperfine state, activities in spinor condensates [46] have recently attracted more and more attention with the additions of four new spin-1 Bose condensate experiments [49, 54, 55, 56], especially on the topics of the dynamics of spin mixing.

In a spinor condensate, atomic hyperfine spin degrees of freedom become accessible with the use of a far-off resonant optical trap instead of a magnetic trap. For atoms in the $F = 1$ ground state manifold, the presence of Zeeman degeneracy and spin dependent atom-atom interaction [45, 46, 49, 50, 51, 52, 93, 102, 63] leads to interesting spin dynamics. A clear experimental demonstration of such macroscopic oscillations remains to be seen though some preliminary work has been done by Chang *et al.* for spin-1 atoms [53] and Schmaljohnn *et al.* [54] and Kuwamoto *et al.* [55] for spin-2 atoms. From an experimental point of view, the main obstacles are dissipative atomic collisions among the condensed atoms and decoherence collisions with the noncondensed atoms [53, 54]. A promising approach to overcome these obstacles relies on increased atomic detection sensitivity, thus on the use of smaller condensates with lower number densities and at lower temperatures, both favorable conditions for

the single spatial mode approximation (SMA). Although some theoretical investigations on spin dynamics of spinor condensate under the SMA have been performed [52, 102], more interesting properties need to be explored in detail, especially when an external magnetic field is present. In this chapter, we study spin mixing dynamics inside a spin-1 condensate [52, 63, 102], focusing on the interaction-driven coherent oscillations in a uniform magnetic field, and the dynamical stability of these oscillations [106]. It is hoped that our study of dynamical instability of a ferromagnetically interacting spin-1 condensate may lead to an explanation for the recently observed multidomain formation.

5.2 Analytical results under SMA

Our system of a spin-1 atomic Bose gas inside an external magnetic field is described by the Hamiltonian given in Eq. (17). The field operators Ψ_i evolve according to the Heisenberg operator equations of motion.

$$\begin{aligned}
i\hbar\frac{\partial}{\partial t}\Psi_+(\vec{r},t) &= \left[-\frac{\hbar^2}{2\mathsf{m}}\nabla^2 + V_{\rm ext}(\vec{r}) + E_+\right]\Psi_+ + c_0\sum_j\left(\Psi_j^\dagger\Psi_j\right)\Psi_+ \\
&\quad + c_2\left(\Psi_+^\dagger\Psi_+ + \Psi_0^\dagger\Psi_0 - \Psi_-^\dagger\Psi_-\right)\Psi_+ + c_2\Psi_-^\dagger\Psi_0\Psi_0, \\
i\hbar\frac{\partial}{\partial t}\Psi_0(\vec{r},t) &= \left[-\frac{\hbar^2}{2\mathsf{m}}\nabla^2 + V_{\rm ext}(\vec{r}) + E_0\right]\Psi_0 + c_0\sum_j\left(\Psi_j^\dagger\Psi_j\right)\Psi_0 \\
&\quad + c_2\left[\left(\Psi_+^\dagger\Psi_+ + \Psi_-^\dagger\Psi_-\right)\Psi_0 + 2\Psi_0^\dagger\Psi_+\Psi_-\right], \\
i\hbar\frac{\partial}{\partial t}\Psi_-(\vec{r},t) &= \left[-\frac{\hbar^2}{2\mathsf{m}}\nabla^2 + V_{\rm ext}(\vec{r}) + E_-\right]\Psi_- + c_0\sum_j\left(\Psi_j^\dagger\Psi_j\right)\Psi_- \\
&\quad + c_2\left(\Psi_-^\dagger\Psi_- + \Psi_0^\dagger\Psi_0 - \Psi_+^\dagger\Psi_+\right)\Psi_- + c_2\Psi_+^\dagger\Psi_0\Psi_0. \qquad (41)
\end{aligned}$$

At near-zero temperature and when the total number of condensed atoms (N) is large, the condensate is essentially described by the mean field $\Phi_i = \langle\Psi_i\rangle$. Neglecting quantum fluctuations, they form the set of coupled Gross-Pitaevskii (GP) equations as expressed in Eq. (36), from which we can simulate the mean field off-equilibrium dynamics accurately at various external magnetic fields without using the SMA.

To gain more physical insight, we have formulated a simple model based on the well-known fact that for both ^{87}Rb (ferromagnetic) and ^{23}Na (anti-ferromagnetic) atoms, the spin dependent interaction $\propto |c_2|$ is much weaker than the density dependent interaction $\propto |c_0|$. This leads to the use of the SMA, where we adopt the mode function $\Phi(\vec{r})$ as determined from the spin-independent part of the Hamiltonian $\mathcal{H}_s = -(\hbar^2/2\mathsf{m})\nabla^2 + V + c_0 n$ as discussed in previous chapters [52, 93, 102]. Thus we define $\Phi_i(\vec{r},t) = \sqrt{N}\xi_i(t)\phi(\vec{r})\exp(-i\mu t/\hbar)$ with $\mathcal{H}_s\phi(\vec{r}) = \mu\phi(\vec{r})$ and $\int d\vec{r}|\phi(\vec{r})|^2 = 1$. We arrive at the coupled spinor equations

$$\begin{aligned} i\hbar\dot{\xi_+} &= E_+\xi_+ + c'[(\rho_+ + \rho_0 - \rho_-)\xi_+ + \xi_0^2\xi_-^*], \\ i\hbar\dot{\xi_0} &= E_0\xi_0 + c'[(\rho_+ + \rho_-)\xi_0 + 2\xi_+\xi_-\xi_0^*], \\ i\hbar\dot{\xi_-} &= E_-\xi_- + c'[(\rho_- + \rho_0 - \rho_+)\xi_- + \xi_0^2\xi_+^*], \end{aligned} \tag{42}$$

with $c' = c_2 N \int d\vec{r}|\phi(\vec{r})|^4$, $\rho_i = |\xi_i|^2$. It is easy to verify that the total atom number and atomic magnetization are conserved, i.e. $\sum_i \rho_i \equiv 1$, $\rho_+ - \rho_- \equiv m$, and $m = (N_+ - N_-)/N$ is a constant of motion.

As before we use $\eta_0 = (E_- - E_+)/2$ and $\delta = (E_- + E_+ - 2E_0)/2$ to parameterize the linear and quadratic Zeeman effect. We further transform $\xi_\pm \to \xi_\pm \exp[-i(E_0 \mp \eta_0)t/\hbar]$ and $\xi_0 \to \xi_0 \exp[-iE_0 t/\hbar]$, to eliminate the E_0 and η_0 dependence, and take $\xi_j = \sqrt{\rho_j}e^{-i\theta_j}$. After some simplification, we obtain the following dynamic equations for spin mixing inside a spin-1 condensate

$$\dot{\rho}_0 = \frac{2c'}{\hbar}\rho_0\sqrt{(1-\rho_0)^2 - m^2}\sin\theta, \tag{43}$$

$$\dot{\theta} = -\frac{2\delta}{\hbar} + \frac{2c'}{\hbar}\left[(1-2\rho_0) + \frac{(1-\rho_0)(1-2\rho_0) - m^2}{\sqrt{(1-\rho_0)^2 - m^2}}\cos\theta\right], \tag{44}$$

where $\theta = \theta_+ + \theta_- - 2\theta_0$ is the relative phase. These two coupled equations give rise to a classical dynamics of a nonrigid pendulum, whose energy functional (or Hamiltonian) can also be derived within the SMA as in [93]

$$\mathcal{E} = c'\rho_0\left[(1-\rho_0) + \sqrt{(1-\rho_0)^2 - m^2}\cos\theta\right] + \delta(1-\rho_0). \tag{45}$$

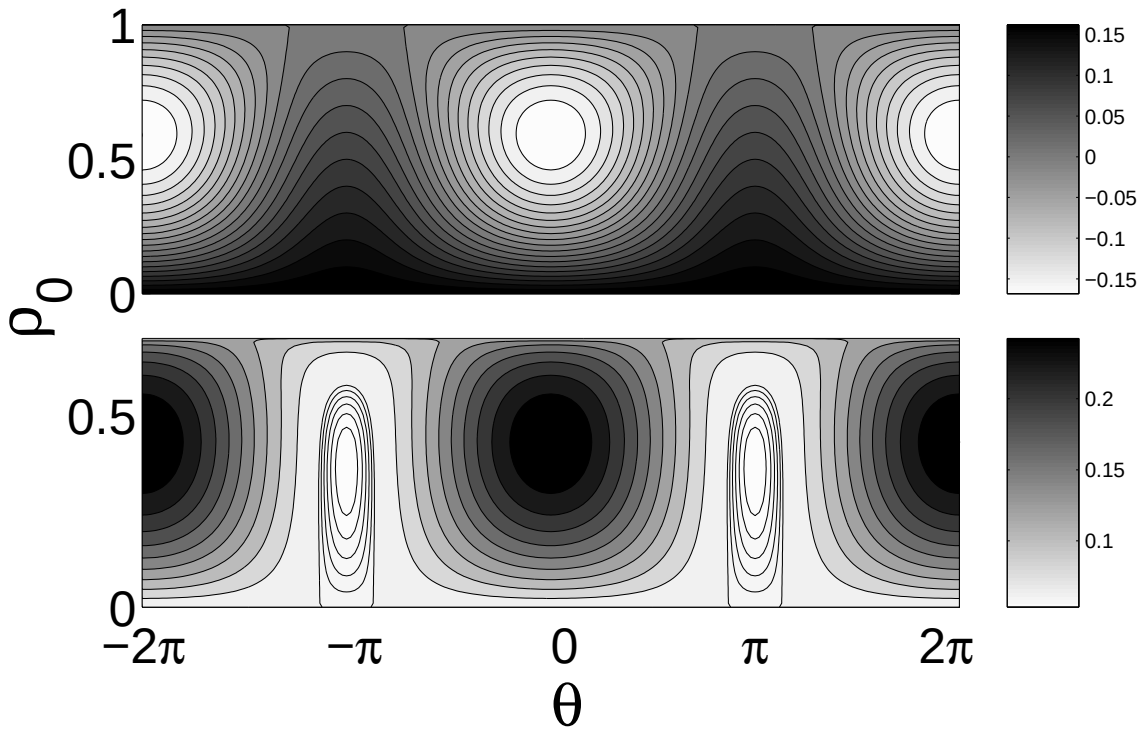

Figure 19: Iso-energy contours for a condensate of ^{87}Rb atoms (upper panel) with $B = 0.05$ Gauss, $|c'| = (2\pi)0.5$ Hz, and $m = 0$; of ^{23}Na atoms (lower panel) with $B = 0.015$ Gauss, $|c'| = (2\pi)0.5$ Hz, and $m = 0.3$.

It is easy to check that $\dot{\rho}_0 = -(2/\hbar)\partial\mathcal{E}/\partial\theta$ and $\dot{\theta} = (2/\hbar)\partial\mathcal{E}/\partial\rho_0$.

The contour plot of $\mathcal{E}$ in Fig. 19 displays several types of oscillation as in a pendulum. The energy is conservative for the spin mixing dynamics described by Eqs. (43, 44) in a magnetic field. The corresponding phase space trajectory is therefore confined to stay on the equal energy contour. Quite generally, ρ_0 oscillates in a magnetic field. Rewriting equation (43) as

$$(\dot{\rho}_0)^2 = \frac{4}{\hbar^2}\{[\mathcal{E} - \delta(1-\rho_0)][(2c'\rho_0 + \delta)(1-\rho_0) - \mathcal{E}] - (c'\rho_0 m)^2\}, \qquad (46)$$

we can compute the oscillation period according to

$$T = \oint \frac{1}{\dot{\rho}_0} d\rho_0 = \frac{\sqrt{2}\hbar}{\sqrt{-\delta c'}} \frac{K\left(\sqrt{\frac{x_2-x_1}{x_3-x_1}}\right)}{\sqrt{x_3-x_1}}, \text{ for } c' < 0, \qquad (47)$$

and

$$T = \frac{\sqrt{2}\hbar}{\sqrt{\delta c'}} \frac{K\left(\sqrt{\frac{x_3-x_2}{x_3-x_1}}\right)}{\sqrt{x_3-x_1}}, \text{ for } c' > 0. \qquad (48)$$

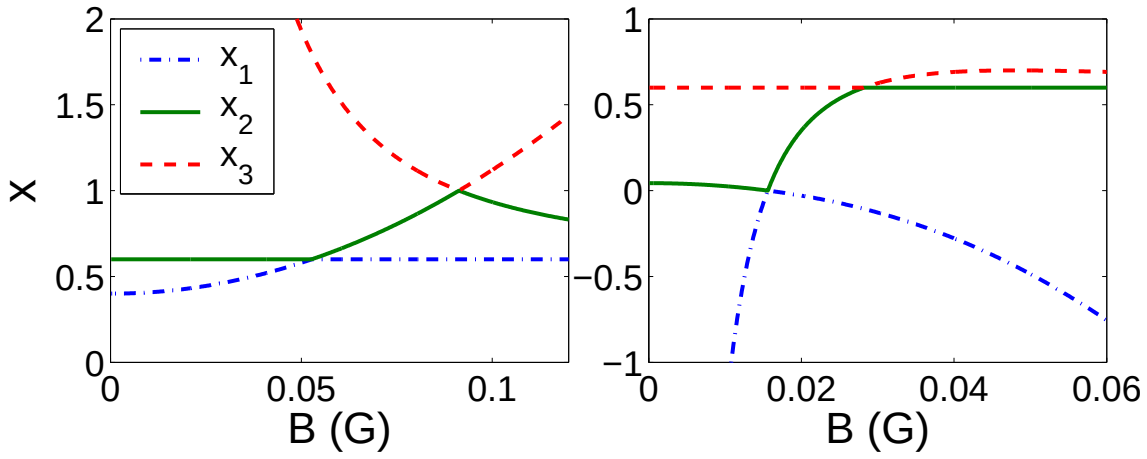

Figure 20: The dependence of cubic roots x_j on the external magnetic field for a ^{87}Rb condensate (left) and a ^{23}Na condensate (right). Other parameters are $|c'| = (2\pi)0.5$ Hz, $\rho_0(0) = 0.6$, $\theta(0) = 0$, and $m = 0$ for ^{87}Rb; $\theta(0) = \pi$ and $m = 0.3$ for ^{23}Na.

$K(k)$ is the elliptic integral of the first kind, and $x_{j=1,2,3}$ are the roots of $\dot{\rho}_0 = 0$ (ordered as $x_1 \leq x_2 \leq x_3$, shown in Fig. 20). The period for a rigid pendulum, described by $\ddot{u} + \sin u = 0$, is $T = 4\sqrt{2}K[\sqrt{2/(E+1)}\,]/\sqrt{E+1}$ at energy $E > 1$ and $T = 4\sqrt{2}F[\arcsin(\sqrt{(E+1)/2}), \sqrt{2/(E+1)}\,]/\sqrt{E+1}$ at energy $-1 \leq E \leq 1$ with E being the energy of the rigid pendulum.

The time evolution of ρ_0 can be expressed in terms of the Jacobian elliptic function cn(.,.),

$$\rho_0(t) \;=\; x_2 - (x_2 - x_1)\mathrm{cn}^2\left[\gamma_0 + t\sqrt{-2\delta c'(x_3 - x_1)}, k\right], \text{for } c' < 0$$

and

$$\rho_0(t) \;=\; x_3 - (x_3 - x_2)\mathrm{cn}^2\left[\gamma_0 + t\sqrt{2\delta c'(x_3 - x_1)}, k\right], \text{for } c' > 0.$$

γ_0 depends on the initial state, $\mathrm{cn}^2(\gamma_0, k) = [x_2 - \rho_0(0)]/(x_2 - x_1)$ if $c' < 0$ and $\mathrm{cn}^2(\gamma_0, k) = [x_3 - \rho_0(0)]/(x_3 - x_2)$ if $c' > 0$. For ^{87}Rb atoms ($c' < 0$), $\gamma_0 = 0$ if $\rho_0(0) = x_1$ and $\gamma_0 = K(k)$ if $\rho_0(0) = x_2$. The solutions of ρ_0 are usually oscillatory between x_1 and x_2 if $c' < 0$ (between x_2 and x_3 if $c' > 0$). When $x_2 = x_3$ ($x_2 = x_1$ if $c' > 0$), the solution becomes homoclinic, i.e., $\lim_{t\to\infty} \rho_0 = 1$ and the corresponding period is infinity for $m = 0$ (Fig. 21).

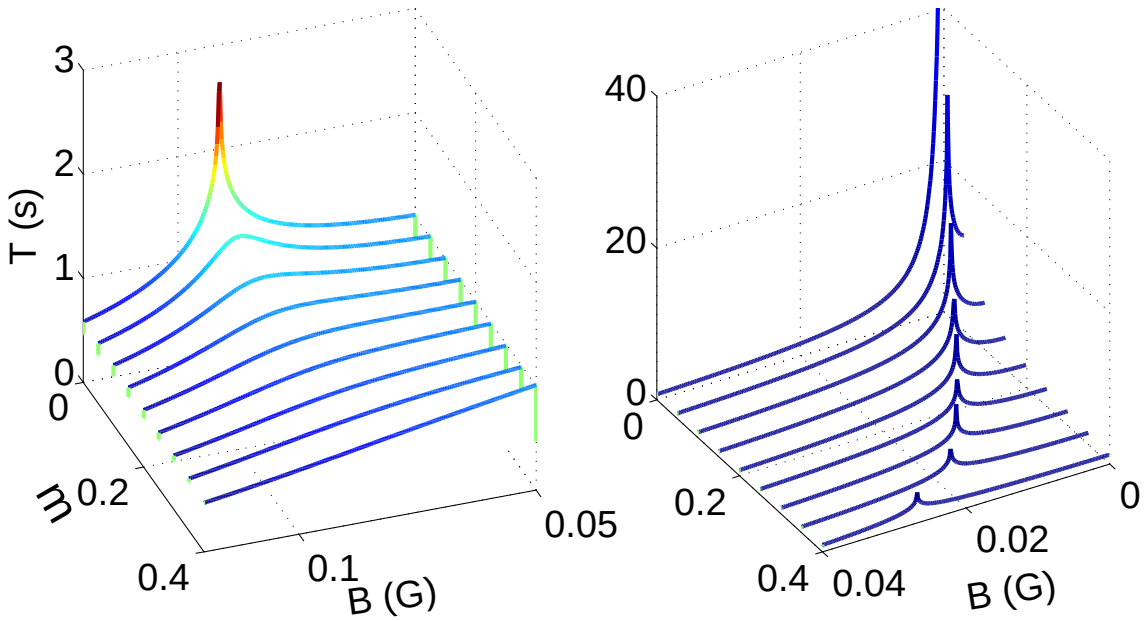

Figure 21: The magnetic field dependence of the oscillation period for a ^{87}Rb condensate (left) and a ^{23}Na condensate (right). parameters are $|c'| = (2\pi)0.5$ Hz, $\rho_0(0) = 0.6$, $\theta(0) = 0$, and $m = 0$ for ^{87}Rb; $\theta(0) = \pi$ and $m = 0.3$ for ^{23}Na.

We further observe from Fig. 21 that when the total magnetization is varied the peak of the oscillation period essentially stays at the same magnetic field for ferromagnetic interactions. The solution becomes periodic when $m \neq 0$ since ρ_0 can at most reach $1 - m$. It turns out that the critical solution of an infinitely long oscillation period occurs when $\rho_0(t \to \infty) = 1$, or equivalently $E = 0$, which gives $\delta(B_c) = |c'|\rho_0(1 + \cos\theta)$ with ρ_0 and θ the initial conditions ($\delta \simeq 72B^2$ Hz/G^2 for ^{87}Rb condensate). At $B = 0$ we reproduce the same result as in Ref. [102]. The rapid decreasing of the period when $B > B_c$ is consistent with the recent calculations by Schmaljohann *et al.* [54]. For anti-ferromagnetic interactions, however, the peak of the oscillation period shows a strong dependence on the magnetization, and asymptotically we find the position of the peak is determined by $\rho_0(t \to \infty) = 0$, i.e., $E = \delta(B_c)$ which is equivalent to $\delta(B_c) = c'[(1 - \rho_0) + \sqrt{(1 - \rho_0)^2 - m^2}\cos\theta]$.

Substituting the solution $\rho_0(t)$ into Eq. (45), we can solve for $\theta(t)$. Furthermore

we can find the time dependence of $\theta_\pm$ and θ_0 through the following

$$\begin{aligned}\dot{\theta}_\pm &= -\frac{1}{\hbar}[\delta + c'\rho_0 + c'\rho_0\sqrt{\frac{1-\rho_0 \mp m}{1-\rho_0 \pm m}}\cos\theta], \\ \dot{\theta}_0 &= -\frac{c'}{\hbar}[(1-\rho_0) + \sqrt{(1-\rho_0)^2 - m^2}\cos\theta].\end{aligned}$$

5.3 Comparison with numerical results

Starting from an equilibrium state of a spin-1 condensate inside an external magnetic field, the initial relative phases among the three components depend on the spin-dependent atom-atom interaction being ferromagnetic (0) or anti-ferromagnetic (π) [94]. Utilizing the SMA, we find previously the off-equilibrium dynamics of a spin-1 condensate corresponds to that of a nonrigid pendulum, which can be characterized by trajectories in the semiclassical phase space. Typical results are as illustrated in Fig. 22 for a spin-1 ^{87}Rb condensate, where we have plotted the SMA orbits and the dependence of oscillation periods on the external magnetic field. The parameters are close to the experiment [107]; where the spin-independent trap is harmonic $V = (\mathsf{m}/2)(\omega_x^2 x^2 + \omega_y^2 y^2 + \omega_z^2 z^2)$ with $\omega_x = \omega_y = (2\pi)240$ Hz and $\omega_z = (2\pi)24$ Hz. The average density of ^{87}Rb condensates are $\langle n\rangle \approx 1.7 \times 10^{13}$ cm^{-3} for $N = 10^3$ and 5.4×10^{13} cm^{-3} for $N = 10^4$. The initial states are taken from the (equilibrium) ground state for $B = 0.07$ Gauss with a zero magnetization ($m = 0$), i.e. $c' = -0.614$ Hz, $\rho_0(0) = 0.644$ and $\theta(0) = 0$, for $N = 10^3$. Similarly the initial state for $N = 10^4$ is the ground state at $B = 0.1$ Gauss with zero m, i.e. $c' = -1.945$ Hz, $\rho_0(0) = 0.595$, and $\theta(0) = 0$.

As illustrated in Fig. 22, the spin mixing dynamics within the SMA corresponds to a typical pendulum, with the quadratic Zeeman energy playing the important role of the total energy by shifting the equilibrium point. At small offset from equilibrium point (small change of the magnetic field before and after $t = 0$), the equivalent pendulum undergoes small amplitude oscillation, approximately harmonic with a period

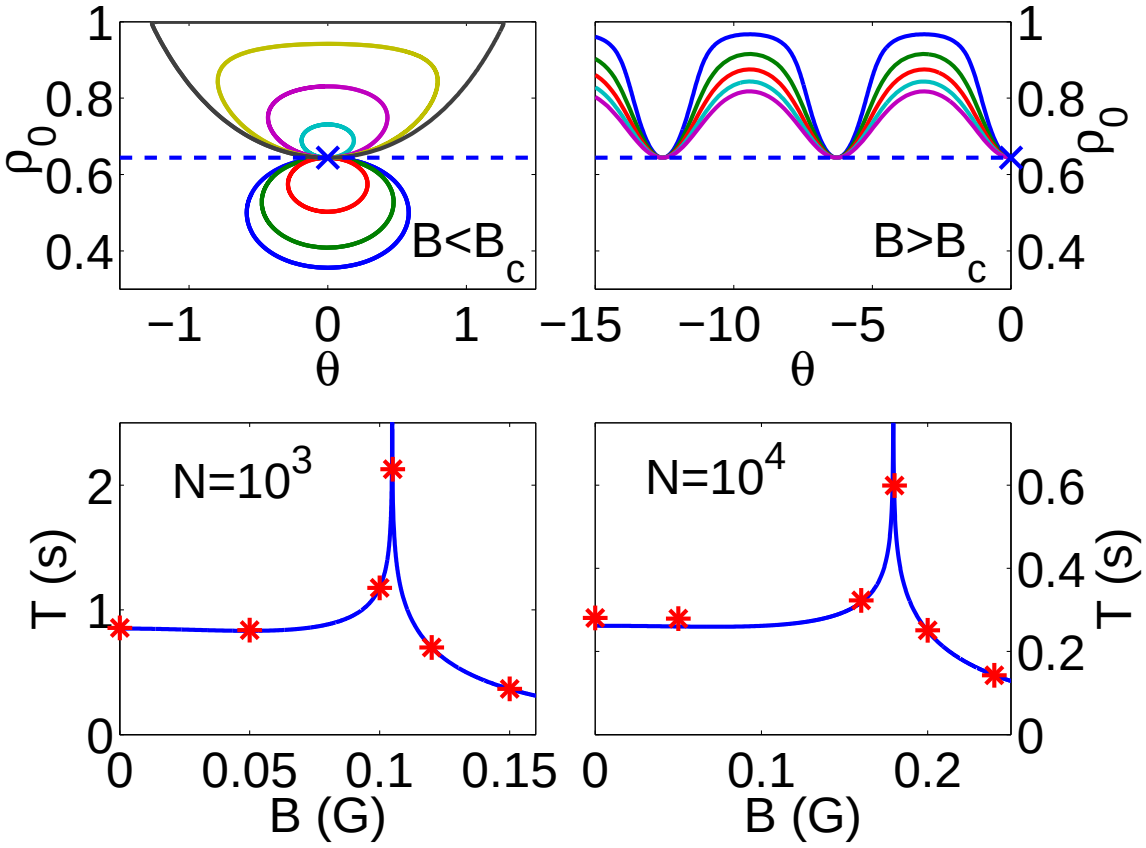

Figure 22: (Color) The upper two panels show typical orbits (solid lines) for different magnetic fields with SMA, starting from the same initial state ($\rho_0(0) = 0.644, \theta(0) = 0, c' = -0.614$, denoted by a crosses). $B = 0$, 0.03, 0.05, 0.08, 0.09, 0.1, 0.1048 (Gauss) from the bottom to the top for the upper left panel and $B = 0.11$, 0.12, 0.13, 0.14, 0.15 (Gauss) from the top to the bottom for the upper right panel. The lower two panels show the dependence of oscillation period T on magnetic field B for a ^{87}Rb condensate from SMA model (solid line, Eq. (47)) with total trapped atoms being $N = 10^3$ (left panel) and $N = 10^4$ (right panel), the results from a full numerical simulation without the use of SMA are denoted by (*).

independent of the energy or oscillation amplitude; increasing of the total energy leads to longer oscillation period as the pendulum becomes increasingly nonlinear. At a critical field B_c, when the effective total energy is just enough to bring the pendulum to the completely up or top position, the period approaches infinity as for the homoclinic orbit of a pendulum; Upon further increasing the energy (or B), the pendulum starts to rotate around and the period becomes smaller with increasing energy as the pendulum rotates faster and faster.

We hope to make some estimates to support the use of the mean field theory, i.e. treating the atomic field operators as c-numbers. Intuitively, we would expect that this is a reasonable approximation as the total numbers of atom, at 1000, although not macroscopic, is definitely 'large'. In fact, the recent double well experiment that confirmed the coherent nonlinear Josephson oscillations of the mean field theory, is at a similar level of numbers of atoms [18]. A rigorous discussion of this point in terms of the quantum phase diffusions in a spin-1 condensate is a rather involved procedure, and will not be reproduced here [109]. Instead, we illuminate the validity of mean field theory as follows. First, we look at the total atom number fluctuations. Approximating the spinor condensate as a one component scalar, and neglecting the internal spin mixing dynamics, its total overall phase spreads after a time of $\tau_c \approx N/[\sigma(N)(c_0\langle n\rangle)]$ [110], with $\sigma(N) \sim \sqrt{N}$ the standard deviation of the atom numbers from taking c-number approximations of the atomic field operators. In our case, this time is about 0.2 second, short compared to a typical Josephson type oscillation period at $\sim$ 1 second. We believe, however, this is not a critical issue as we are not studying phase sensitive phenomena involving the overall phase as in an interference experiment. Instead, we are interested here in the relative phase dynamics between different condensate components, whose oscillation time scale is given by the much smaller value of the spin-dependent interaction coefficient c_2; thus we should compare the coherent classical oscillation period of $\sim$ 1 second with the

much longer time $\tau_c' \approx N/[\sigma(N)(c_2\langle n\rangle)]$ [52], ~ 50 seconds (for ^{87}Rb). This then leads to a favorable condition for adopting the mean field theory in our study. Alternatively, we can reach the same conclusion from a direct investigation of the oscillation period T in Eq. (47), which contains a simple N dependence $\propto 1/\sqrt{N}$. We find that $|T(N \pm \sqrt{N}) - T(N)|/T(N) = 1/(2\sqrt{N})$, is only about 2%, indicating the overall validity of the mean field theory.

5.4 Averaged spin evolutions

In a recent experiment, the collective precessing of the magnetization of a spin-1 condensate were imaged, leading to a beautiful display of spinor coherence in the condensate [56]. Prompted by this, we now consider the evolution of the averaged total spin. We first illustrate the quadratic Zeeman effect on the spin dynamics of a noninteracting condensate. Assuming an initial state $\hat{\xi}(0) = (\xi_+, \xi_0, \xi_-)^T$, the total spin average is $\langle \vec{F}(t)\rangle = \langle \hat{\xi}(t)|F_x\hat{x} + F_y\hat{y} + F_z\hat{z}|\hat{\xi}(t)\rangle$ with

$$\begin{aligned}
\langle F_x\rangle &= \sqrt{2}\Re\Big[|\xi_0|\left(|\xi_+|e^{i(\theta_0-\theta_+)} + |\xi_-|e^{i(\theta_0-\theta_-)}\right)\Big], \\
\langle F_y\rangle &= \sqrt{2}\Im\Big[|\xi_0|\left(|\xi_+|e^{i(\theta_0-\theta_+)} - |\xi_-|e^{i(\theta_0-\theta_-)}\right)\Big], \\
\langle F_z\rangle &= |\xi_+|^2 - |\xi_-|^2 = m.
\end{aligned}$$

As an interesting case, we take $\hat{\xi}(0) = [\sqrt{(1-\rho_0)/2}, \sqrt{\rho_0}, \sqrt{(1-\rho_0)/2}\,]^T$, $\theta_0 = 0$, and $\theta_\pm = (\delta \mp \eta_0)t/\hbar$. ρ_0 is a constant. We find

$$\begin{aligned}
\langle F_x\rangle + i\langle F_y\rangle &= 2\sqrt{\rho_0(1-\rho_0)}\cos(\delta t/\hbar)\, e^{-i\eta_0 t/\hbar}, \\
\langle F_z\rangle &= m = 0.
\end{aligned} \tag{49}$$

It spirals toward and away from the origin in the $\langle F_x\rangle$-$\langle F_y\rangle$ plane. The linear Zeeman effect causes spin precessing around the magnetic field ($\hat{z}$ axis), while the quadratic Zeeman effect makes the magnitude of the spin average oscillate.

The spin evolution becomes quite different when atomic interaction is included. For the same initial conditions (of the above), the total averaged spin at time t

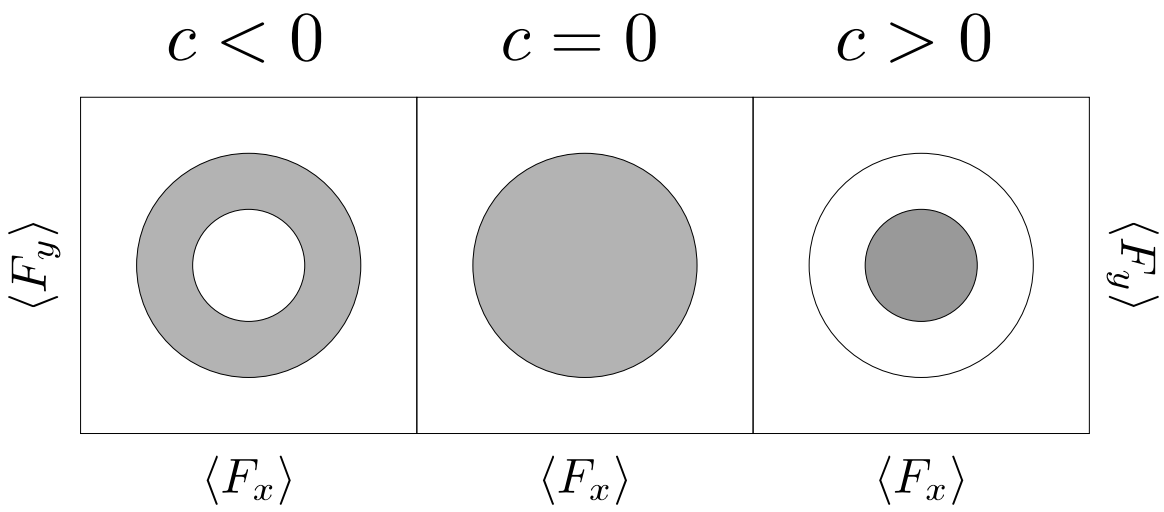

Figure 23: Two dimensional projections of the averaged spin evolution (shaded region) for a condensate with zero magnetization of noninteracting atoms (middle), in comparison with atoms of ferromagnetic (left) and antiferromagnetic interactions (right).

becomes

$$\begin{aligned} \langle F_x \rangle + i\langle F_y \rangle &= 2\sqrt{\rho_0(1-\rho_0)}\cos(\theta/2)\, e^{-i\eta_0 t/\hbar}, \\ \langle F_z \rangle &= 0, \end{aligned} \tag{50}$$

which can be conveniently confirmed from the phase space contour plot of Fig. 19, where θ is confined to oscillate around zero for ferromagnetic interactions and around π for antiferromagnetic interactions if $B < B_c$. Note that ρ_0 and θ are time-dependent for interacting condensates. Figure 23 exemplifies this oscillation in terms of the allowed regions (shaded) of $\langle F_x \rangle$ and $\langle F_y \rangle$ for interacting condensates in contrast to non-interacting ones. For ferromagnetic interactions, the allowed region is defined by two radii. One of them, $r_I = \sqrt{2\rho_0(0)[(1-\rho_0(0)) + \sqrt{(1-\rho_0(0))^2 - m^2}\,]}$, depends on the initial condition, while the other (r_B) is solely determined by the quadratic Zeeman effect. We find $r_B > r_I$ if $B < B_0$, $0 < r_B < r_I$ if $B_0 < B < B_c$, and $r_B = 0$ if $B \geq B_c$. There exists a forbidden region at the center for a ferromagnetically interacting condensate if $B < B_c$. This region shrinks to zero when $B \geq B_c$. Exactly at $B = B_c$, an interesting attractor-like feature arises and the average spin gradually

spirals towards the origin (at the center) and becomes trapped eventually after an infinitely long time. For antiferromagnetic interactions, the allowed region generally becomes smaller than that for a noninteracting condensate as shown in Fig. 23 for $m = 0$ (or $B_c = 0$). The radius of the shaded (allowed) region depends on the quadratic Zeeman effect, while the forbidden region approaches zero as $B \to \infty$.

For the general case of $m \neq 0$, the allowed region is in between the two radii $\sqrt{2\rho_0(0)[(1-\rho_0(0)) \pm \sqrt{(1-\rho_0(0))^2 - m^2}\,]}$ for a noninteracting gas. For ferromagnetic interactions, the averaged spin behaves similar to the case of $m = 0$ considered above, except now the forbidden region shrinks gradually to a minimum nonzero value of $\sqrt{2\rho_0(0)[(1-\rho_0(0)) - \sqrt{(1-\rho_0(0))^2 - m^2}\,]}$ when $B \to \infty$. In this case, there exists no B_c or homoclinic orbits. For antiferromagnetic interactions, the analogous radius r_B decreases from $r_I = \sqrt{2\rho_0(0)[(1-\rho_0(0)) - \sqrt{(1-\rho_0(0))^2 - m^2}\,]}$ to zero while B increases from zero to B_c. At $B = B_c$ the attractor-like feature remains. When B is increased from B_c, r_B increases from zero, and crosses r_I at $B = B_0$, finally approaches the radius of the allowed region for a non-interacting condensate when $B \to \infty$.

5.5 Beyond SMA: Dynamical instabilities and spatial domains

Finally, we consider the stability of these orbits, $(\rho_0(t), \theta(t))$, when small external noises are present, for example, noises from stray magnetic fields. We first discuss a ferromagnetically interacting ^{87}Rb atomic condensate whose $|+\rangle$ and $|-\rangle$ components are known to be immiscible [97]. The SMA-based spin mixing dynamics model predicts that the state consists mostly of the $|+\rangle$ and $|-\rangle$ components after $T/2$ evolution if starting from $\rho_0 \approx 1.0$ and $\theta = 0$ without an external magnetic field. At this time, the system is obviously unstable against external noises, because the $|+\rangle$ and $|-\rangle$ components tend to be phase separate. This extreme case reveals that semiclassical orbits are not always stable. As we show later these orbits are indeed dynamically

unstable. The intrinsic instability of the orbit can well be the reason of the formation of domains. On the other hand, domains always occur for large condensate when the SMA fails, consistent with several experimental observations [107].

We now address the topic of dynamical stability for a ferromagnetically interacting homogeneous spin-1 condensate without an magnetic field. The energy of the system, including all parts, is

$$\frac{E}{N} = \frac{1}{2}c_0\rho^2 + \frac{1}{2}c_2\left[m^2 + 2\rho_0(1-\rho_0) + 2\rho_0\sqrt{(1-\rho_0)^2 - m^2}\cos\theta\right], \qquad (51)$$

where $\rho = \rho_+ + \rho_0 + \rho_- = 1$ is the normalized total density of the homogeneous condensate and m is the magnetization. The energy is a constant of motion thus the sum of the second and the third terms must also be a constant. It turns out that $2\rho_0(1-\rho_0) + 2\rho_0\sqrt{(1-\rho_0)^2 - m^2}\cos\theta = \langle F_x\rangle^2 + \langle F_y\rangle^2 = f_x^2 + f_y^2$. Within the mean field approximation, the x- and y-component of the averaged spin are independently conserved in the absence of an external B-field. Thus the total averaged spin is conserved $f = \sqrt{m^2 + f_x^2 + f_y^2}$. The energy then simplifies to

$$\frac{E}{N} = \frac{1}{2}c_0\rho^2 + \frac{1}{2}c_2\left(m^2 + f_x^2 + f_y^2\right).$$

To investigate the stability of an orbit, we transform to a rotating frame where each orbit essentially collapses to a single point in the phase space diagram. For the system we consider here the free energy in the "rotating" frame becomes

$$\mathcal{F} = \frac{F}{N} = \frac{1}{2}c_0\rho^2 + \frac{1}{2}c_2\left(m^2 + f_x^2 + f_y^2\right) - \mu\rho - \eta m - \delta_x f_x - \delta_y f_y,$$

where parameters μ, η, δ_x, and δ_y define the "rotating" frame, and are Lagrange multiplies to conserve ρ, m, f_x, and f_y, respectively. This is similar to the case of a condensate in a rotating frame described with a Hamiltonian $H^{\rm rot} = H^{\rm lab} - \Omega L_z$, where Ω is the rotating angular speed, and L_z is the z-component of the angular momentum. Either Ω or L_z can be conserved with the one being physical observable, and the other serving as a Lagrange multiplier.

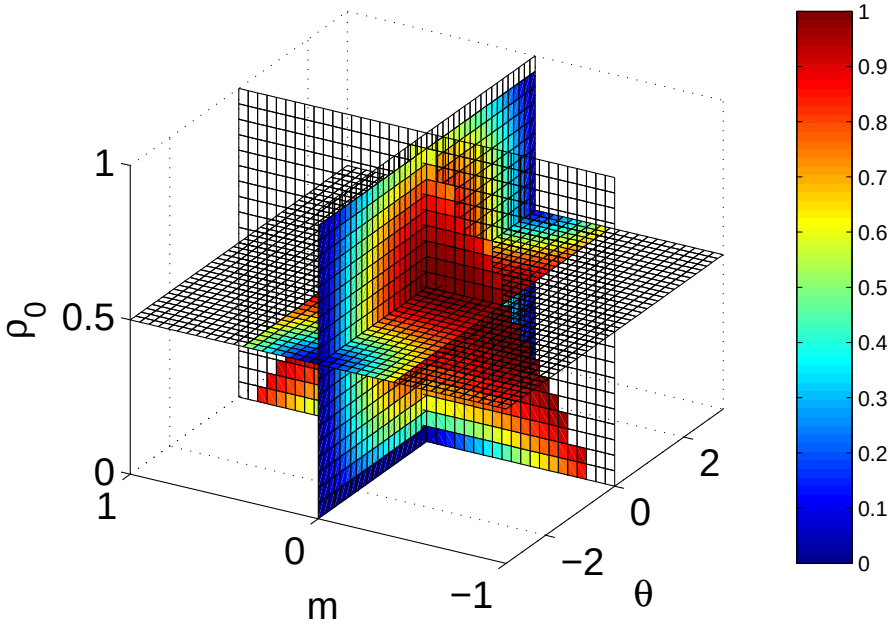

Figure 24: (Color) The dependence of the total spin f of a homogeneous spin-1 ^{87}Rb condensate on the magnetization m, the relative phase θ, and the $|0\rangle$ component fraction ρ_0. f ranges from 0 to 1 as denoted by the legend to the right.

The stationary state is obtained by finding the local minimum, maximum, or saddle points of $\mathcal{F}$ from

$$\frac{\partial \mathcal{F}}{\partial \rho} = 0, \quad \frac{\partial \mathcal{F}}{\partial m} = 0, \quad \frac{\partial \mathcal{F}}{\partial f_x} = 0, \quad \frac{\partial \mathcal{F}}{\partial f_y} = 0,$$

which lead to

$$\begin{aligned} \mu &= c_0 \rho, \\ \eta &= c_2 m, \\ \delta_x &= c_2 f_x, \\ \delta_y &= c_2 f_y. \end{aligned}$$

The stability of our system of a spin-1 condensate at a stationary state is determined by the second order derivatives of $\mathcal{F}$ described by a Hessian matrix,

$$\begin{pmatrix} \frac{\partial^2 \mathcal{F}}{\partial \rho^2} & \frac{\partial^2 \mathcal{F}}{\partial \rho \partial m} & \frac{\partial^2 \mathcal{F}}{\partial \rho \partial f_x} & \frac{\partial^2 \mathcal{F}}{\partial \rho \partial f_y} \\ \frac{\partial^2 \mathcal{F}}{\partial m \partial \rho} & \frac{\partial^2 \mathcal{F}}{\partial m^2} & \frac{\partial^2 \mathcal{F}}{\partial m \partial f_x} & \frac{\partial^2 \mathcal{F}}{\partial m \partial f_y} \\ \frac{\partial^2 \mathcal{F}}{\partial f_x \partial \rho} & \frac{\partial^2 \mathcal{F}}{\partial f_x \partial m} & \frac{\partial^2 \mathcal{F}}{\partial f_x^2} & \frac{\partial^2 \mathcal{F}}{\partial f_x \partial f_y} \\ \frac{\partial^2 \mathcal{F}}{\partial f_y \partial \rho} & \frac{\partial^2 \mathcal{F}}{\partial f_y \partial m} & \frac{\partial^2 \mathcal{F}}{\partial f_y \partial f_y} & \frac{\partial^2 \mathcal{F}}{\partial f_y^2} \end{pmatrix} = \begin{pmatrix} c_0 & 0 & 0 & 0 \\ 0 & c_2 & 0 & 0 \\ 0 & 0 & c_2 & 0 \\ 0 & 0 & 0 & c_2 \end{pmatrix}. \tag{52}$$

The system is dynamically stable if the Hessian matrix is positive definite, i.e., all the eigenvalues of the Hessian matrix are positive. The stationary state then corresponds to a local minimum of $\mathcal{F}$, and the system dynamics consists of oscillations around the minimum if perturbed by small external forces. On the other hand, the system is dynamically unstable if any eigenvalue is negative, which implies the stationary state is a saddle point or maximum and will be destabilized by an infinitesimal force along the direction of negative second order derivative.

The eigenvalues of the above Hessian matrix for a homogeneous spin-1 condensate are c_0, c_2, c_2, and c_2. Unfortunately homogeneous spin-1 condensates with ferromagnetic interactions ($c_2 < 0$) are always dynamically instable. This might be one of the reasons why it has been difficult to study experimentally the dynamics of a ^{87}Rb

spin-1 condensate. But for antiferromagnetically interacting spin-1 condensates such as ^{23}Na condensates, the dynamics is always stable ($c_2 > 0$).

Before proceeding further with our investigation of the spin mixing dynamics, we would like to comment on the studies of dynamical instabilities. Many phenomena, such as parametric instability [111], modulational instability [112], and cross phase modulational instability [113], and so on, rely on essentially the same idea as dynamical instability. A system is unstable if one or more of its eigenfrequencies are imaginary which is equivalent to the appearance of a negative eigenvalue of the above Hessian matrix. The amplitude of the corresponding eigenmode(s) with imaginary frequency would increase or decrease exponentially with time under presumed small perturbations. The phenomena of dynamically instability have been studied extensively in nonlinear optics [114] and recently in Bose-Einstein condensates which are in fact nothing but nonlinear interacting matter waves. Most of these studies have focused on single-component systems with conserved number of particles [111]. Some have also investigated two-component condensates either with conserved numbers for each species [113, 115] or with a linear coupling between the two components that can be decoupled by a linear transformation [116]. A spin-1 Bose condensate system distinguishes itself uniquely from these studied systems by the presence of spin mixing interaction, $2|0\rangle \leftrightarrow |+\rangle + |-\rangle$. It is not necessary for a spin-1 condensate to conserve the number of atoms for each component though the total atom number is usually conserved.

Robins *et al.* first studied the dynamical instability of a spin-1 condensate [112]. They found a special stationary state which is dynamically instable for a ferromagnetically interacting ^{87}Rb spin-1 condensate. Starting from this stationary state they showed the system collapses suddenly due to numerical truncation errors. Other more general studies of the dynamical instability in spin-1 condensates are not yet available to our knowledge.

Our analysis in the above shows that a homogeneous spin-1 condensate is dynamically instable. We can use the Bogoliubov-de-Genns transformation to find out more detailed information of the instability, such as what consists of the instable modes. Based on the stationary state we find above, we apply the Bogoliubov-de-Genns approximation to describe the elementary excitations in a spin-1 condensate in a matrix form as

$$M \cdot \vec{x} \;=\; \hbar\omega\vec{x}, \tag{53}$$

where the vector $\vec{x} = (\delta\psi_+,\ \delta\psi_0,\ \delta\psi_-,\ \delta\psi_+^*,\ \delta\psi_0^*,\ \delta\psi_-^*)^T$, and M is the associated matrix

$$M \;=\; \begin{pmatrix} A & B \\ -B^* & -A^* \end{pmatrix},$$

with

$$A \;=\; \begin{pmatrix} \varepsilon_k + (c_0+c_2)n_+ + c_2 n_0 & c_0\phi_0^*\phi_+ + c_2\phi_0\phi_-^* & (c_0-c_2)\phi_-^*\phi_+ \\ c_0\phi_0\phi_+^* + c_2\phi_0^*\phi_- & \varepsilon_k + c_0 n_0 + c_2(n_+ + n_-) & c_0\phi_0\phi_-^* + c_2\phi_0^*\phi_+ \\ (c_0-c_2)\phi_-\phi_+^* & c_0\phi_0^*\phi_- + c_2\phi_0\phi_+^* & \varepsilon_k + (c_0+c_2)n_- + c_2 n_0 \end{pmatrix}$$

and

$$B \;=\; \begin{pmatrix} (c_0+c_2)\phi_+^2 & (c_0+c_2)\phi_0\phi_+ & c_2\phi_0^2 + (c_0-c_2)\phi_-\phi_+ \\ (c_0+c_2)\phi_0\phi_+ & c_0\phi_0^2 + 2c_2\phi_-\phi_+ & (c_0+c_2)\phi_0\phi_- \\ c_2\phi_0^2 + (c_0-c_2)\phi_-\phi_+ & (c_0+c_2)\phi_0\phi_- & (c_0+c_2)\phi_-^2 \end{pmatrix}.$$

$\varepsilon_k = \hbar^2k^2/2\mathsf{m}$ is the kinetic energy of an elementary excitation with wave vector k.

The eigenfrequencies of these Bogoliubov modes can be found by solving the characteristic equation for $M - \hbar\omega I$. Let $y = (\hbar\omega)^2$, it turns out after some calculation that the characteristic equation becomes

$$y^3 + ry^2 + sy + t = 0, \tag{54}$$

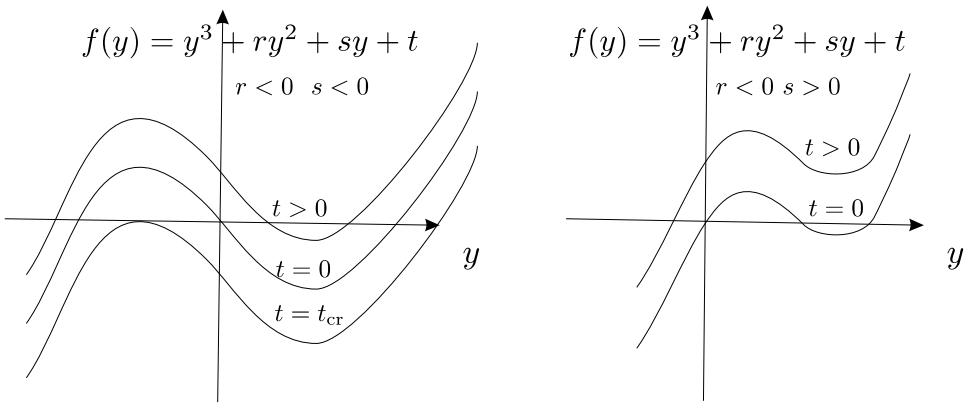

Figure 25: Cubic roots. For currently available spin-1 condensates, $r < 0$ is always satisfied. We find just one negative root under these three situations, (1) $t > 0$ and (2) $t = t_{cr}$ for $s < 0$, and (3) $t > 0$ for $s > 0$. We find two negative roots if $s < 0$ and $t_{cr} < t < 0$.

where

$$
\begin{aligned}
r &= -3\varepsilon_k^2 - 2\varepsilon_k(c_0 + 2c_2) - c_2^2 f^2, \\
s &= 3\varepsilon_k^4 + 4\varepsilon_k^3(c_0 + 2c_2) + 2\varepsilon_k^2\left[2c_2(c_2 + 2c_0) + c_2(c_2 - 2c_0)f^2\right] + 2\varepsilon_k c_2^2(c_2 + c_0)f^2, \\
t &= -\varepsilon_k^6 - 2\varepsilon_k^5(c_0 + 2c_2) - \varepsilon_k^4 c_2[4c_0(2 - f^2) + c_2(4 + f^2)] \\
&\quad -2\varepsilon_k^3 c_2^2\left[4c_0 + (c_2 - 3c_0)f^2\right] + 4\varepsilon_k^2 c_0 c_2^3 f^2(f^2 - 1).
\end{aligned}
$$

If $c_0 + 2c_2 > 0$, as true for both spin-1 ^{87}Rb and ^{23}Na condensates, we find always $r < 0$. By drawing the graph of $y^3 + ry^2 + sy + t$ for $s > 0$ and $s < 0$ (Fig. 25), we find the conditions under which y has at least one negative root,

$$
t \;\geq\; t_{\rm cr}, \quad \text{where } t_{\rm cr} = -\frac{1}{27}\left[2r^3 - 9rs + 2(r^2 - 3s)^{3/2}\right] \tag{55}
$$

for $s < 0$ or

$$
t \;>\; 0 \tag{56}
$$

for $s > 0$. Figure 25 shows that the larger the t, the more negative the root. The eigenfrequencies become imaginary if $y = (\hbar\omega)^2$ takes a negative root(s). The larger in value a negative root(s), the more rapidly decaying or increasing a mode(s) is. Figure

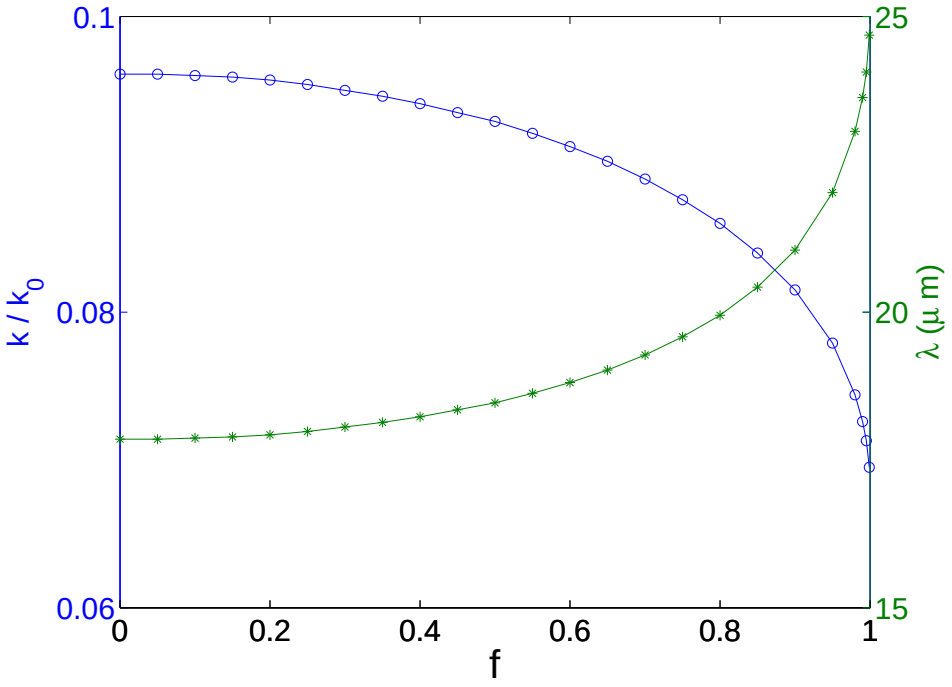

Figure 26: Elementary excitations of a homogeneous spin-1 ^{87}Rb condensate. The curve with circles denotes the wave vector of elementary excitations and the curve with asterisks denotes the corresponding wavelength to the label on the right. $k_0 = \sqrt{2mc_0n}/\hbar \approx 3.2\ \mu\text{m}^{-1}$ if $n = 1 \times 10^{14}$ cm^{-3}.

26 displays the largest wave vector with an imaginary frequency for a given f and the corresponding wavelength of the elementary excitations at density $n = 1 \times 10^{14}$ cm^{-3} for a homogeneous ^{87}Rb spin-1 condensate.

We find explicitly a ferromagnetically interacting homogeneous spin-1 condensate is dynamically instable. The direct consequence of the dynamical instability is the formation of spin domains. But the road map to the domain formation is not so obvious from above analysis. We have to give a clearer picture of the domain formation in the lab reference frame instead of in the rotating frame since experimental observations are sometimes easier to understand in lab frame.

We focus on the partial derivative of $\mathcal{E} = E/V$ from Eq. (51) with respect to m, $d\mathcal{E}/dm$, which is related to the formation of spin domain for ferromagnetically

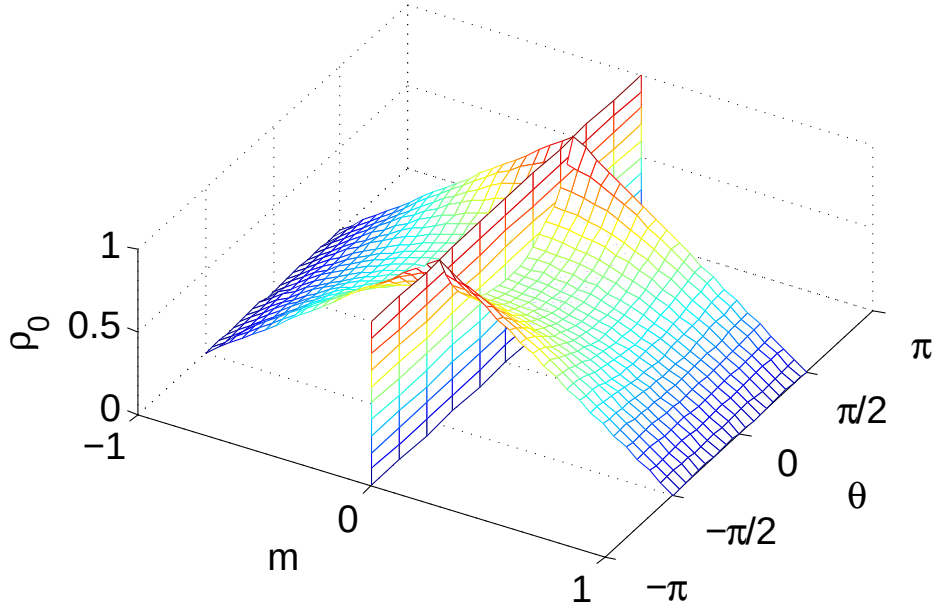

Figure 27: (Color) Surfaces of $d\mathcal{E}/dm = 0$.

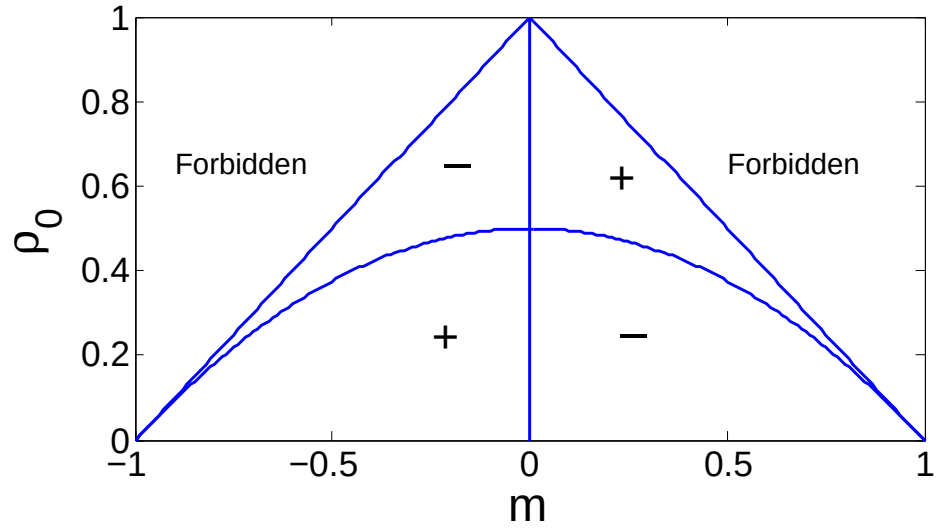

Figure 28: Cross-section of Fig. 27 at $\theta = 0$. Plus signs denote $d\mathcal{E}/dm > 0$ and minus signs denote $d\mathcal{E}/dm < 0$.

interacting homogeneous spin-1 condensates. We find

$$\frac{d\mathcal{E}}{dm} = c_2 m \left[1 - \frac{\rho_0 \cos\theta}{\sqrt{(1-\rho_0)^2 - m^2}} \right]. \quad (57)$$

Figure 27 shows the surfaces where the above first order derivative is zero. The part above the saddle surface in Fig. 27 of an orbit is stable and the part below is unstable if $c_2 < 0$. Here the meaning of "stable" is generalized, referring to the dynamical property where the local magnetization tends to oscillate around $m = 0$. For example, in the top right allowed region of $d\mathcal{E}/dm > 0$. To lower the configuration energy $\mathcal{E} \approx \mathcal{E}(m) + (d\mathcal{E}/dm)\Delta m$, $\Delta m < 0$ is required. Thus m tends to decrease to zero. While in the left top allowed region $\Delta m > 0$ is required and m tends to increase to zero. Thus the whole top allowed region (including left and right) tends to have m oscillate around zero. On the contrary the bottom allowed region tends to have m run away from zero and form spin domains. The net effect leads to orbits being dynamically instable and eventually formation of spin domains.

For an antiferromagnetically interacting spin-1 condensate ($c_2 > 0$), θ usually oscillates around π. Thus $d\mathcal{E}/dm > 0$ for $m > 0$ and $d\mathcal{E}/dm < 0$ for $m < 0$. So the magnetization always oscillates around zero and no domain forms. This coincides with the conclusion of dynamical stability analysis for an antiferromagnetically interacting spin-1 condensate.

To justify the above analysis for the instability we have performed two simulations with the same initial condition for a ^{87}Rb condensate ($\rho_0(0) = 0.744, \theta(0) = 0$, which is the ground state for $N = 2.0 \times 10^5$ at $B = 0.3$ G and $M = 0$), in a trap $V_{\rm ext}(\vec{r}) = (\mathsf{m}/2)(\omega_x^2 x^2 + \omega_y^2 y^2 + \omega_z^2 z^2)$ with $\omega_x = \omega_y = (2\pi)240$ Hz and $\omega_z = (2\pi)24$ Hz. For one simulation, we intentionally add small white noise ($\sim 1.0 \times 10^{-5}$) to the wave function during the evolution. It is not done for the other. Our numerical results show that it takes a shorter time for the $|+\rangle$ and $|-\rangle$ components to separate with a white-noise-perturbed condensate. This is due to the fact that the truncation error is much smaller than the added white noise in our simulations [111] . Figure 29 shows

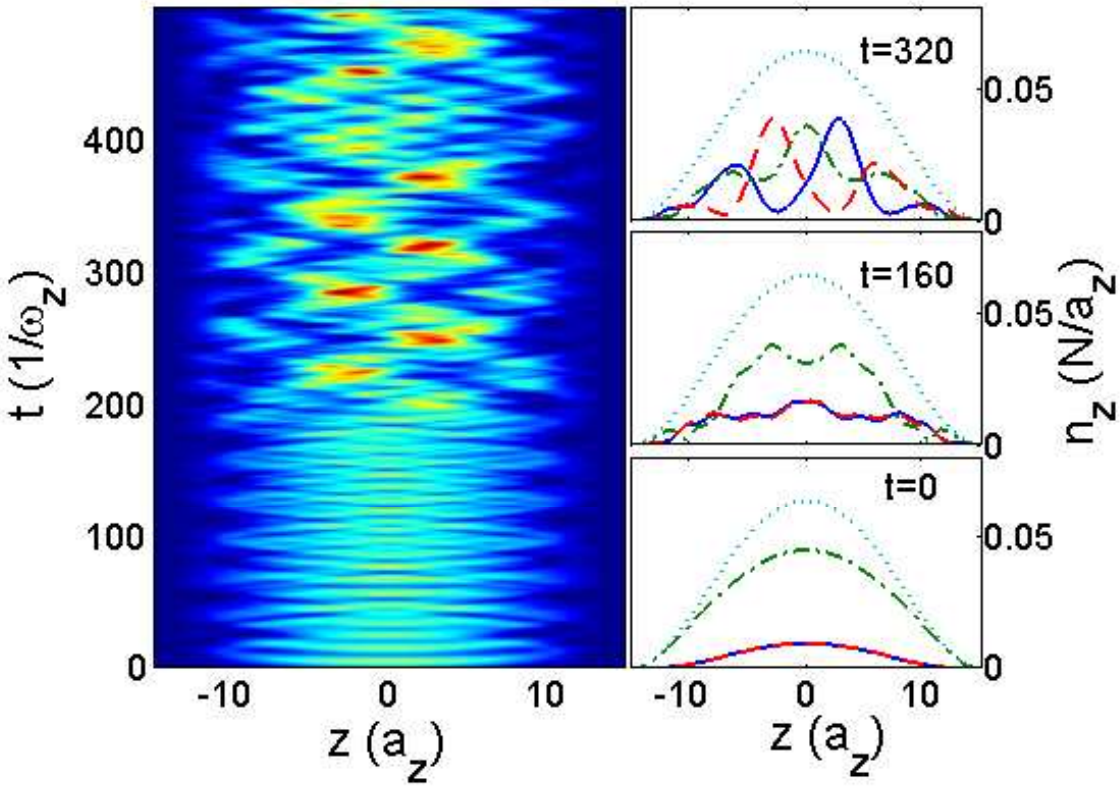

Figure 29: (Color) Typical evolution for a ^{87}Rb condensate and the formation of spin domains due to a dynamical instability. The initial state is the ground state at $B = 0.3$ G. The magnetic field is then set to zero and a small white noises are added throughout the evolution. The left contour plot is the evolution of the $|+\rangle$ component. The right column shows the density distribution of all three components at times $t = 0, 160, 320$ $(1/\omega_z)$. Solid lines denote the $|+\rangle$ component, dash-doted lines refer to the $|0\rangle$ component, dashed lines label the $|-\rangle$ component, and dotted lines are for the total density. $n_z = \int |\phi|^2 2\pi r dr$ is the density along z-direction.

the evolution of the density distribution along z-direction (r-direction is integrated out). We see that the phase separation between $|+\rangle$ and $|-\rangle$ components actually indicates the formation of domains (note the total magnetization, M/N, is conserved to within 1.0×10^{-5}). So we can safely infer that the formation of domains for ^{87}Rb is due to the dynamical instability. The domain width (an upper limit) can be estimated by the spin healing length (or penetration depth), $\xi = h/\sqrt{2\mathsf{m}|c'|} \simeq 8(a_z) \approx 17\mu$m, where $a_z = \sqrt{\hbar/\mathsf{m}\omega_z}$ and the average condensate density used is about 1.9×10^{14} cm^{-3}.

5.6 Conclusions

In conclusion we have studied the interaction driven off-equilibrium collective oscillations of an atomic spin-1 condensate in a uniform magnetic field. The dynamics of spin mixing is found to be well described by a nonrigid pendulum due to the conservations of atom numbers, atomic magnetization, and the total energy. In particular, we find that there exists an interesting class of critical trajectories whose oscillation periods approach infinity. The dynamical instability of these orbits can lead to a phase separation of the $|+\rangle$ and $|-\rangle$ components for a ^{87}Rb condensate and subsequently to the formation of spin domains. Our study suggests the use of quadratic Zeeman shift to probe pendulum-like oscillations in a spin-1 condensate and provides the complete spin mixing dynamics analytically.

Finally we would like to point out that we have excluded some extreme cases, such as $\rho_0(t = 0) = 0$ and $\rho_0(t = 0) = 1$ from our mean field studies, as these situations cannot be accurately described by the mean field theory and will require higher order corrections, for instance, inclusion of quantum fluctuations and coupling to the environment.

CHAPTER VI

SOLITON IN A TRAPPED SPIN-1 CONDENSATE

6.1 Introduction

A solitonic condensate state is an excited eigenstate of the nonlinear Schrödinger equation (NLSE). Solitons have been extensively studied in nonlinear optics [114] and also recently in atomic Bose condensates [117], particularly for homogeneous spin-1 condensates with a restricted form of ferromagnetic interaction [118]. From the experimental point of view, a spin-1 Bose condensate is usually confined in an optical trap, which can significantly affect the spatial propagation of a soliton. Instead of adopting the analytical method as in [118], we employ numerical approaches to find soliton states in a trapped spin-1 condensate. We observe that the density of the obtained soliton state becomes time-independent under a special canonical transformation.

6.2 An effective quasi-one-dimensional description

Although our ability to perform numerical simulations keeps increasing with computer technology, full 3D time dependent calculations still represent a significant challenge. In many situations, one explores the inherent system symmetries, e.g. cylindrical and spherical symmetries in space, to reduce the numbers of spatial dimension from 3D to 2D or even 1D. The description of atomic condensate dynamics in terms of a mean field theory is such an example. With a tight radial confinement, a condensate becomes cigar-shaped. Several effective 1D approaches have been developed [117, 119, 120, 121, 122], with the simplest of them assuming a fixed transverse Gaussian profile.

Recent studies, however, have indicated that the effective quasi-1D non-polynomial Schrödinger equation (NPSE) is the most powerful and efficient tool, at least for a weakly interacting atomic condensate [117, 119, 120]. In this section, we generalize such an NPSE approach to the case of a spin-1 atomic condensate in a cigar-shaped trap [123].

Several recent experiments of the spin-1 condensate use a single running wave optical trap, i.e. in a cigar-shaped trap [54, 55, 56, 107]. To provide a proper theoretical description for these observations, numerical approaches have been used to study the nonlinear spatial-temporal dynamics for a spin-1 condensate. It is therefore desirable to have a more efficient theoretical approach instead of the 3D coupled Gross-Pitaevskii (GP) equations that is uniformly valid to both strongly and weakly interacting limits.

A spin-1 Bose condensate is described by the Hamiltonian in second quantized form by Eq. (17). Adopting the mean field theory when the condensate consists of a large number of atoms, we introduce the condensate order parameter or wave function $\Phi_i = \langle \Psi_i \rangle$ for the ith component. Neglecting quantum fluctuations we arrive at the mean field energy functional,

$$\begin{aligned} E[\Phi_i, \Phi_i^*] &= \int d\vec{r} \left[\Phi_i^* \left(-\frac{\hbar^2}{2\mathsf{m}} \nabla^2 + V_{\rm ext} + E_i \right) \Phi_i \right. \\ &+ \left. \frac{c_0}{2} \Phi_i^* \Phi_j^* \Phi_j \Phi_i + \frac{c_2}{2} \Phi_k^* \Phi_i^* \left(F_\alpha\right)_{ij} \left(F_\alpha\right)_{kl} \Phi_j \Phi_l \right], \end{aligned} \tag{58}$$

from which the coupled GP equations can be derived according to $i\hbar\, \partial \Phi_i / \partial t = \delta E / \delta \Phi_i^*$. They are given in explicit form in Eq. (36).

The external trap is assumed harmonic $V_{\rm ext} = \mathsf{m}(\omega_\perp^2 r_\perp^2 + \omega_z^2 z^2)/2$ with cylindrical symmetry $\omega_x = \omega_y = \omega_\perp$, and $\omega_z \ll \omega_\perp$, i.e. cigar shaped. Following the successful approach of the NPSE description as for a single component scalar condensate [120], we factor the wave function into transversal and longitudinal functions as

$$\Phi_i(\vec{r}_\perp, z; t) = \sqrt{N}\, \Phi_\perp(\vec{r}_\perp; \chi(z,t)) f_i(z,t), \tag{59}$$

where χ and f_i are variational functions which depend on z and t. $\Phi_\perp$ is the transversal wave function, satisfying $\int d\vec{r}_\perp |\Phi_\perp|^2 = 1$, and is assumed identical for all components. Substituting Eq. (59) into Eq. (36), we obtain the Lagrangian of our system as

$$\begin{aligned}
\mathcal{L} &= \int d\vec{r} \sum_i \Phi_i^*(\vec{r},t)\left[i\hbar\frac{\partial}{\partial t} + \frac{\hbar^2}{2\mathsf{m}}\nabla^2 - V_{\rm ext} - E_i - \frac{c_0 N}{2}\sum_j |\Phi_j|^2\right]\Phi_i(\vec{r},t) \\
&\quad -\frac{c_2 N}{2}\int d\vec{r}\Big[|\Phi_+|^4 + |\Phi_-|^4 + 2|\Phi_+|^2|\Phi_0|^2 + 2|\Phi_-|^2|\Phi_0|^2 - 2|\Phi_+|^2|\Phi_-|^2 \\
&\quad +2\Phi_0^{*2}\Phi_+\Phi_- + 2\Phi_+^*\Phi_-^*\Phi_0^2\Big] \\
&= \int dz\left\{\sum_i f_i^*(z,t)\left[i\hbar\frac{\partial}{\partial t} + \frac{\hbar^2}{2\mathsf{m}}\frac{\partial^2}{\partial z^2} - V(z) - E_i - E_\perp(\chi)\right.\right. \\
&\quad \left.\left. -\tilde{\eta}(\chi)\frac{c_0 N}{2}\tilde{n}(z)\right] f_i(z,t) - \tilde{\eta}(\chi)\frac{c_2 N}{2}S_2\right\}, \qquad (60)
\end{aligned}$$

where $V(z) = \mathsf{m}\omega_z^2 z^2/2$. $E_\perp$ is the transverse mode energy,

$$E_\perp(\chi) = \int d\vec{r}_\perp \Phi_\perp^*[-(\hbar^2\nabla_\perp^2/2\mathsf{m}) + (\mathsf{m}\omega_\perp^2 r_\perp^2/2)]\Phi_\perp.$$

$\tilde{\eta}$ is the scaling factor of the nonlinear interaction strength, $\tilde{\eta}(\chi) = \int d\vec{r}_\perp |\Phi_\perp|^4$. $\tilde{n}(z) = \sum_i |f_i|^2$, and S_2 is independent of χ and given by

$$S_2 = \left(|f_+|^4 + |f_-|^4 + 2|f_+|^2|f_0|^2 + 2|f_-|^2|f_0|^2 - 2|f_+|^2|f_-|^2 + 2f_0^{*2}f_+f_- + 2f_+^*f_-^*f_0^2\right).$$

To obtain the above result, we have also assumed a weak time and z dependence of the transverse wave function, i.e. $\partial\Phi_\perp/\partial t \simeq 0$ and $\nabla^2\Phi_\perp \simeq \nabla_\perp^2\Phi_\perp$. The effective quasi-1D NPSE for a spin-1 condensate can now be derived from the least action principle of the above Lagrangian,

$$\begin{aligned}
i\hbar\frac{\partial}{\partial t}f_+ &= \left[-\frac{\hbar^2}{2\mathsf{m}}\frac{\partial^2}{\partial z^2} + V(z) + E_+ + E_\perp + c_0 N\tilde{\eta}\tilde{n} + c_2 N\tilde{\eta}(\tilde{n}_+ + \tilde{n}_0 - \tilde{n}_-)\right] f_+ \\
&\quad +c_2 N\tilde{\eta} f_0^2 f_-^*, \\
i\hbar\frac{\partial}{\partial t}f_0 &= \left[-\frac{\hbar^2}{2\mathsf{m}}\frac{\partial^2}{\partial z^2} + V(z) + E_0 + E_\perp + c_0 N\tilde{\eta}\tilde{n} + c_2 N\tilde{\eta}(\tilde{n}_+ + \tilde{n}_-)\right] f_0 \\
&\quad +2c_2 N\tilde{\eta} f_+ f_- f_0^*, \\
i\hbar\frac{\partial}{\partial t}f_- &= \left[-\frac{\hbar^2}{2\mathsf{m}}\frac{\partial^2}{\partial z^2} + V(z) + E_- + E_\perp + c_0 N\tilde{\eta}\tilde{n} + c_2 N\tilde{\eta}(\tilde{n}_- + \tilde{n}_0 - \tilde{n}_+)\right] f_- \\
&\quad +c_2 N\tilde{\eta} f_0^2 f_+^*, \\
\tilde{n}\frac{\partial E_\perp}{\partial\chi} &+ \left(\frac{c_0 N}{2}\tilde{n}^2 + \frac{c_2 N}{2}S_2\right)\frac{\partial\tilde{\eta}}{\partial\chi} = 0, \qquad (61)
\end{aligned}$$

where $\tilde{n} = \sum_i \tilde{n}_i$ is the total density and $\tilde{n}_i = |f_i|^2$ is the density of the ith component.

We discuss two separate ansatzs for the transverse function applicable respectively for the case of weak and strong atomic interactions.

- **A Gaussian ansatz**

  For weak atomic interaction when $\mu - E_\perp \ll \hbar\omega_\perp$ is satisfied, the transverse wave function can be taken as a Gaussian function of a variable width,

$$\Phi_\perp(\vec{r}_\perp; \chi(z,t)) = \frac{1}{\pi^{1/2}\chi} \exp[-r_\perp^2/2\chi^2]. \tag{62}$$

  The transverse mode energy and scaling factor are then given by

$$E_\perp = \frac{\hbar\omega_\perp}{2}\left(\frac{a_\perp^2}{\chi^2} + \frac{\chi^2}{a_\perp^2}\right), \tag{63}$$

$$\tilde{\eta} = \frac{1}{2\pi\chi^2}, \tag{64}$$

  where $a_\perp = \sqrt{\hbar/\mathsf{m}\omega_\perp}$.

- **A Thomas-Fermi ansatz**

  For strong atomic interactions when $\mu - E_\perp \gg \hbar\omega_\perp$ holds, the transverse wave function is taken as a Thomas-Fermi (TF) ansatz,

$$\Phi_\perp(\vec{r}_\perp; \chi(z,t)) = \begin{cases} \sqrt{\frac{2}{\pi}}\,\frac{1}{\chi}\sqrt{1-\left(\frac{r_\perp}{\chi}\right)^2}, & r_\perp \le \chi; \\ 0, & r_\perp > \chi. \end{cases} \tag{65}$$

  The kinetic energy in the transverse direction is neglected, leading to the transverse mode energy and scaling factor as

$$E_\perp = \frac{\hbar\omega_\perp}{6}\left(\frac{\chi^2}{a_\perp^2}\right), \tag{66}$$

$$\tilde{\eta} = \frac{4}{3\pi\chi^2}. \tag{67}$$

We have performed extensive numerical simulations to illustrate the efficiency and effectiveness of the NPSE as developed by us for a spin-1 condensate in a cigar-shaped trap. For the first example, we computed the ground state of a ^{87}Rb spin-1

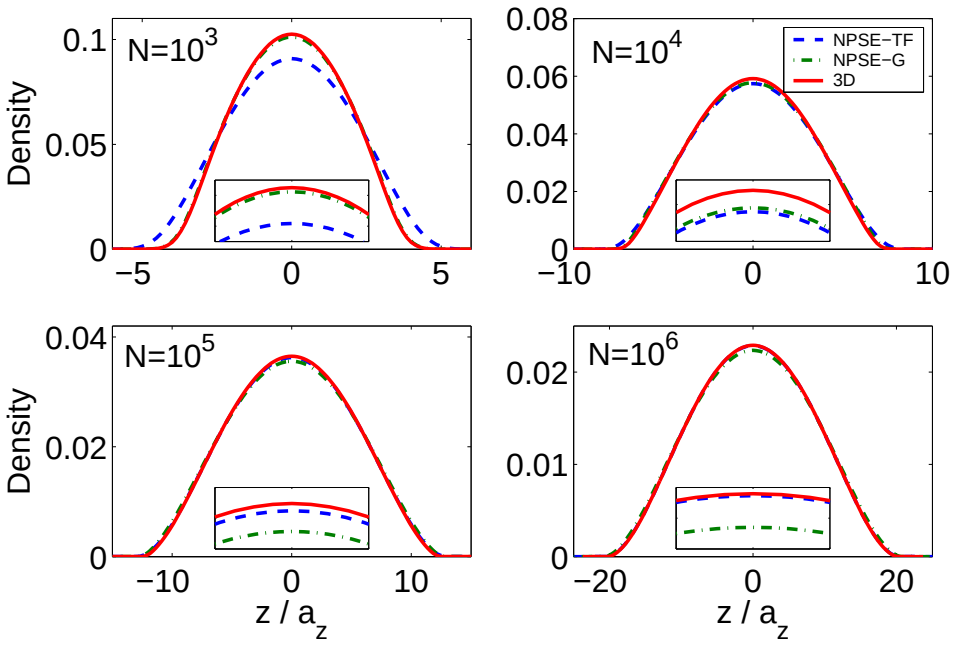

Figure 30: The ground state density distribution of the condensate in $|0\rangle$ component along the axis of a cigar-shaped trap, for ^{87}Rb atoms and without an external magnetic field. The inset shows the zoom-in central region. The solid line denotes the "exact", while the dashed and dash-dot lines denote respectively the results from our NPSE with a TF or a Gaussian ansatz for the transverse profile.

condensate by propagating the GP equations and the effective 1D NPSE with an imaginary time. The atomic parameters of ^{87}Rb are $a_0 = 101.8\,a_{\rm B}$ and $a_2 = 100.4\,a_{\rm B}$ [95]. The trap frequencies are $\omega_\perp = (2\pi)240$ Hz and $\omega_z = (2\pi)24$ Hz. The "exact" solution as given by the ground state of the full 3D coupled GP equations (36) is calibrated by its effective 1D distribution according to $|f_i(z)|^2 = \int d\vec{r}_\perp |\Phi_i|^2$. Figure 30 illustrates the results for several cases of different total number of atoms, N. We note that with increasing N, the mean field interaction becomes stronger. For weak interactions the quasi-1D NPSE with a Gaussian variational ansatz gives a better result, while for strong interactions the quasi-1D NPSE with a TF ansatz is a better choice. Here "better" means the result obtained from an NPSE is closer to that of the full 3D solution. We also observe that the quasi-1D NPSE with a TF ansatz gives a lower central density and over-estimates the TF radius in the weak interaction regime, while the quasi-1D NPSE with a Gaussian ansatz gives a lower central density

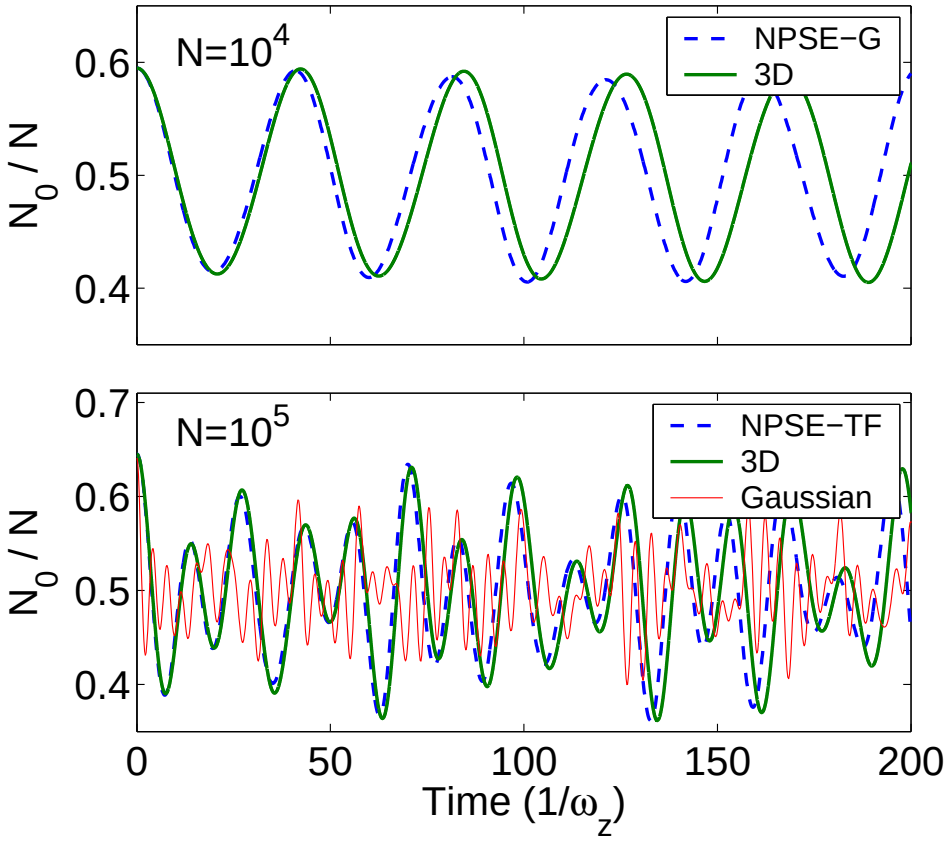

Figure 31: Time dependence of the fractional condensate population in the $|0\rangle$ state N_0/N. Thick solid curve denotes the full 3D simulation while the dashed curve denotes the simulation with our effective quasi-1D NPSE. We have used $N = 10^4$ for the top part and $N = 10^5$ for the bottom. As a comparison we also presented the result obtained from a widely adopted time-independent Gaussian ansatz (thin solid curve in the bottom panel), which is shown to give a poor agreement in the strong interaction regime.

and a correspondingly larger width in the strong interaction regime. Over all, it is interesting to point out that the quasi-1D NPSE with a Gaussian ansatz is not too bad even in the strong interaction regime.

To test the quasi-1D NPSE more strictly we study the dynamics of a spin-1 condensate out of equilibrium configuration and compare the results with those from a full 3D simulation with the coupled GP equations (36). The initial state is taken as the ground state in a given magnetic field. The simulation starts after the magnetic field is set zero, and we follow the spatial-temporal dynamics. With our NPSE, it

becomes essentially a trivial task, and we find that excellent agreements are obtained with a Gaussian ansatz, e.g. with $N = 10^3$ atoms for weak interactions, and a TF ansatz for strong interactions with $N = 10^6$ atoms. In the results to be given below, we instead use the effective quasi-1D NPSE to simulate the dynamics in the limit between the strong and weak interactions, i.e. for $\mu - \hbar\omega_\perp \sim \hbar\omega_\perp$. For the quasi-1D NPSE approach, we use a Gaussian ansatz with $N = 10^4$ atoms ($E - \hbar\omega_\perp = 1.74\,\hbar\omega_\perp$) and a TF ansatz with $N = 10^5$ atoms ($E - \hbar\omega_\perp = 4.98\,\hbar\omega_\perp$). Figure 31 displays the time evolution of the fractional condensate in the $|0\rangle$ state. For weak interactions, all three components share the space profile along the z axis, and the out of equilibrium dynamics is periodic [53, 63, 102]. Figure 31 also clearly shows the periodic motion for $N = 10^4$ atoms, although we do find that the quasi-1D NPSE gives a slightly shorter period than that of the full 3D simulation. For strong interactions, the apparent spatial profiles of the three spin components clearly becomes different, and the out of equilibrium dynamics also becomes complicated. Yet still, the quasi-1D NPSE simulations give results very close to the "exact" 3D solution, especially in the short time range. Figure 32 compares the dependence of the density distribution of the $|0\rangle$ state component on time and space from quasi-1D NPSE and full 3D simulation. The excellent agreement clearly demonstrates the efficiency and effectiveness of the quasi-1D NPSE approach, although we do find that it always seems to give a slightly shorter oscillation period as compared to the "exact" result.

We now discuss the conditions under which our quasi-1D NPSE description is applicable. For a true 1D condensate which enters the Tonks gas regime [27, 30], our result is obviously not applicable. In the derivations of the quasi-1D NPSE, we have assumed a weak time- and z-dependence of the transverse mode. This assumption is valid only for weak excitations of the condensate such that the excitation in the transverse direction is negligible. In other words, the wavelength of the excitation is longer than the transverse size of the condensate. Under this condition, the transverse

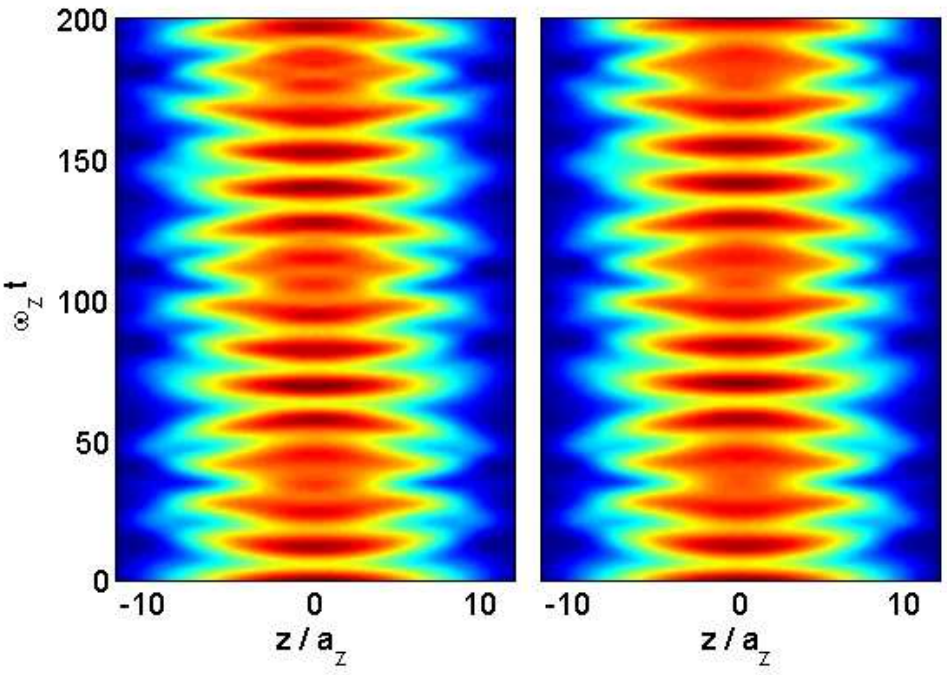

Figure 32: (Color) Contour plot of the density of the $|0\rangle$ component of a condensate with respect to time and z. The left one is from the quasi-1D NPSE while the right one is the "exact" result from a full 3D simulation. Parameters are the same as in Fig. 31.

mode is reduced to the ground state which is a Gaussian in the weakly interacting limit and a TF profile in the strongly interacting limit. For spin-1 condensates widely discussed now, either of ^{23}Na or ^{87}Rb atoms, the spin-dependent excitation is always weak since c_2 is two or three orders of magnitude smaller than c_0. The wavelength of the spin wave is thus larger than the transversal size of the condensate for a cigar-shaped trap [41, 45, 46, 54, 55, 56, 107]. Our resulting NPSE model can thus be directly applied. For a strongly excited system, one has to include the transverse motion, with a more general approach as developed by Kamchatnov and Shchesnovich in [124] and Salasnich *et al.* in [125].

6.3 Soliton in a trapped spin-1 Bose condensate

Condensate solitons are loosely defined as high energy eigenstates of the GP equation (36). Armed with the quasi-1D NPSE approach and the imaginary time propagation method, we have performed extensive search for solitonic states. Numerically we first find the ground state, then we propagate the GP equation in imaginary time domain but subtract out the ground state projection at each time step during evolution,

$$\Phi^{(n)} \quad \rightarrow \quad \Phi^{(n)} - \langle \Phi_0 | \Phi^{(n)} \rangle | \Phi_0 \rangle. \tag{68}$$

For the second excited soliton state, we subtract the projections of both the ground state and the first excited state, and analogously for higher energy soliton states. The main restriction is the numerical precision which limits us to be capable of finding only one soliton state accurately.

An example of the soliton we find in a trapped spin-1 ^{87}Rb condensate is illustrated in Fig. 33. We see a π phase shift in the $|0\rangle$ component near the central region, and also notice that the $|+\rangle$ and $|-\rangle$ components are symmetric with respect to the trap center $z = 0$. Starting from this solitonic state we have propagated the GP equation, and the time dependence of the $|0\rangle$ component fraction is as shown in Fig. 34. We see clearly periodic oscillations in the fractional population of each component from

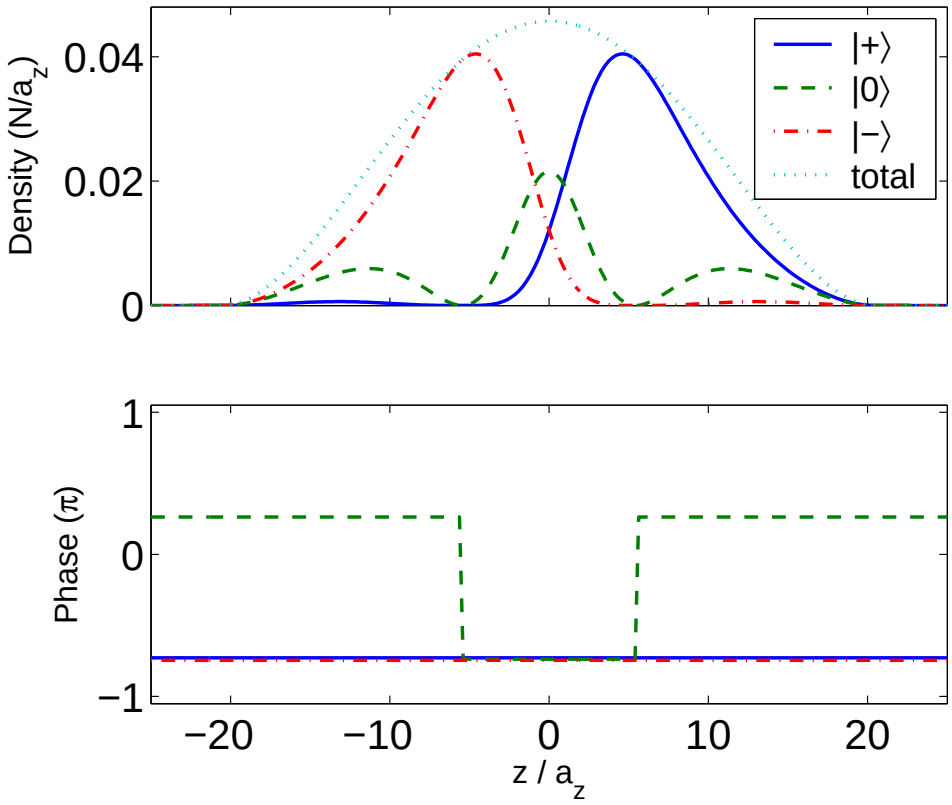

Figure 33: The wave function of a soliton state in a trapped spin-1 ^{87}Rb condensate. The trap parameters are $\omega_x = \omega_y = (2\pi)240$ Hz and $\omega_z = (2\pi)24$ Hz. The total number of atoms in the trap is $N = 10^6$ and the total magnetization is zero. The solid curves denote the density (the upper panel) and the phase (the lower panel) for the $|+\rangle$ component, the dash-dotted curves denote the $|0\rangle$ component, the dashed curves denote the $|-\rangle$ component, and the dotted curve (the upper panel) denotes the total density.

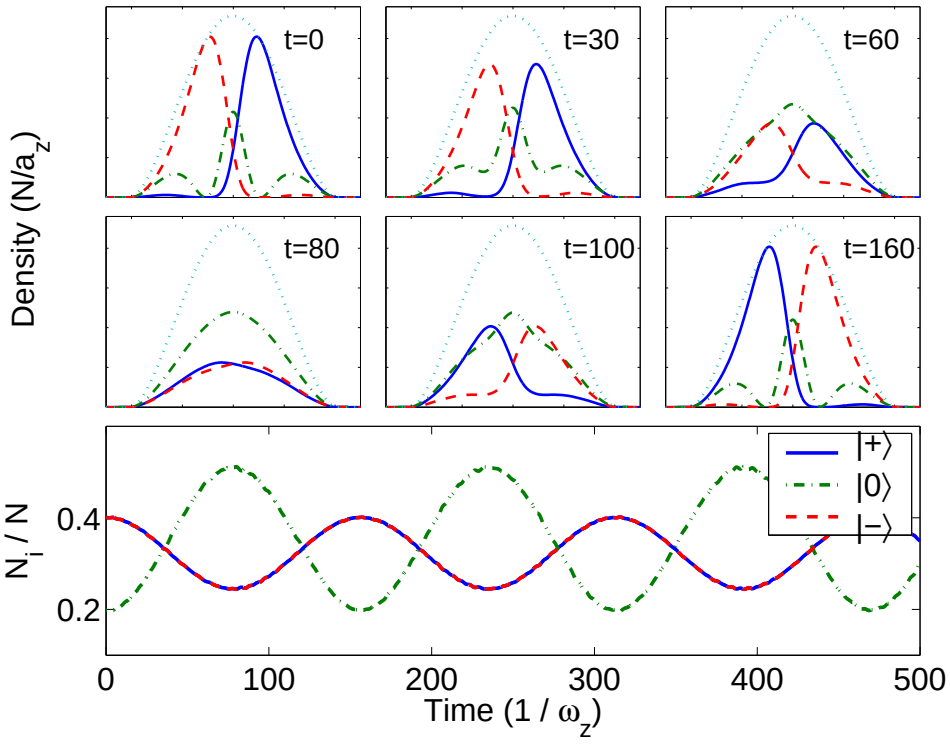

Figure 34: Propagation of a soliton in a trap. The upper and the middle rows display the density distribution of the soliton at different times. The lower row shows the time dependence of the fractional populations of every spin components. The parameters and notations are the same as in Fig. 33.

the curves in the lower row of Fig. 34. From the upper and middle rows we see the density distribution varies with time. The $|+\rangle$ and $|-\rangle$ components tunnel through each other with the assistance of the $|0\rangle$ component. The tunnelling process would be much slower if $|0\rangle$ component is absent. Such a process is often called a soliton collision in nonlinear science [118]. This collision was explained in terms of a mutual precession among the three components as in Ref. [118]. We can actually extract the precession angles for both the $|+\rangle$ and $|-\rangle$ components as π since they just exchange their positions after the collision, i.e., spin up becomes spin down and vice versa. The interesting feature for a trapped system, distinct from the homogeneous one, is that the collision process repeats itself cyclically upon reflections from the boundaries.

A propagating soliton with a constant speed is actually stationary in a special moving frame. A wonderful story of this is that J. S. Russell once followed the water

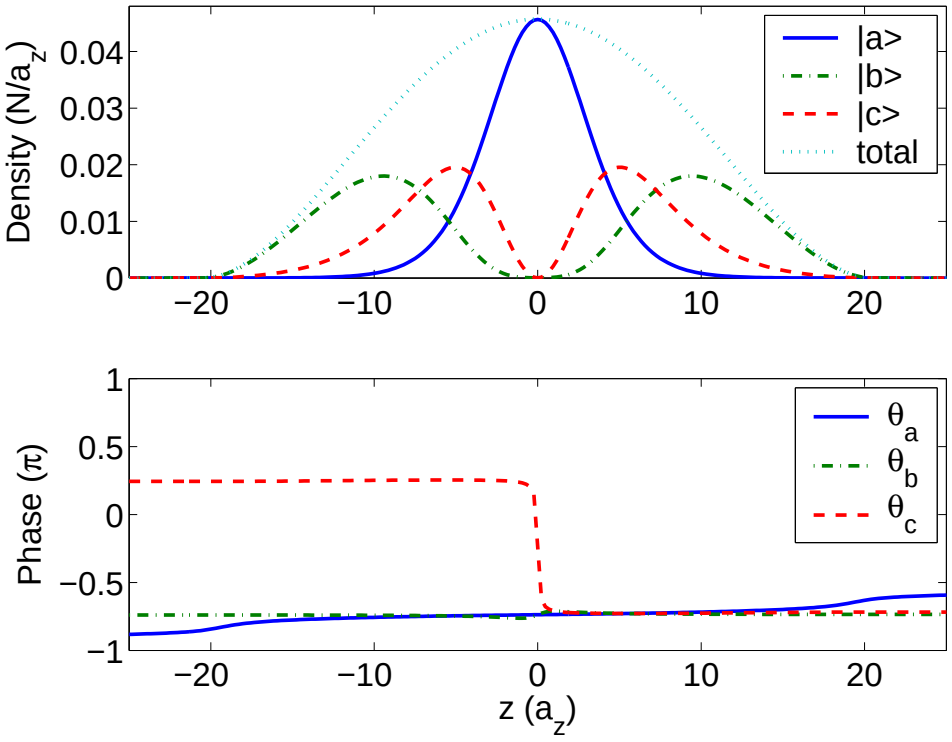

Figure 35: Density and phase distributions of the soliton after the transformation (Eq. 69). The density becomes time independent. This is actually a one dimensional Mermin-Ho vortex.

wave soliton for a few miles. This is also true for a soliton in a spin-1 condensate. We find that the density of the soliton becomes time independent with the following canonical transformation,

$$\begin{aligned} \Phi_a &= \frac{1}{\sqrt{2}}(\Phi_+ - \Phi_-), \\ \Phi_b &= \frac{1}{\sqrt{2}}\left[\frac{1}{\sqrt{2}}(\Phi_+ + \Phi_-) + \Phi_0\right], \\ \Phi_c &= \frac{1}{\sqrt{2}}\left[\frac{1}{\sqrt{2}}(\Phi_+ + \Phi_-) - \Phi_0\right]. \end{aligned} \tag{69}$$

Figure 35 shows the density and phase distributions of component $|a\rangle$, $|b\rangle$, and $|c\rangle$. The density is time independent after the transformation. According to Ref. [79], we find that this is in fact simply a 1D Mermin-Ho vortex.

6.4 Conclusions

In summary, we have extended the successful effective quasi-1D non-polynomial Schrödinger equation (NPSE) for a single component scalar condensate to a multi-component spin-1 condensate in a cigar-shaped trap. We have demonstrated its validity with a Gaussian ansatz for the transverse profile in the weak interaction regime and with a Thomas-Fermi (TF) ansatz in the strong interaction regime. We have further demonstrated its effectiveness with studies on both the static (ground state) and dynamic properties of a spin-1 ^{87}Rb condensate in a cigar-shaped harmonic trap. With the effective quasi-1D NPSE, simulations for out of equilibrium condensate dynamics become rather efficient, thus allowing for detailed comparisons with the recently observed spatial temporal dynamics in spin-1 condensates.

Armed with the quasi-1D NPSE, we have searched for collectively excited, or soliton states in a trapped spin-1 ^{87}Rb Bose condensate. Starting from a soliton state we find, the soliton propagates in the trap. This propagation process is explained as mutual precession among different components. We also find a canonical transformation which leads the time dependent propagation of the soliton into a time independent density profile. The state after the transformation is found to resemble a one dimensional Mermin-Ho vortex state.

APPENDIX A

FINDING THE GROUND STATE NUMERICALLY: IMAGINARY TIME PROPAGATION METHOD

We employ the imaginary time propagation method [126, 127] to search for the ground state. We give a rather brief summary of this algorithm in the following. More detailed discussions can be found in Ref. [128]. For a quantum system described by a Hamiltonian H, the Schrödinger equation is,

$$i\hbar\frac{\partial\psi}{\partial t} = H\psi.$$

In imaginary time domain $\tau = it$ the above Schrödinger equation becomes (setting $\hbar = 1$)

$$-\frac{\partial\psi}{\partial\tau} = H\psi,$$

where we have shifted to make sure all eigenvalues of H are positive. Numerically the time derivative is approximated by a first-order forward difference formula with a time step $\Delta\tau$

$$\frac{\psi^{(n+1)} - \psi^{(n)}}{\Delta\tau} = -H\psi^{(n)}.$$

Spatial derivatives in H are also approximated by a finite difference method or can be computed by fast Fourier transform (FFT). Given an initial wave function $\psi^{(0)}$, we propagate numerically the wave function according to

$$\psi^{(n+1)} = \psi^{(n)} - \Delta\tau H\psi^{(n)},$$

until a stable convergent solution is found. We normalize ψ at the end of each iteration. The initial wave function is usually taken as a Gaussian for weak interaction or parabola shaped for strong interaction (TF limit).

The imaginary time propagation method is a quantum version of the steepest descent method or downhill search method in an infinite dimensional configuration space expanded by $\psi(x)$ and $\psi^*(x)$. Physically, it corresponds to decay process from initial state to the final ground state. Expanding the initial wave function $\psi^{(0)}$ according to the eigenfunctions ϕ_i of H,

$$\psi^{(0)} = \sum_i c_i^{(0)} \phi_i,$$

at step n,

$$\psi^{(n)} = \sum_i c_i^{(0)} e^{-E_i n \Delta\tau} \phi_i^{(0)}.$$

The higher the energy of an eigenstate, the more rapidly it decays. Since we normalize the wave function at each step, the converged wave function contains essentially only the ground state component.

Strictly speaking, the above explanation is applicable only to a linear system. In practice this method is also applicable to nonlinear interacting systems such as for atomic Bose-Einstein condensate, especially for the ground state configuration.

APPENDIX B

DIAGONALIZATION OF A QUADRATIC HAMILTONIAN FOR INTERACTING BOSONS

We provide here a brief summary of a procedure for diagonalizing a quadratic Hamiltonian of bosons. See Ref. [129, 130] for more details.

A general form of a quadratic Hamiltonian for a bosonic system with N internal degrees of freedom ($N = 3$ for a spin-1 system) is

$$H_2 = \frac{1}{2}\sum_{i,j=1}^{N}\left[A_{ij}(a_i^\dagger a_j + a_i a_j^\dagger) + B_{ij}a_i^\dagger a_j^\dagger + B_{ji}^* a_i a_j\right],$$

where a_i ($a_i^\dagger$) are the annihilation (creation) operators for the ith component which satisfy the commutation relations

$$\left[a_i, a_j^\dagger\right] = \delta_{ij},\ [a_i, a_j] = \left[a_i^\dagger, a_j^\dagger\right] = 0,$$

A is an $N \times N$ Hermitian matrix, $A^\dagger = A$, and B is a symmetric matrix, $B^T = B$.

The task of diagonalization is to find a canonical transformation of a_i and $a_i^\dagger$ such that H_2 takes the form

$$H_2 = \sum_{i=1}^{N}\hbar\omega_i b_i^\dagger b_i,$$

where b_i ($b_i^\dagger$) are the new bosonic annihilation (creation) operators. Let us define the *associated matrix*

$$M_{2N\times 2N} = \begin{pmatrix} A & B \\ -B^* & -A^* \end{pmatrix},$$

then we just diagonalize M. The characteristic equation of M, $\det(M - \hbar\omega I_{2N})$, is a real polynomial in $(\hbar\omega)^2$. The appearance of zero eigenvalue is due to Goldstone modes and imaginary eigenvalues are usually related to dynamical instability.

APPENDIX C

NOTATIONS

Symbol	Meaning
a_0	s-wave scattering length for total $F = 0$ channel
a_2	s-wave scattering length for total $F = 2$ channel
$a_{\rm sc}$	s-wave scattering length for scalar condensate
B	External magnetic field
B'	Magnetic field gradient
c	Normalized spin interaction, $(c_2/2)\langle n\rangle$
c'	Normalized spin interaction, $c_2\langle n\rangle$
c_0	Spin independent interaction strength
c_2	Spin dependent interaction strength
E	Total energy of the system
$E[\Phi, \Phi^*]$	Energy functional for condensate wave function
E_i	Zeeman shift for ith component
$\mathcal{E}$	Energy per atom under SMA
F	Angular momentum of atom's hyperfine state
$F_{\rm high}$	Hyperfine state with high energy
$F_{\rm low}$	Hyperfine state with low energy
$F_{\rm tot}$	Collision channel for two atoms
$F_{1,2}$	Hyperfine state of two colliding atoms
F_α	Spin matrices, $\alpha = x, y, z$
f	Average spin per atom
$\mathcal{F}$	Free energy in rotating frame
G	Gibbs free energy
g	Interaction strength for scalar condensate
$g_{0,2}$	Interaction strength for channel $F_{\rm tot} = 0, 2$
g_I	Landé g-factor for nucleons
$g_\nu(x)$	Bose function
H	Hamiltonian, expressed as integration of field operators
H_{ZM}	Zeeman energy matrix
H_S	Spin independent Hamiltonian
$\hbar$	Plank's constant
I	Nuclear spin
J	Angular momentum
i, j, k, l	Internal state, $i = +, 0, -$
$\mathcal{L}$	Linear operator in H

Symbol	Meaning
m	Mass of atom
M	Total magnetization
m	Fractional magnetization, $\mathcal{M}/N$
m_F	z-component of the angular momentum F
N	Total number of atoms
$N_{i,j}$	Number of atoms in ith component and jth level
N^T	Total number of atoms of noncondensed part
N_i^T	Total number of atoms of noncondensed ith component
N_C	Total number of atoms of condensate
N_c	Critical number of atoms with attractive interaction
n	Total density, $n_+ + n_0 + n_-$
n^T	Total density of noncondensed part
n_i	Density of ith component $(n_i^T + n_i^C)$
n_i^T	Density of ith component of noncondensed part
n_i^C	Density of ith component of condensate
$\tilde{n}_i$	Density of ith component of quasi-1D system
$P_{0,2}$	Projection operator (onto $F_{\rm tot} = 0, 2$)
r, s, t	Coefficients in cubic equation
$V_{\rm ext}$	External trapping potential
x, y, z	Cartesian coordinates
δ	Quadratic Zeeman energy
η	Fictitious magnetic field, used to conserve M
η_0	Linear Zeeman energy if a B field is applied
$\tilde{\eta}$	Scaling factor for quasi-1D system
μ	Chemical potential, used to conserve N
$\Psi(\Psi^\dagger)$	Field creating (annihilating) operator
$\Phi(\Phi^*)$	Condensate wave function, normalized to N
$\phi(\phi^*)$	Condensate wave function, normalized to unit
ρ_i	Fraction of ith component $(i = +, 0, -)$
θ	Relative phase among components
θ_i	Phase of the ith component
ξ_i	ith component of spin degree of freedom

REFERENCES

[1] S. N. Bose, Z. Phys. **26**, 178 (1924).

[2] A. Einstein, Sitzber. Kgl. Preuss. Akad. Wiss., 261 (1924).

[3] M. H. Anderson, J. R. Ensher, M. R. Matthews, C. E. Wieman, and E. A. Cornell, Science **269**, 198 (1995).

[4] K. B. Davis, M. -O. Mewes, M. R. Andrews, N. J. van Druten, D. S. Durfee, D. M. Stamper-Kurn, and W. Ketterle, Phys. Rev. Lett. **75**, 3969 (1995).

[5] C. C. Bradley, C. A. Sackett, J. J. Tollett, and R. G. Hulet, Phys. Rev. Lett. **75**, 1687 (1995); Erratum: *ibid* **79**, 1170 (1997).

[6] A. E. Leanhardt, T. A. Pasquini, M. Saba, A. Schirotzek, Y. Shin, D. Kielpinski, D. E. Pritchard, and W. Ketterle, Science **301**, 1513 (2003).

[7] See http://amo.phy.gasou.edu/bec.html/bibliography.html

[8] J. E. Williams and M. J. Holland, Nature (London) **401**, 568 (1999).

[9] M. R. Matthews, B. P. Anderson, P. C. Haljan, D. S. Hall, C. E. Wieman, and E. A. Cornell, Phys. Rev. Lett. **83**, 2498 (1999).

[10] K. W. Madison, F. Chevy, W. Wohlleben, and J. Dalibard, Phys. Rev. Lett. **84**, 806 (2000).

[11] J. R. Abo-Shaeer, C. Raman, J. M. Vogels, and W. Ketterle, Science **292**, 476 (2001).

[12] C. Raman, J. R. Abo-Shaeer, J. M. Vogels, K. Xu, and W. Ketterle, Phys. Rev. Lett. **87**, 210402 (2001).

[13] E. Hodby, G. Hechenblaikner, S. A. Hopkins, O. M. Maragó, and C. J. Foot, Phys. Rev. Lett. **88**, 010405 (2002).

[14] P. Engels, I. Coddington, P. C. Haljan, and E. A. Cornell, Phys. Rev. Lett. **89**, 100403 (2002).

[15] V. Bretin, S. Stock, Y. Seurin, and J. Dalibard, Phys. Rev. Lett. **92**, 050403 (2004).

[16] A. Smerzi, S. Fantoni, S. Giovanazzi, and S. R. Shenoy, Phys. Rev. Lett. **79**, 4950 (1997).

[17] S. Raghavan, A. Smerzi, S. Fantoni, and S. R. Shenoy, Phys. Rev. A **59**, 620 (1999).

[18] M. Albiez, R. Gati, J. Fölling, S. Hunsmann, M. Cristiani, and M. K. Oberthaler, e-print cond-mat/0411757 v2.

[19] B. P. Anderson and M. A. Kasevich, Science **282**, 1686 (1998).

[20] P. Pedri, L. Pitaevskii, and S. Stringari, Phys. Rev. Lett. **87**, 220401 (2001).

[21] D. Jaksch, C. Bruder, J. I. Cirac, C. W. Gardiner, and P. Zoller, Phys. Rev. Lett. **81**, 3108 (1998).

[22] M. Greiner, O. Mandel, T. Esslinger, T. W. Hänsch, and I. Bloch, Nature (London) **415**, 39 (2002).

[23] O. Mandel, M. Greiner, A. Widera, T. Rom, T. W. Haïsch, and I. Bloch, Nature (London) **425**, 937 (2004).

[24] D. I. Choi and Q. Niu, Phys. Rev. Lett. **82**, 2022 (1999).

[25] O. Morsch, J. H. Müller, M. Cristiani, D. Ciampini, and E. Arimondo, Phys. Rev. Lett. **87**, 140402 (2001).

[26] D. Jaksch and P. Zoller, New J. Phys. **5**, 56 (2003).

[27] M. Olshanii, Phys. Rev. Lett. **81**, 938 (1998).

[28] D. S. Petrov, G. V. Shlyapnikov, and J. T. M. Walraven, Phys. Rev. Lett. **85**, 3745 (2000).

[29] E. B. Kolomeisky, T. J. Newman, J. P. Straley, and X. Qi, Phys. Rev. Lett. **85**, 1146 (2000).

[30] A. Görlitz, J. M. Vogels, A. E. Leanhardt, C. Raman, T. L. Gustavson, J. R. Abo-Shaeer, A. P. Chikkatur, S. Gupta, S. Inouye, T. Rosenband, and W. Ketterle, Phys. Rev. Lett. **87**, 130402 (2001).

[31] V. Dunjko, V. Lorent, and M. Olshanii, Phys. Rev. Lett. **86**, 5413 (2001).

[32] C. A. Regal, M. Greiner, and D. S. Jin, Phys. Rev. Lett. **92**, 040403 (2004).

[33] M. W. Zwierlein, C. A. Stan, C. H. Schunck, S. M. F. Raupach, A. J. Kerman, and W. Ketterle, Phys. Rev. Lett. **92**, 120403 (2004).

[34] T. -L. Ho, Phys. Rev. Lett. **92**, 090402 (2004).

[35] H. Hu, A. Minguzzi, X. Liu, and M. P. Tosi, Phys. Rev. Lett. **93**, 190403 (2004).

[36] S. Stringari, Europhys. Lett. **65**, 749 (2004).

[37] M. H. Szymariska, B. D. Simons, and K. Burnett, e-print cond-mat/0412454 v2.

[38] Q. Chen, J. Stajic, and K. Levin, e-print cond-mat/0411090 v2.

[39] C. Chin, e-print cond-mat/0409489 v2.

[40] Y. Ohashi and A. Griffin, Phys. Rev. Lett. **89**, 140302 (2002).

[41] C. J. Myatt, E. A. Burt, R. W. Ghrist, E. A. Cornell, and C. E. Wieman, Phys. Rev. Lett. **78**, 586 (1997).

[42] D. S. Hall, M. R. Matthews, J. R. Ensher, C. E. Wieman, and E. A. Cornell, Phys. Rev. Lett. **81**, 1539 (1998); Erratum: *ibid* 4531.

[43] D. S. Hall, M. R. Matthews, C. E. Wieman, and E. A. Cornell, Phys. Rev. Lett. **81**, 1543 (1998).

[44] M. R. Matthews, D. S. Hall, D. S. Jin, J. R. Ensher, C. E. Wieman, and E. A. Cornell, Phys. Rev. Lett. **81**, 243 (1998).

[45] J. Stenger, S. Inouye, D. M. Stamper-Kurn, H. -J. Miesner, A. P. Chikkatur, and W. Ketterle, Nature (London) **396**, 345 (1998).

[46] D. M. Stamper-Kurn, M. R. Andrews, A. P. Chikkatur, S. Inouye, H. -J. Miesner, J. Stenger, and W. Ketterle, Phys. Rev. Lett. **80**, 2027 (1998).

[47] H. -J. Miesner, D. M. Stamper-Kurn, J. Stenger, S. Inouye, A. P. Chikkatur, and W. Ketterle, Phys. Rev. Lett. **82**, 2228 (1999).

[48] D. M. Stamper-Kurn, H. -J. Miesner, A. P. Chikkatur, S. Inouye, J. Stenger, and W. Ketterle, Phys. Rev. Lett. **83**, 661 (1999).

[49] M. D. Barrett, J. A. Sauer, and M. S. Chapman, Phys. Rev. Lett. **87**, 010404 (2001).

[50] T. -L. Ho, Phys. Rev. Lett. **81**, 742 (1998).

[51] T. Ohmi and K. Machida, J. Phys. Soc. Jpn. **67**, 1822 (1998).

[52] C. K. Law, H. Pu, and N. P. Bigelow, Phys. Rev. Lett. **81**, 5257 (1998).

[53] M. -S. Chang, C. D. Hamley, M. D. Barrett, J. A. Sauer, K. M. Fortier, W. Zhang, L. You, and M. S. Chapman, Phys. Rev. Lett. **92**, 140403 (2004).

[54] H. Schmaljohann, M. Erhard, J. Kronjäger, M. Kottke, S. van Staa, L. Cacciapuoti, J. J. Arlt, K. Bongs, and K. Sengstock, Phys. Rev. Lett. **92**, 040402 (2004).

[55] T. Kuwamoto, K. Araki, T. Eno, and T. Hirano, Phys. Rev. A **69**, 063604 (2004).

[56] J. M. Higbie, L. E. Sadler, S. Inouye, A. P. Chikkatur, S. R. Leslie, K. L. Moore, V. Savalli, and D. M. Stamper-Kurn, e-print cond-mat/0502517.

[57] H. Feshbach, Ann. Phys. **19**, 287 (1962).

[58] J. Stenger, S. Inouye, M.R. Andrews, H.-J. Miesner, D.M. Stamper-Kurn, and W. Ketterle, Phys. Rev. Lett. **82**, 2422 (1999).

[59] S. L. Cornish, N. R. Claussen, J. L. Roberts, E. A. Cornell, and C. E. Wieman, Phys. Rev. Lett. **85**, 1795 (2000).

[60] A. J. Moerdijk, B. J. Verhaar, and A. Axelsson, Phys. Rev. A **51**, 4852 (1995).

[61] T. L. Ho and S. K. Yip, Phys. Rev. Lett. **84**, 4031 (2000).

[62] M. Koashi and M. Ueda, Phys. Rev. Lett. **84**, 1066 (2000).

[63] H. Pu, S. Raghavan, and N. P. Bigelow, Phys. Rev. A **61**, 023602 (2000).

[64] E. P. Gross, Nuovo Cimento **20**, 454 (1961).

[65] E. P. Gross, J. Math. Phys. **4**, 195 (1963).

[66] L. P. Pitaevskii, Zh. Eksp. Teor. Fiz. **40**, 646 (1961) [Sov. Phys. JETP **13**, 451 (1961)].

[67] C. J. Pethick and H. Smith, *Bose-Einstein condensation in dilute gases*, (Cambridge University Press, 2002).

[68] L. Pitaevskii and S. Stringari, *Bose-Einstein condensation*, (Clarendon Press, Oxford, 2003).

[69] F. Dalfovo, S. Giorgini, L. P. Pitaevskii, and S. Stringari, Rev. Mod. Phys. **71**, 463 (1999).

[70] K. Huang, *Statistical Mechanics*, 2^{nd} edition, (John Wiley & Sons, New York, 1987).

[71] H. T. C. Stoof, Phys. Rev. A **49**, 3824 (1994).

[72] P. A. Ruprecht, M. J. Holland, K. Burnett, and M. Edwards, Phys. Rev. A **51**, 4704 (1995).

[73] Y. Kagan, G. V. Shlyapnikov, and J. T. M. Walraven, Phys. Rev. Lett. **76**, 2670 (1996).

[74] A. Gallagher and D. E. Pritchard, Phys. Rev. Lett. **63**, 957 (1989).

[75] M. V. Simkin and E. G. D. Cohen, Phys. Rev. A **59**, 1528 (1999).

[76] A. Görlitz, T. L. Gustavson, A. E. Leanhardt, R. Löw, A. P. Chikkatur, S. Gupta, S. Inouye, D. E. Pritchard, and W. Ketterle, Phys. Rev. Lett. **90**, 090401 (2003).

[77] M. Erhard, H. Schmaljohann, J. Kronjäger, K. Bongs, and K. Sengstock, Phys. Rev. A **70**, 031602 (2004).

[78] S. -K. Yip, Phys. Rev. Lett. **83**, 4677 (1999).

[79] T. Mizushima, K. Machida, and T. Kita, Phys. Rev. Lett. **89**, 030401 (2002).

[80] A. E. Leanhardt, Y. Shin, D. Kielpinski, D. E. Pritchard, and W. Ketterle, Phys. Rev. Lett. **90**, 140403 (2003).

[81] J. -P. Martikainen, A. Collin, and K. -A. Suominen, Phys. Rev. A **66**, 053604 (2002).

[82] T. Isoshima, T. Ohmi, and K. Machida, J. Phys. Soc. Jpn. **69**, 3864 (2000).

[83] W. -J. Huang, S. -C. Gou, and Y. -C. Tsai, Phys. Rev. A **65**, 063610 (2002).

[84] F. Gerbier, J. H. Thywissen, S. Richard, M. Hugbart, P. Bouyer, and A. Aspect, Phys. Rev. A **70**, 013607 (2004).

[85] W. Zhang, S. Yi, and L. You, Phys. Rev. A **70**, 043611 (2004).

[86] R. K. Pathria, *Statistical mechanics*, second edition, (Butterworth-Heinemann, Oxford, Boston, 1996).

[87] V. Bagnato, D. E. Pritchard, and D. Kleppner, Phys. Rev. A **35**, 4354 (1987).

[88] W. Ketterle and N. J. van Druten, Phys. Rev. A **54**, 656 (1996).

[89] S. Giorgini, L. P. Pitaevskii, and S. Stringari, J. Low Temp. Phys. **109**, 309 (1997).

[90] S. Giorgini, L. P. Pitaevskii, and S. Stringari, Phys. Rev. A **54**, 4633(R) (1996).

[91] X. Liu, H. Hu, A. Minguzzi, and M. P. Tosi, Phys. Rev. A **69**, 043605 (2004).

[92] A. Minguzzi, S. Conti, and M. P. Tosi, J. Phys.: Condens. Matter **9**, L33 (1997).

[93] S. Yi, Ö. E. Müstecaplıoğlu, C. P. Sun, and L. You, Phys. Rev. A **66**, 011601 (2002).

[94] W. Zhang, S. Yi, and L. You, New J. Phys. **5**, 77 (2003).

[95] E. G. M. van Kempen, S. J. J. M. F. Kokkelmans, D. J. Heinzen, and B. J. Verhaar, Phys. Rev. Lett. **88**, 093201 (2002).

[96] A. Crubellier, O. Dulieu, F. Masnou-Seeuws, M. Elbs, H. Knöckel, and E. Tiemann, Eur. Phys. J. D **6**, 211 (1999).

[97] D. M. Stamper-Kurn and W. Ketterle, in *Coherent Atomic Matter Waves*, Proceedings of the Les Houches Summer School in Theoretic Physics, Session LXXII, 1999, edited by R. Kaiser, C. Westbrook, and F. David (Springer, New York, 2001), pp. 137-217.

[98] A. J. Leggett, Rev. Mod. Phys. **73**, 307 (2001).

[99] M. Holzmann, G. Baym, J. Blaizot, and F. Laloë, Phys. Rev. Lett. **87**, 120403 (2001).

[100] Q. Gu and R. A. Klemm, Phys. Rev. A **68**, 031604(R) (2003).

[101] F. Dalfovo, S. Giorgini, L. P. Pitaevskii, and S. Stringari, Rev. Mod. Phys. **71**, 463 (1999).

[102] H. Pu, C. K. Law, S. Raghavan, J. H. Eberly, and N. P. Bigelow, Phys. Rev. A **60**, 1463 (1999).

[103] H. Pu, C. K. Law, and N. P. Bigelow, Physica B **280**, 27 (2000).

[104] J. Vanier and C. Audoin, *The quantum physics of atomic frequency standards*, (A. Hilger, Philadelphia, 1988).

[105] T. Isoshima, M. Nakahara, T. Ohmi, and K. Machida, Phys. Rev. A **61**, 063610 (2000).

[106] W. Zhang, D. L. Zhou, M. -S. Chang, M. S. Chapman, and L. You, e-print cond-mat/0502061.

[107] The parameters are taken from M. -S. Chang and M. S. Chapman's new experiment set up (different from [53]).

[108] D. R. Romano and E. J. V. de Passos, Phys. Rev. A **70**, 043614 (2004).

[109] S. Yi, Ö. E. Müstecaplıoğlu, and L. You, Phys. Rev. Lett. **90**, 140404 (2003).

[110] A. Imamoğlu, M. Lewenstein, and L. You, Phys. Rev. Lett. **78**, 2511 (1997).

[111] M. Krämer, C. Tozzo, and F. Dalfovo, e-print cond-mat/0410122 v1.

[112] N. P. Robins, W. Zhang, E. A. Ostrovskaya, and Y. S. Kivshar, Phys. Rev. A **64**, 021601(R) (2001).

[113] K. Kasamatsu and M. Tsubota, Phys. Rev. Lett. **93**, 100402 (2004).

[114] G. P. Agrawal, *Nonlinear fiber optics*, (Academic Press, Boston, 1989).

[115] B. A. Malomed, H. E. Nistazakis, D. J. Frantzeskakis, and P. R. Kevrekidis, e-print cond-mat/0409123 v1.

[116] B. Deconinck, P. G. Kevrekidis, H. E. Nistazakis, and D. J. Frantzeskakis, e-print cond-mat/0409113 v1.

[117] A. D. Jackson, G. M. Kavoulakis, and C. J. Pethick, Phys. Rev. A **58**, 2417 (1998).

[118] J. Ieda, T. Miyakawa, and M. Wadati, Phys. Rev. Lett. **93**, 194102 (2004).

[119] L. Salasnich, A. Parola, and L. Reatto, Phys. Rev. A **65**, 043614 (2002).

[120] L. Salasnich, Phys. Rev. A **70**, 053617 (2004).

[121] M. L. Chiofalo and M. P. Tosi, Phys. Lett. A **268**, 406 (2000).

[122] F. Gerbier, Europhys. Lett. **66**, 771 (2004).

[123] W. Zhang and L. You, Phys. Rev. A **71**, 025603 (2005).

[124] A. M. Kamchatnov and V. S. Shchesnovich, Phys. Rev. A **70**, 023604 (2004).

[125] L. Salasnich, A. Parola, and L. Reatto, Phys. Rev. A **69**, 045601 (2004).

[126] F. Dalfovo and S. Stringari, Phys. Rev. A **53**, 2477 (1996).

[127] S. Yi, *Properties of trapped dipolar condensates*, Ph. D. thesis of Georgia Institute of Technology (2002).

[128] S. E. Koonin, *Computational Physics*, (Addison-Wesley Publishing Com., Redwood City, CA, 1986).

[129] O. Maldonado, J. Math. Phys. **34**, 5016 (1993).

[130] J.-P. Blaizot and G. Ripka, *Quantum theory of finite systems*, (MIT Press, Cambridge, MA, 1986).

VITA

Wenxian (Wingham) Zhang was born in Zhengzhou, Henan Province, P. R. China on October 23, 1974. He entered Fudan University after high school in 1992 and received his B. S. degree in Physics in 1997 and M. S. degree in Optical Science in 2000 from Fudan University. His interest was on the neutral nanoclusters. He came to the U. S. A. for more development in August 2000, studying at Georgia Institute of Technology. He received M. S. degree in 2004 from School of Electrical and Computer Engineering of Georgia Institute of Technology. Since Fall 2000, he was a Teaching Assistant then a Research Assistant at School of Physics. His work in Georgia Institute of Technology has concentrated on ultra-cold dilute spin-1 quantum Bose gases. His immediate postgraduate plan involve post-doctoral work. His scientific publications during this Ph. D. study include:

(1) M.-S. Chang, Q. Qin, W. Zhang, L. You, and M. S. Chapman, "Coherent spinor dynamics in a spin-1 Bose condensate", submitted, e-print cond-mat/0509341.

(2) Wenxian Zhang, D. L. Zhou, and L. You, "Dynamical instability and domain formation in spin-1 Bose condensates", accepted by Phys. Rev. Lett..

(3) Wenxian Zhang and L. You, "Soliton state in trapped ferromagnetic spin-1 Bose condensates", in preparation.

(4) Wenxian Zhang, D. L. Zhou, M. -S. Chang, M. S. Chapman, and L. You, "Coherent spin mixing dynamics of spin-1 atomic condensate in magnetic field", Phys. Rev. A **72**, 013602 (2005).

(5) Wenxian Zhang and L. You, "An effective quasi-one-dimensional description of a spin-1 atomic condensate", Phys. Rev. A **71**, 025603 (2005).

(6) M. -S. Chang, C. D. Hamley, M. D. Barrett, J. A. Saucer, K. M. Fortier, W. Zhang, L. You, and M. S. Chapman, "Observation of spinor dynamics in optically

trapped ^{87}Rb Bose-Einstein condensates", Phys. Rev. Lett. **92**, 140403 (2004).

(7) Wenxian Zhang, Su Yi, and L. You, "Bose-Einstein condensation of trapped interacting spin-1 atoms", Phys. Rev. A **70**, 043611 (2004).

(8) J. Zhuang, Z. Sun, W. Zhang, M. Zhuang, X. Ning, L. Liu, and Y. Li, "Structures and magic numbers of adatom clusters on metal fcc (001) surfaces", Phys. Rev. B **69**, 165421 (2004).

(9) Wenxian Zhang, Su Yi, and Li You, "Mean field ground state of a spin-1 condensate in a magnetic field", New J. Phys. **5**, 77 (2003).

(10) J. Zhuang, T. Kojima, W. Zhang, L. Liu, L. Zhao, and Y. Li, "Structure of clusters on embedded-atom-method metal fcc (111) surfaces", Phys. Rev. B **65**, 045411 (2002).